Geological Field Trips and Maps

SOCIETÀ GEOLOGICA ITALIANA
FONDATA NEL 1881 - ENTE MORALE R. D. 17 OTTOBRE 1885

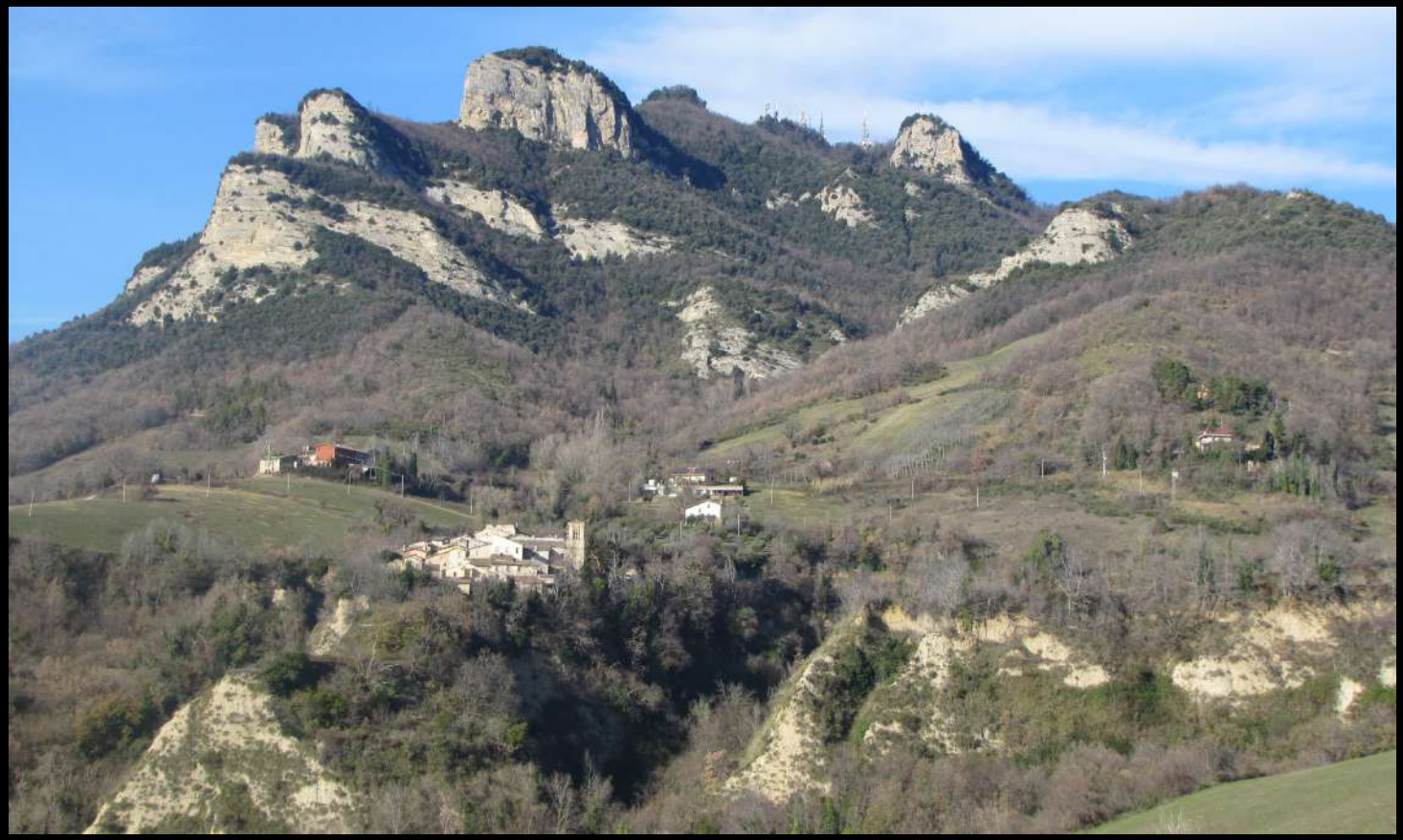

ISPRA
Istituto Superiore per la Protezione e la Ricerca Ambientale

Sistema Nazionale per la Protezione dell'Ambiente

2023
Vol. 15 (1.2)

INDEXED IN EMERGING SOURCES CITATION INDEX THOMSON REUTERS

ISSN: 2038-4947

Pleistocene slope, shallow-marine and continental deposits of eastern central Italy wedge-top basin: a record of sea-level changes and mountain building

PRE-3 Pre-congress Field Trip of the XXI Inqua Congress "A Mediterranean perspective on Quaternary Sciences", Rome 14th-20th July 2023

https://doi.org/10.3301/GFT.2023.03

GFT&M - *Geological Field Trips and Maps*

Periodico semestrale del Servizio Geologico d'Italia - ISPRA e della Società Geologica Italiana
Geol. F. Trips Maps, Vol.**15** No.1.3 (2023), 75 pp., 37 figs., 1 tab. (https://doi.org/10.3301/GFT.2023.03)

Pleistocene slope, shallow-marine and continental deposits of eastern central Italy wedge-top basin: a record of sea-level changes and mountain building

PRE-3 Pre-congress Field Trip of the XXI Inqua Congress "A Mediterranean perspective on Quaternary Sciences", Rome 14th-20th July 2023

Claudio Di Celma[1], Andrea Artoni[2], Danica Jablonská[1], Elisa Mammoliti[1], Michele Malavolta[1], Michela Principi[1], Mauro Caffau[3], Petros Didaskalou[1], Gino Cantalamessa[1]

[1] Scuola di Scienze e Tecnologie, Università degli Studi di Camerino, Via Gentile III da Varano 7, 62032 Camerino (MC), Italy.
[2] Dipartimento di Scienze Chimiche, della Vita e della Sostenibilità Ambientale, Università degli Studi di Parma, Parco Area delle Scienze 157/A, 43124 Parma, Italy.
[3] Istituto Nazionale di Oceanografia e di Geofisica Sperimentale, OGS, Borgo Grotta Gigante 42/C 34010 – Sgonico (TS), Italy.

Corresponding author e-mail: claudio.dicelma@unicam.it

Cover page Figure: Panoramic view of the Gelasian canyon-fill conglomerates of Mt. Ascensione (Photo courtesy of C. Di Celma).

ISSN: 2038-4947 [online]

http://gftm.socgeol.it/

https://doi.org/10.3301/GFT.2023.03

INDEX

INFORMATION

EXCURSION NOTES

ITINERARY

https://doi.org/10.3301/GFT.2023.03

ABSTRACT

This guidebook to Pleistocene sediments exposed in eastern central Italy has been prepared for the PRE-3 geological field trip accompanying the XXI INQUA Congress held in Rome, Italy, in July 2023. It is designed to provide an overview of the sedimentological features, stratigraphic architecture and basin evolutionary steps during the Pleistocene of the central portion of the Periadriatic basin (Central Periadriatic Basin), a N-S oriented foreland basin system associated to the Central Apennine Outer Orogenic Wedge. The Central Periadriatic Basin stretches along the Marche and Abruzzo regions and is an excellent example of an evolving mountain chain and associated deep-marine to fluvial-alluvial foredeep and wedge-top basin system. By integrating surface and subsurface datasets, this field trip affords a fine west to east transect through the Pleistocene basin-fill in southern Marche, where exposures allow a close examination of sedimentary facies and architecture of depositional systems. The basin-fill succession includes coarse-grained submarine canyon-fills encased in slope mudstones, mixed beachface-shoreface conglomerates and sandstones, and alternating conglomerate and mudstone bodies interpreted as fluvial-channel and floodplain deposits, respectively. The analysis of facies architecture and discontinuity surfaces will allow the attendees to understand the relative role of sea-level changes, sediment supply, and thrust front propagation inside the foreland basins system as several factors controlling the stratigraphic record.

Key words: Apennine, Adriatic Sea, Orogenic wedge, Foreland basin, Quaternary, Tectono-sedimentary evolution.

PROGRAM SUMMARY

The field trip sections contain far more stops than can possibly be visited in the actual 3-day 2023 INQUA excursion from Rome (Fig. 1). We have included extra stops (indicated as optional) in order to provide a field-trip guide that will have lasting utility for those who may have more time or may want to emphasise one particular area. Specific stops on the 2023 INQUA excursion will reflect the necessary logistic and time constraints.

DAY 1 – The morning of this day will be spent travelling by bus from Rome to the area of interest. The afternoon of the first day is intended to set up the background geology and stratigraphy of the basin and to examine the sedimentology and stratigraphic architecture of the coarse-grained turbidites filling the Early Pleistocene Mt. Ascensione slope canyon, which provides an opportunity for assessing, from an outcrop perspective, how this type of deepwater depositional systems evolves and fills. This sediment conduit is a transfer zone that records an intermediate step in sediment transport from tectonically-uplifted Apennine source regions to ultimate sinks in the deeper parts of the adjacent basin and is deeply entrenched into a thick succession of hemipelagic mudstones representing background slope deposits laid down by suspension settling and very dilute gravity flows.
Six outcrops, presented along depositional dip and strike, are featured from the Mt. Ascensione canyon system. The field trip itinerary starts at Fosso Morignano (Stop 1.1) by looking at the Messinian and Pliocene mudstones directly underlaying the Pleistocene conglomerates of Mt. Ascensione. Then we move to Polesio to get a scenic panoramic view of the Upper Pleistocene *glacis* deposits laid down along the slope

https://doi.org/10.3301/GFT.2023.03

of Mt. Ascensione (Stop 1.2), to Castel di Croce to get a panoramic view of the proximal portion of the Mt. Ascensione canyon fill (Stop 1.3), and Rotella, where excellent exposures of mud-prone mass-transport deposits (Stop 1.4), coarse-grained channel-fill deposits (Stop 1.5), and thin-bedded mixed sandstones and mudstones deposited in channel-related levee margins (Stop 1.6) can be observed. The day finishes at Castignano.

DAY 2 – The second day of the trip is mostly devoted to the observation of the large-scale geometry of two additional slope canyons. It will begin in the Castignano area, which offers various exposures to reconstruct the stratal architecture of the Castignano canyon (Stops 2.1 and 2.2). We will then travel east to Offida where participants will have the opportunity to examine excellent depositional strike– and dip–oriented sections of the Offida slope canyon (Stops 2.3 and 2.4, respectively). The day finishes at Castignano.

DAY 3 – The third day will be dedicated to describe and discuss the complex stratigraphic architecture as well as the details of environmental variability within

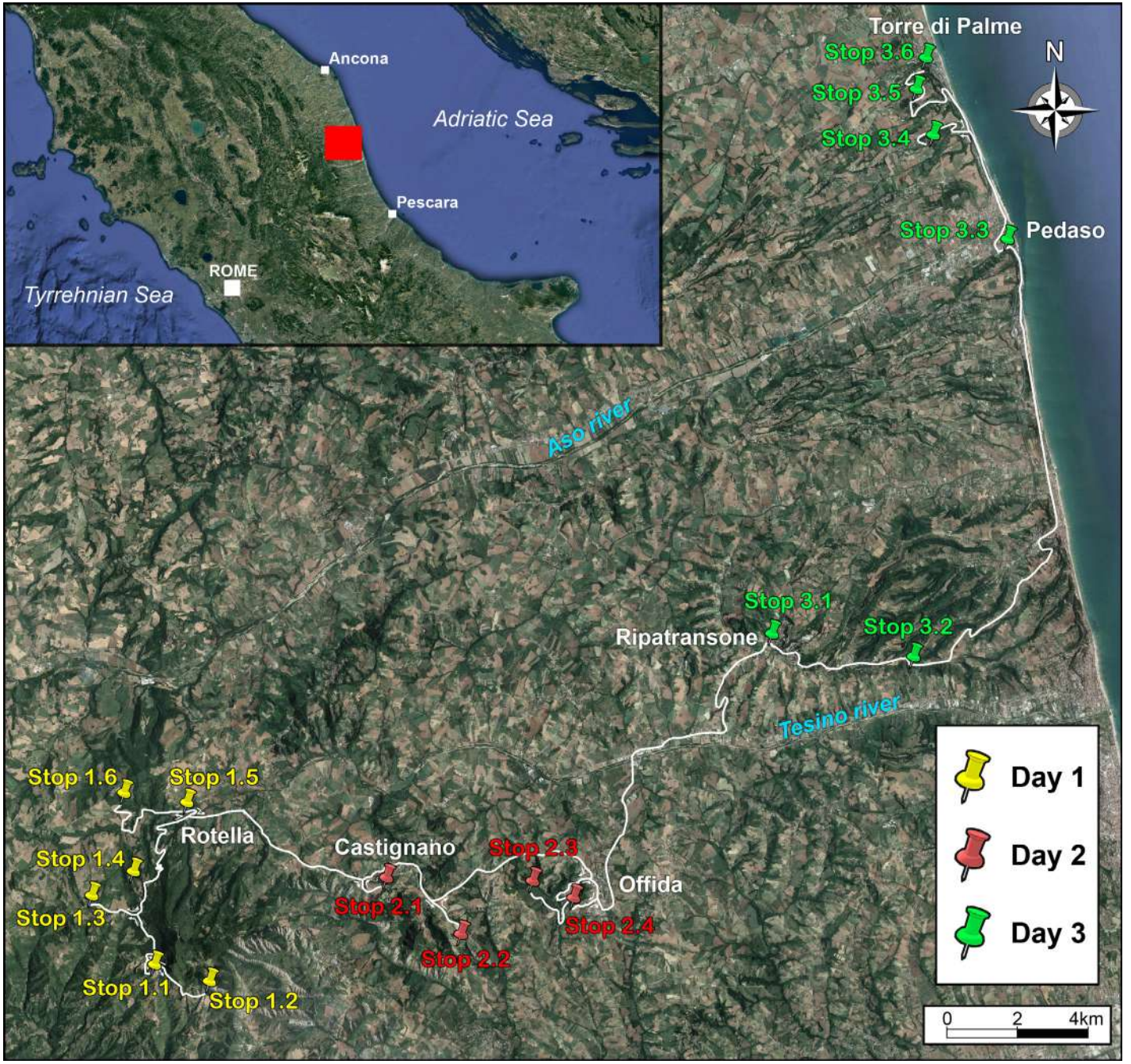

Fig. 1 - Google Earth view of the 3 days field trip itinerary with locations of the stops.

https://doi.org/10.3301/GFT.2023.03

the topset of a prograding, margin-scale clinoforms system deposited during a period of high-frequency sea-level changes superimposed on long-term, syndepositional uplift. The slightly easterly dipping topset, comprising beachface conglomerates, shoreface sandstones, gravel-filled incised-valleys, and back-barrier lagoon mudstones, developed in response to repeated cross- shelf shoreline transgressions and regressions, thereby hosting the shelf portion of high-frequency sequences. The day will start at Ripatransone with a close examination of: i) the transition from mud-prone slope foreset to coarse-grained shelf topset of the prograding clinoforms system (Stop 3.1); and ii) beachface-shoreface strata containing sedimentary structures interpreted to have been formed by storm-generated, offshore-directed flows during the transition in flow regime from supercritical to subcritical (Stop 3.2). The field trip continues with a series of stops (Stop 3.3, 3.4, and 3.5), where we will examine different aspects of the sedimentology and large-scale architecture of these coarse-grained, storm-dominated shallow-water systems developed under the control of relative fall and successive rise of sea level, and will end at the charming village of Torre di Palme (Stop 3.6) with a north-looking panoramic view of the Porto San Giorgio and Mt. Conero thrust-related anticlines exposed along the Adriatic coastline. The day finishes at Rome.

SAFETY

Some of the stops will involve panoramic views, some others include road cuts along narrow roads (be aware of fast-moving traffic and look both ways before attempting to cross a road), and short walks along easy paths and shallow stream crossings. In this area, July is warm and pleasant with average temperatures approximately between 18 to 27 degrees Celsius; however, it's not unusual to get heat waves and occasional summer rainstorms. Suitable field clothing and sturdy footwear, such as jumpers, wind-jackets, heavy socks, waterproof trekking boots, long trousers, hat and suncream are strongly recommended. Trekking shoes are necessary for the field trip, as some parts of the trails are steep. Mobile phone coverage is generally good, although in some place it can be absent.

If you find yourself in serious difficulty and need help, the single number to call for emergencies in Italy is **112**, a free number you dial without any area code: operator will forward the call to the relevant service depending on the type of emergency.
For needs limited to specific issues, you can also call the following numbers:
State Police: 113 (accidents, theft, etc.)
Fire Brigade: 115 (fires, weather emergencies)
Urgent and emergency medical service: 118 (must concern health issues)

https://doi.org/10.3301/GFT.2023.03

Responsibilities of field trip participants:

- follow the leader's instructions and directions;
- advise the excursion leader of any medical or physical problems prior to the start of a trip (e.g. asthma, diabetes, epilepsy, vertigo, heart condition, back problems, carsickness, lung disease, allergies etc.);
- carry any personal medicines you may require (antihistamines, anti-inflammatories, asthma medication, etc.);
- know your limitations and fitness before undertaking any field trip;
- advising the leader if you want to stop. Leader can then make arrangements to assist you safely back to the starting point, arrange a companion to stay with them or arrange to meet them on the return;
- always stay with the group. Short cuts can be dangerous;
- be responsible for taking plenty of fluids and food (including extra energy sources);
- have enough comfortable clothing adequate for any weather changes, suitable footwear and a good raincoat;
- take care in the field such as when hammering rocks, using chisels. Wearing eye protection is recommended.

Credit and permissions

https://doi.org/10.3301/GFT.2023.03

HOSPITALS

The nearest hospitals are located at:
DAY 1 and DAY 2: Ascoli Piceno (Ospedale “C. e G. Mazzoni”, Via degli Iris, 1, 63100; Phone: +39 0736 358111); San Benedetto del Tronto (Ospedale “Madonna del Soccorso”, via Luciano Manara, 8, 63074; Phone: +39 0735 7931).
DAY 3: Fermo (Ospedale “Augusto Murri”, Via Augusto Murri, 21, 63900; Phone: +39 0734 625111).

OVERNIGHT ACCOMMODATION

Ascoli Piceno and its surroundings offer many options for hotel and farm-house accommodations; it is possible to browse and book from websites dedicated to hotel reservations.

https://doi.org/10.3301/GFT.2023.03

GEOLOGICAL OVERVIEW

This section will acquaint the user with the geologic framework and the stratigraphic terminology of the Periadriatic Basin, thus providing a context for specific discussions at the road log. The Central portion of the Periadriatic Basin (Central Periadriatic Basin), also known as the Pescara Basin (Ghielmi et al., 2013), is a N-S oriented foreland basin system associated to the Central Apennine Outer Orogenic Wedge (CAOOW, Figs. 2 and 3). It is located between an extensional range to the west and the foreland area to the east (Fig. 3); the latter is a relatively undeformed zone in the middle of the Adriatic basin and it is also the foreland area for the Dinarides (Fig. 2). The Central Periadriatic Basin is a segment of the Apennine mountain chain which is connected to the Alps toward north and continues in the Calabrian Arc and the Maghrebian mountain chain toward the south (Fig. 2). These mountain chains are the result of the convergent movements of Eurasia, Africa, Corsica-

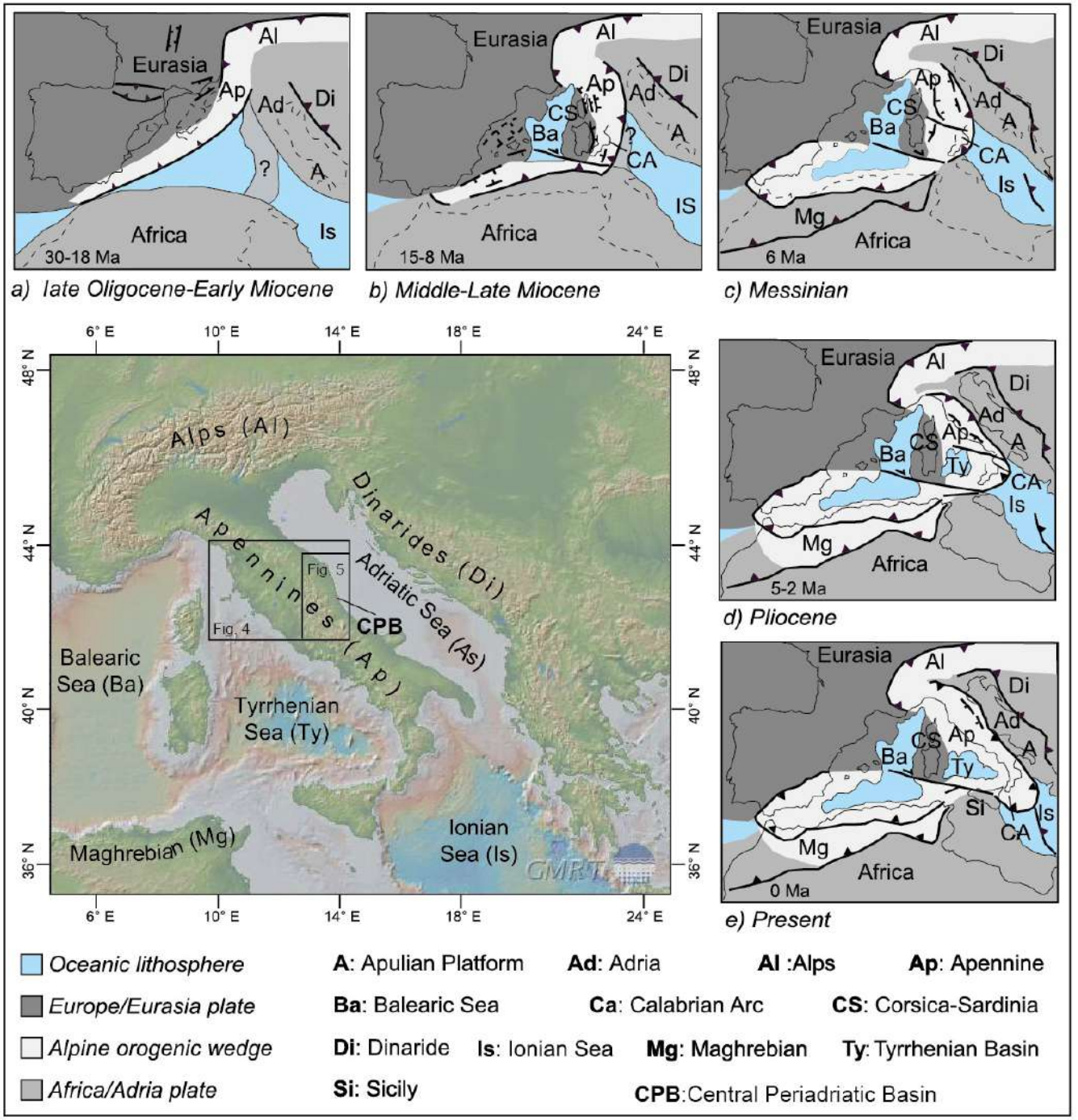

Fig. 2 - Location of the visited area (CPB: Central Periadriatic Basin) and regional geological evolution of the Mediterranean area (modified after Faccenna et al., 2004; Rosenbaum et al., 2002). The location map in this and the following figures is from GMRT Data Portal (http://www.marine-geo.org/tools/maps_grids.php) (Ryan et al., 2009).

https://doi.org/10.3301/GFT.2023.03

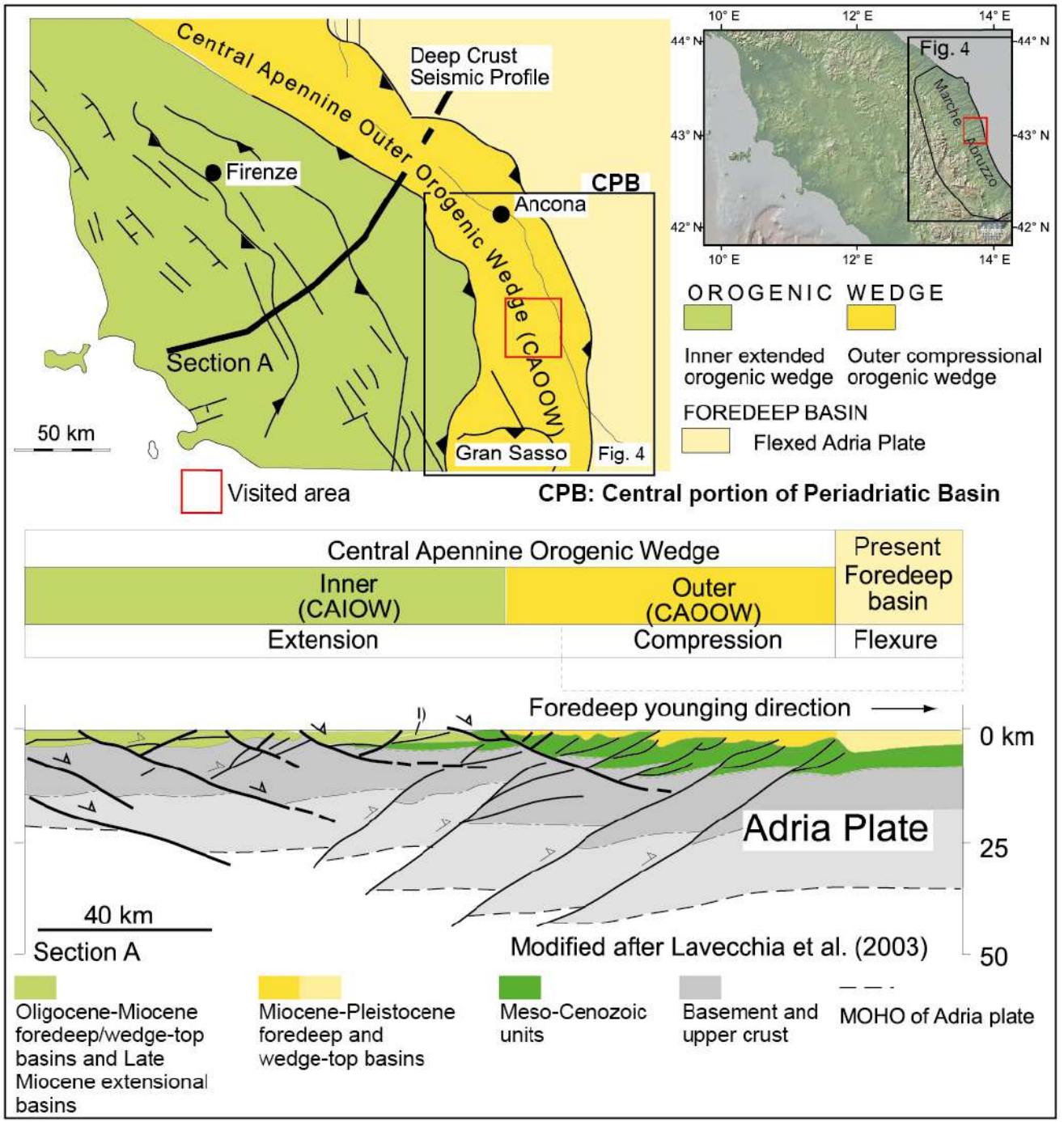

Sardinia and Adria plate that are the remnants of Mesozoic-Cenozoic continental blocks and associated passive margins (Dercourt et al., 1986; Boccaletti et al., 1990; Argnani, 2002; Rosenbaum et al., 2002; Cavazza et al., 2004; Faccenna et al., 2004) (Fig. 2a-e).

The Apennines started as an Alpine back-thrust belt or retro-wedge; the latter was associated to an east-verging accretionary prism in the frame of the westward subduction of the Alpine Tethys oceanic crust since Late Cretaceous (Dercourt et al., 1986; Doglioni et al., 1998; Molli et al., 2010; Carminati and Doglioni, 2012; Marroni et al., 2017). During Europe-Africa collision (post-Oligocene), the lithosphere and mantle behaviour induced the uplift of the Apenninic orogenic wedge, asthenosphere wedging and lithosphere delamination (Doglioni et al., 1998; Argnani, 2002; Faccenna et al., 2004; Carminati and Doglioni, 2012). At the same time, the segmented Adria plate collided with the Corsica-Sardinia block and underwent flexure (Royden and Karner, 1984; Kruse and

Fig. 3 - Location of the visited area (inset red rectangle) within the Central Apennine and regional cross-section (section A) derived from deep seismic profile north of the visited area. Note the thick-skinned tectonics of outer orogenic wedge. The Central Apennine Outer Orogenic Wedge (CAOOW) and the associated Central Apennine Foreland Basins System are evidenced (modified after Lavecchia et al., 2003).

https://doi.org/10.3301/GFT.2023.03

Royden, 1994; Van Der Meulen et al., 1998) and eastward retreat (Malinverno and Ryan, 1986; Doglioni et al., 1999; Argnani, 2002; Scrocca et al., 2007; Mantovani et al., 2009). On the western side of the Apennines, these processes are associated to the lithospheric boudinage of the earlier Alpine belt, which produced the collapse of the Apennine belt (Doglioni et al., 1998; Mantovani et al., 2009). On the Adriatic side, the coupling between mountain uplift and flexure/retreat created a series of Oligocene to Recent foredeep basins; from the oldest to the youngest these are: Macigno (Chattian-Aquitanian), Cervarola (Aquitanian-Burdigalian), Marnosa-arenacea (Langhian-Tortonian), Laga (Messinian), and Pliocene-Pleistocene foredeep basins (Ricci Lucchi, 1986; Boccaletti et al., 1990; Argnani and Ricci Lucchi, 2001). Within the Oligocene to Recent collisional history, two major phases can be distinguished. During the Oligocene-Miocene phase (Fig. 2a, b, c), the lithospheric collision occurred during a major counterclockwise rotation of the Corsica-Sardinia block (Rosenbaum et al., 2002; Faccenna et al., 2004; Rosenbaum and Lister, 2004) and caused the welding of Adria plate to the Alpine accretionary prism. During the following Pliocene to Recent phases (Fig. 2d, e), the Adria plate was shortened by crustal scale and thick-skinned tectonic (Barchi et al., 1998, 2003, 2012; Tozer et al., 2002; Lavecchia et al., 2003; Carboni et al., 2020; Giacomuzzi et al., 2022) or thin-skinned tectonic (Bally et al., 1986) and the Apenninic mountain chain was built.

The Pliocene-Pleistocene Central Apennine Foreland Basin System is the youngest foreland basins system of the Apennines (Ricci Lucchi, 1986; Argnani and Ricci Lucchi, 2001; Ghielmi et al., 2010). It forms on and seals the shortened pre-Messinian and Messinian foredeep basins whose depocentres are located west and south of the visited area (Fig. 4) (Artoni, 2003; Centamore et al., 1991; Casnedi et al., 2006; Milli et al., 2007; Bigi et al., 2009; Fantoni and Franciosi, 2010). Towards east, the Pliocene-Pleistocene deposits extend into the Adriatic Sea where they reach their maximum thickness, up to 6 km (Fantoni and Franciosi, 2010).

Structural framework

This large-scale collisional dynamic is associated to tectono-sedimentary processes, which controlled the Central Apennine Foreland Basins System (*sensu* DeCelles and Giles, 1996) by locating the positions of the foredeep and wedge-top basins. The visited area is now ~70 km west of the outermost thrust fronts of the orogenic wedge; the leading edges thrust fronts of the Central Apennine are now in the Central Adriatic (Fig. 4) (Argnani et al., 1991; Argnani and Gamberi, 1995; Argnani and Frugoni, 1997; Scrocca et al., 2007; Artoni, 2013). However, from Messinian to Pleistocene, the leading edge of the Apennines migrated eastward by creating thrust fronts and related anticlines. In the Central Apennine Outer Orogenic Wedge of the Central Periadriatic Basin, six main NNW-SSE trending thrust stacks can be recognised based on their alignment along strike and timing (Fig. 4). Four of these thrust stacks extend all along the Marche and Abruzzo regions (Artoni and Casero, 1997; Artoni, 2007 and reference therein) and two of them are in the central part of the Adriatic Sea (Argnani et al., 1991; Argnani and Gamberi, 1995; Argnani and Frugoni, 1997). From west to east (Fig. 4), the six thrust stacks are named: 1) Mt. Acuto-M.gna dei Fiori front (MAF); 2) Strada-Roccafinadamo front (SR); 3) Jesi-Nereto-Zaccheo front (JNZ); 4) Conero-Tortoreto front (CT); 5) Elga Adriatic front (EA); 6) Central Adriatic front (CA). At present, the thrust stacks form imbricate thrust fans at various scales, which generate folds of a few hundred metres wavelength at

https://doi.org/10.3301/GFT.2023.03

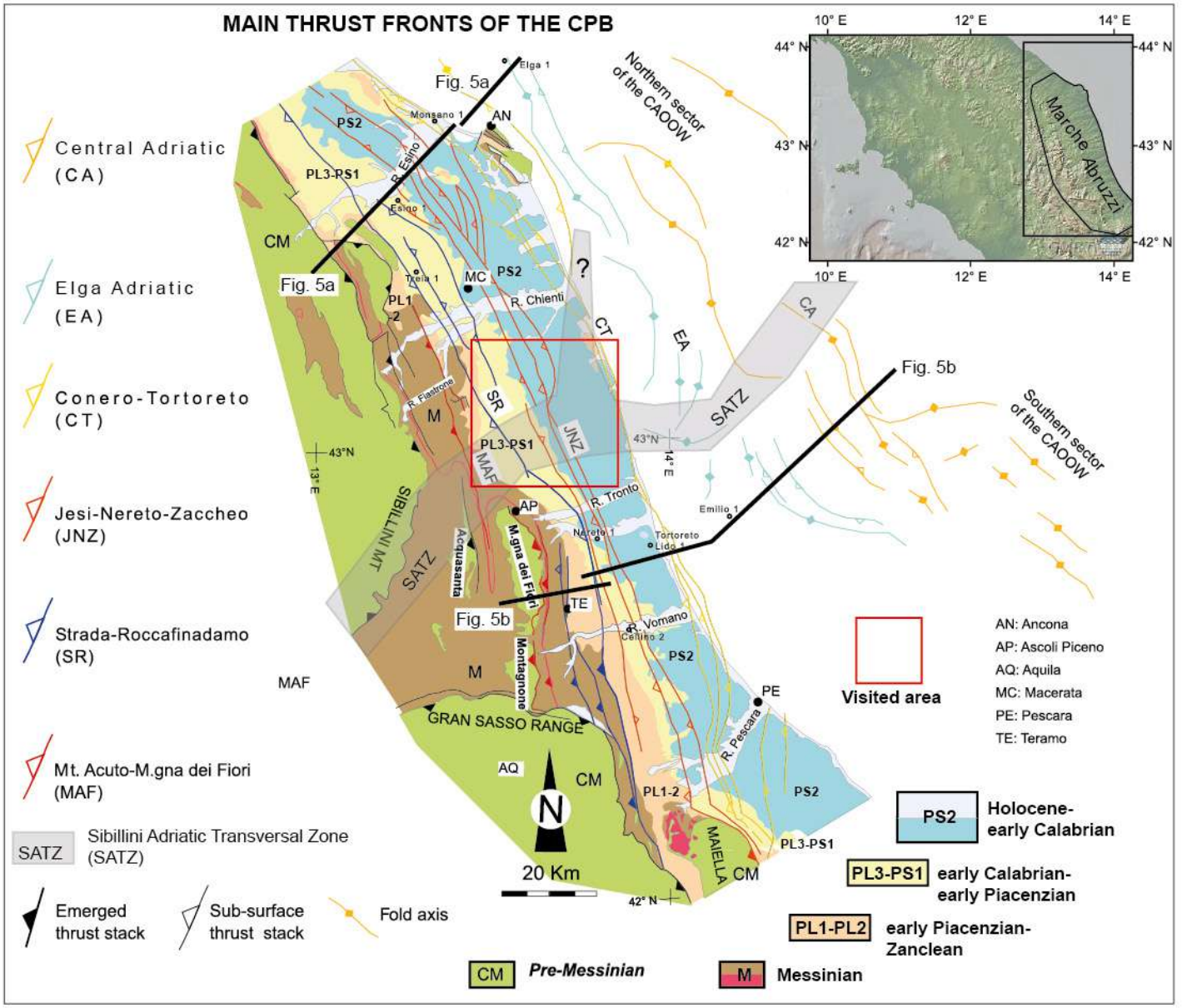

Fig. 4 - Structural sketch map of the Central Periadriatic Basin (CPB) with the traces of the major thrust front and fold axis derived from integrated surface and subsurface studies. The structures are from Artoni (1993, 2007) and, in the Adriatic Sea, are modified after Argnani et al. (1991) and Argnani and Gamberi (1995). Further details about the six thrust stacks and the literature data of each structure can be found in Artoni (2013).

the trailing edge of the major thrust faults (Figs. 4 and 5). Detailed descriptions of these structures can be found in specific studies (see Artoni, 2013). Two regional cross sections cutting through the six thrust stacks have been constructed based on surface and subsurface data (Fig. 5); seismic profiles were depth-converted applying interval velocities to the distinguished stratigraphic units as reported in Figure 5C. The wedge top basin visited in this field trip is bounded by the Mt. Acuto-M.gna dei Fiori front (MAF) to the west and by the Conero-Tortoreto front (CT) to the east (Figs. 4 and 5).

All thrust fronts show significant along-strike variations in geometry, detachment levels (Fig. 5) and most of them are interpreted to involve the basement. In particular, the thrust stacks show geometrical changes in coincidence with a NE-SW zone separating the southern and northern sector of the Central Apennine Outer Orogenic Wedge; this zone is oblique to the major thrust fronts and it is here named the Sibillini Adriatic Transversal Zone (SATZ in Fig. 4). North of this zone, northern sector of the Central Apennine

https://doi.org/10.3301/GFT.2023.03

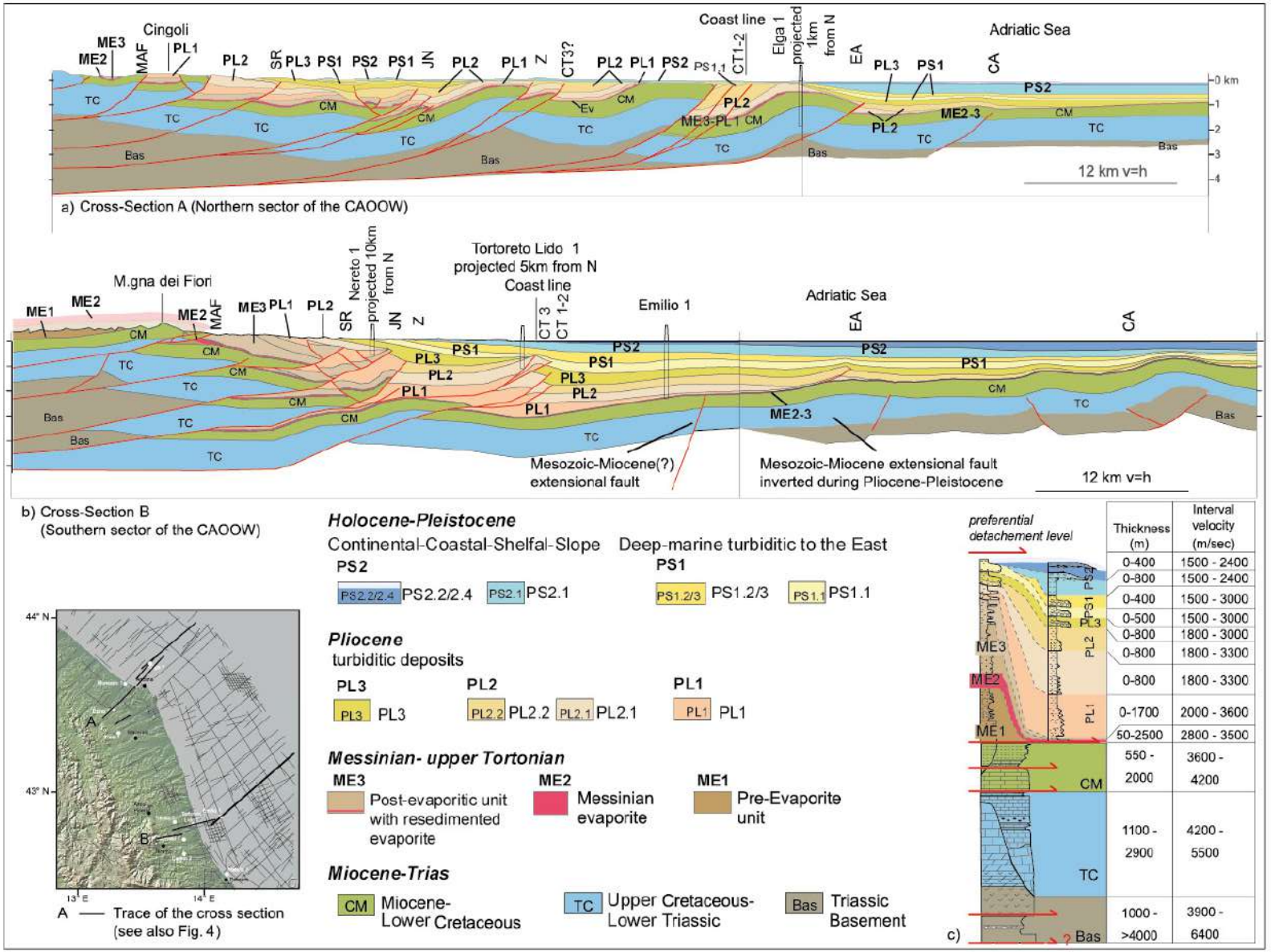

Fig. 5 – (A) Northern and (B) southern cross-sections modified after Artoni (1993, 2007) and in part used for structural modelling. The cross-sections have been constructed by integrating surface and subsurface data. The seismic reflection profiles are depth converted using available velocities (see C); (C) Schematic stratigraphy and thicknesses of the Central Periadriatic Basin stratigraphic units. Average interval velocities are derived from wells along the seismic profiles or calculated for each stratigraphic unit from the available sonic logs in wells (Artoni, 1993). Preferential detachment levels are also reported; "Bas" (Trias basement) includes possible detachment level localised inside Palaeozoic sedimentary units (modified after Scisciani and Montefalcone, 2006).

https://doi.org/10.3301/GFT.2023.03

Outer Orogenic Wedge, the Mt. Acuto-M.gna dei Fiori (MAF), Strada-Roccafinadamo (SR), Jesi-Nereto-Zaccheo (JNZ) and Conero-Tortoreto (CT) thrust stacks branch and have more pronounced arcuate structures, whereas Elga Adriatic (EA) and Central Adriatic (CA) fronts do not exhibit straight thrusts and the folds show E-W-oriented axis within this transversal zone (Fig. 4). South of the Sibillini Adriatic Transversal Zone, southern sector of the Central Apennine Outer Orogenic Wedge, the thrust stacks are NW-SE striking and straighter. The Mt. Acuto-M.gna dei Fiori (MAF), Strada-Roccafinadamo (SR), Jesi-Nereto-Zaccheo (JNZ) and Conero-Tortoreto (CT) gently bend to NNW-SSE striking near the Pescara river (Fig. 4), and the Elga Adriatic (EA) and Central Adriatic (CA) are relatively straighter compared to the northern sector (Fig. 4). In the northern sector, the Conero-Tortoreto (CT) thrust stack involves basement, or pre-Triassic detachment level, whereas, in the southern sector, the Conero-Tortoreto (CT) front detaches both on the Messinian horizon (evaporites) after involving basement to the west (CT3 in Fig. 5B), and on the deeper Triassic evaporites (CT1, CT2 in Fig. 5B). The Elga Adriatic (EA) thrust front displays similar features of Conero-Tortoreto (CT). In the northern sector, the EA is related to a thrust detaching within the basement (or pre-Triassic evaporites?), whereas in the southern sector, it is related to the emergence, almost at the same position, of two thrusts (Fig. 5B). The upper thrust detaches on Messinian evaporites, whereas the lower thrust has to detach on a level deeper than the Messinian seismic horizon and it is interpreted as a basement-involved structure that inverts Mesozoic to Miocene extensional faults (Fig. 5B). The inherited extensional faults are evidenced by a thickened Mesozoic to Miocene succession in the hanging wall of the fault (Fig. 5). Also the Central Adriatic (CA) thrust front is a composite and along-strike variable structure (Fig. 5): a mildly deformed, very open fault-propagation fold in the northern sector; a complex pop-up structure in the southern sector. The complex pop-up structure also displays several evidence of Mesozoic-Miocene extensional faults inverted during Pliocene-Pleistocene along detachment horizon/s deeper than the Messinian reflector, as also recently recognised by Costa et al. (2021).

In other outer orogenic wedges, along strike variations in geometries of the wedge are related to arcuate thrust front geometries, breaching back-thrusting, back-thrusting, lateral variation in thicknesses/facies of detachment horizons and variations in the amount of shortening (Davis and Engelder, 1985; De Donatis and Mazzoli, 1994; Mascle et al., 1998; Coward et al., 1999; Costa and Vendeville, 2002; Mazzoli et al., 2005; Scisciani and Montefalcone, 2005; Kryzywiec and Vergés, 2007).

In the Central Apennine Outer Orogenic Wedge (CAOOW), the major changes in thrust front geometries and styles occur along the SW-NE-striking Sibillini Adriatic Transversal Zone (SATZ), which is approximately aligned with the NE prosecution of the Mt. Sibillini front and partly coincides with the Ancona-Anzio line (Castellarin et al., 1978). This zone is transversal to the main structural trends of the CAOOW and forms a NE-SW-oriented lineament that separates the northern and southern sectors of the CAOOW (Fig. 4). Transversal structures have been recognised to be transcurrent faults systems separating different sectors of the subducting Adria plate (Kruse and Royden, 1994; van der Meulen et al., 1998; Scrocca, 2006) and, in upper crustal level, they might separate zones with different thrust geometries. However, the occurrence of inherited Mesozoic to Miocene extensional faults, as in the Apennine chain, has to be considered to explain along strike variations in structural styles (e.g., Scisciani et al., 2002; Calamita et al., 2003; Tavarnelli et al., 2004; Mazzoli et al., 2005; D'Ambrosio et al., 2021). In the southern sector, complex geometries of the pre-Messinian units suggest the occurrence of Mesozoic-Miocene structural highs

https://doi.org/10.3301/GFT.2023.03

that were involved in post-Messinian inversion structures when the Central Apennine Outer Orogenic Wedge underwent compression. The Ancona-Anzio Line, at least in the exposed portion, is also a Mesozoic inherited extensional structure that, prosecuting in the subsurface, has been likely inverted in post-Messinian times. At present, the transversal zone Sibillini Adriatic Transversal Zone (SATZ) constitutes a complex faults and folds system, still to be described in detail, that contributes to generate variable amount of shortening (13 km, 14.5%, in the northern sector and 33 km, 36% in the southern sector) (Fig. 12 in Artoni, 2013; see also Fig. 10 of this guide).

Since the Late Pliocene-Early Pleistocene times, this sector of the Central Apennine Outer Orogenic Wedge underwent a pronounced regional uplift (San Jose et al., 2020, Sembroni et al., 2020), the greatest being recorded by the Mt. Ascensione canyon fill, which has risen at least 1500 m since earliest-Pleistocene times, as suggested by the epibathyal (400 to 500 m palaeodepth) Lower Pleistocene marine sediments now exposed at ~1,100 m above sea level at the summit of Mt. Ascensione, and by the Middle Pleistocene beachface deposits now exposed at 470 m above sea level at Ripatransone. The uplift is inferred to have been triggered by either out-of-sequence thrusting which continues to shorten and uplift the more internal Strada-Roccafinadamo (SR) and Jesi-Nereto-Zaccheo (JNZ) thrust stacks (Figs. 4 and 5) or the isostatic rebound following the break-off of the subducting Adria plate beneath the Apennines fold-and-thrust belt (Mancinelli et al., 2018; Fellin et al., 2022), or mantle upwelling processes (D'Agostino et al., 2001). Increased erosion and sediment supply rates, because of Quaternary tectonic uplift of the hinterland, along with a relatively narrow shelf were important factors in keeping the Gelasian slope turbidite systems of the Periadriatic basin charged with coarse-grained sediments locally trapped in confined to unconfined wedge-top basins.

Stratigraphic framework

Concepts of genetic sequence stratigraphy, designed to define stratigraphic units bounded by unconformities, have been applied to the stratigraphic analysis of the Pliocene-Pleistocene marine succession exposed in front of the Apennine orogenic belt since the early 1980s (e.g., Ricci Lucchi et al., 1982; Cantalamessa et al., 1986; Ori et al., 1986, 1991), mostly focusing on the analysis of low-resolution sequences at the regional or seismic scale. Over the last decades, new observations and advances in conceptual models and methods contributed to the identification of stratigraphic surfaces at several hierarchical levels and provided new data to refine earlier sequence stratigraphic and chronostratigraphic schemes that could be framed into and allowed to better constrain the tectonic evolution of the Apenninic foreland basin system (e.g., Amorosi et al., 1998; Bracone et al., 2012; Artoni, 2013; Ghielmi et al., 2019). In this guide, which is focused on the Pleistocene succession exposed in the Central Perdiadriatic Basin, we combine surface and subsurface data to outline the tectono-sedimentary evolution of the frontal zone of this sector of the Central Apennine Outer Orogenic Wedge during the final stages of foredeep infilling and its subsequent inclusion in the wedge-top depozone and coeval eastward shift of the foredeep depozone.

Seismostratigraphic analysis of seismic reflection profiles, well logs integrated with the stratigraphy of the exposed Messinian to Pleistocene deposits, and recently published stratigraphic schemes (Casnedi et al., 1981; Casnedi, 1983; Ori et al., 1991; Centamore et al., 1992, 2003; Bigi et al., 1999; Dattilo et al., 1999; Crescenti et al., 2004; Carruba et al., 2006; Artoni, 2007, 2013; Ghielmi et al., 2010, 2013, 2019)

https://doi.org/10.3301/GFT.2023.03

allowed to recognise eight large-scale stratigraphic units bounded by regional tectonically-induced unconformities (U.B.S.U. *sensu* Salvador, 1994) (Fig. 6) developed in response to major phases of compressional deformation and depocentre migration towards the foreland eastward. Some of this large-scale units, spanning in time 1.5-2.5 Myr and some thousands of metres of thickness in the foredeep depocentres, comprise smaller scale stratal subunits bounded by minor unconformities that do not mark significant changes in basin configuration. In particular, during the Gelasian to Calabrian time interval, deposition of the mudstone-dominated basin fill succession was characterised by two main periods when the graded progradational margin was represented by clinoforms in which depositional profiles advanced into the basin and no erosion occurred (units PS1 and PS2), separated by two main phases of out-of-grade slope degradation, canyon incision and sediment bypass onto the base of the slope (u7 and u8 unconformities) in response to stages of basin reorganisation (Ori et al., 1991; Artoni, 2013; Ghielmi et al., 2019).

The Messinian-Pleistocene unconformity bounded stratigraphic units and subunits have been described by Ghielmi et al. (2019) and their distribution is presented on a synthetic geological map derived from published maps (Fig. 7). Although precise dating can be further improved, this basic anatomy of ~million-year-scale unconformity bounded units is now widely accepted for the Late Miocene-Pleistocene complex of foredeep depocentres of the Periadriatic Basin (e.g., Ghielmi et al., 2013), with these surfaces traceable into the subsurface (Artoni, 2013).

The Messinian-Pliocene unconformity bounded stratigraphic units and subunits are not the object of this field guide. For more details on these sediment packages the reader is referred to Ghielmi et al. (2019) and reference therein.

Unit PS1 (lower Gelasian-lower Calabrian)

At surface, the PS1 Unit is composed of a thick succession of hemipelagic slope mudstones that are intermittently cut by submarine canyons infilled by a variety of coarse-grained lithologies. The PS1 Unit comprises three subunits (namely, PS1.1, PS1.2, and PS1.3 from the oldest to the youngest) separated by basin-wide unconformities, which record relatively protracted periods of slope progradation via accretion of sediment to clinoform foresets and degradation in response to canyon incision, respectively. The time-equivalent up-dip configuration during the deepwater phase is unknown, due to later uplift and erosional removal of the laterally equivalent shelf and continental stratigraphy.

The PS1.1 subunit is separated from the underlying PL3.2 subunit by the u7 unconfomity (MP2 unconformity in Ori et al., 1991) exposed at Mt. Ascensione (Stop 1.1). This unconformity is directly overlain by channelised conglomerates associated with sand-rich and mud-rich sediment packages showing a well-defined cyclic arrangement that is inferred to be strictly related to high frequency glacio-eustatic oscillations of sea-level regulating the supply of clastic sediments to the shelf and deep-sea environments (Cantalamessa et al., 2009; Di Celma and Cantalamessa, 2012). Unit PS1.1 shows considerable thickness changes at the scale of the outcrop and from west to east at the scale of the seismic lines. The channelised conglomerates of PS1.1 contain limestone clasts derived from nearby relief to the west, suggesting the occurrence of a short transfer system connecting the source to the depositional area. The u7 unconformity passes to a correlative conformity toward east where, especially east of the present-day coastline, it is difficult to locate with accuracy owing to feeble or missing lithological contrasts.

https://doi.org/10.3301/GFT.2023.03

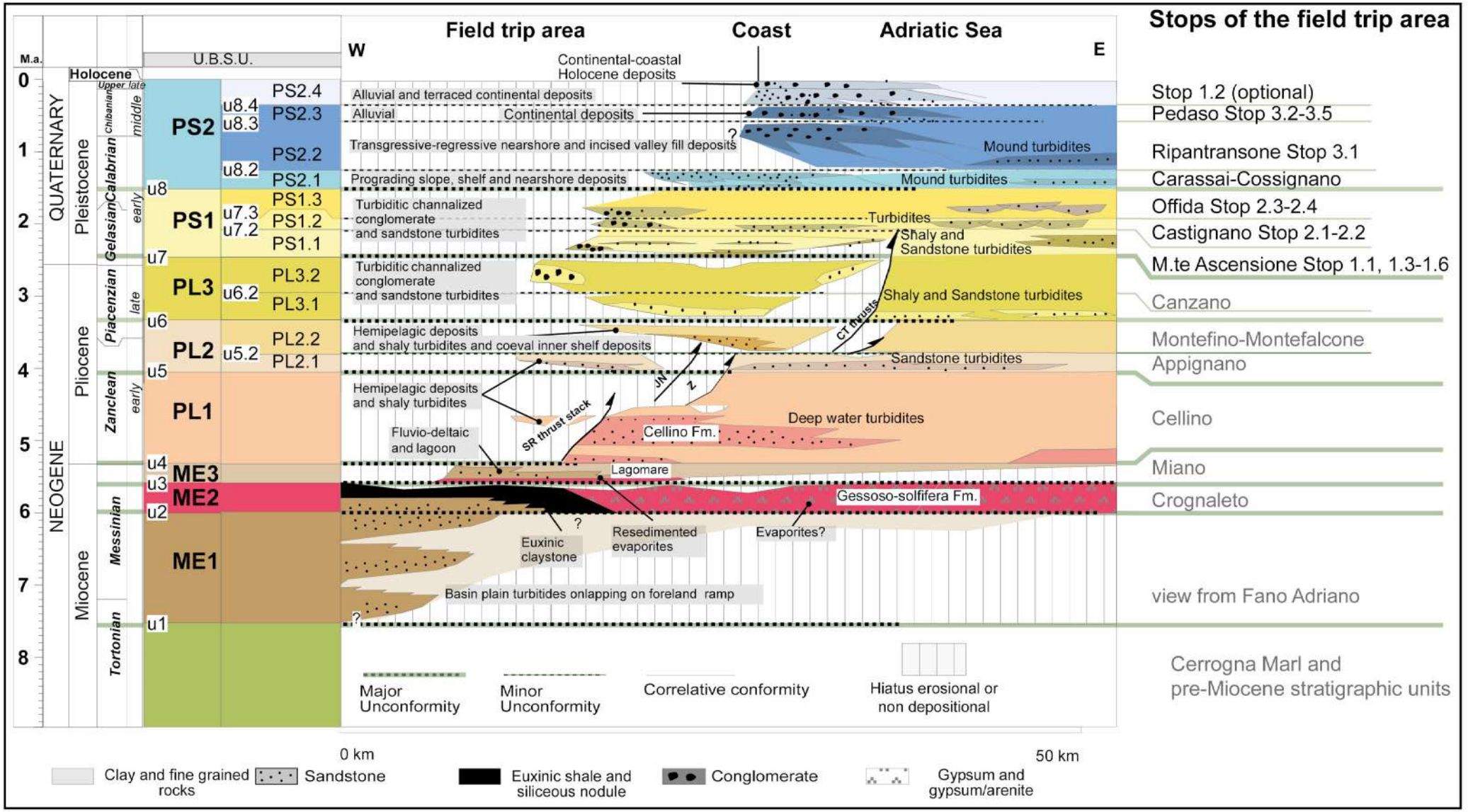

Fig. 6 - Synthetic stratigraphic scheme of Messinian-Pleistocene of the Central Periadriatic Basin including stratigraphic schemes from previous studies (Ori et al., 1991; Roveri et al., 2001; Centamore and Nisio, 2003; Crescenti et al., 2004; Carruba et al., 2006; Ghielmi et al., 2010, 2013, 2019; Artoni, 2013).

https://doi.org/10.3301/GFT.2023.03

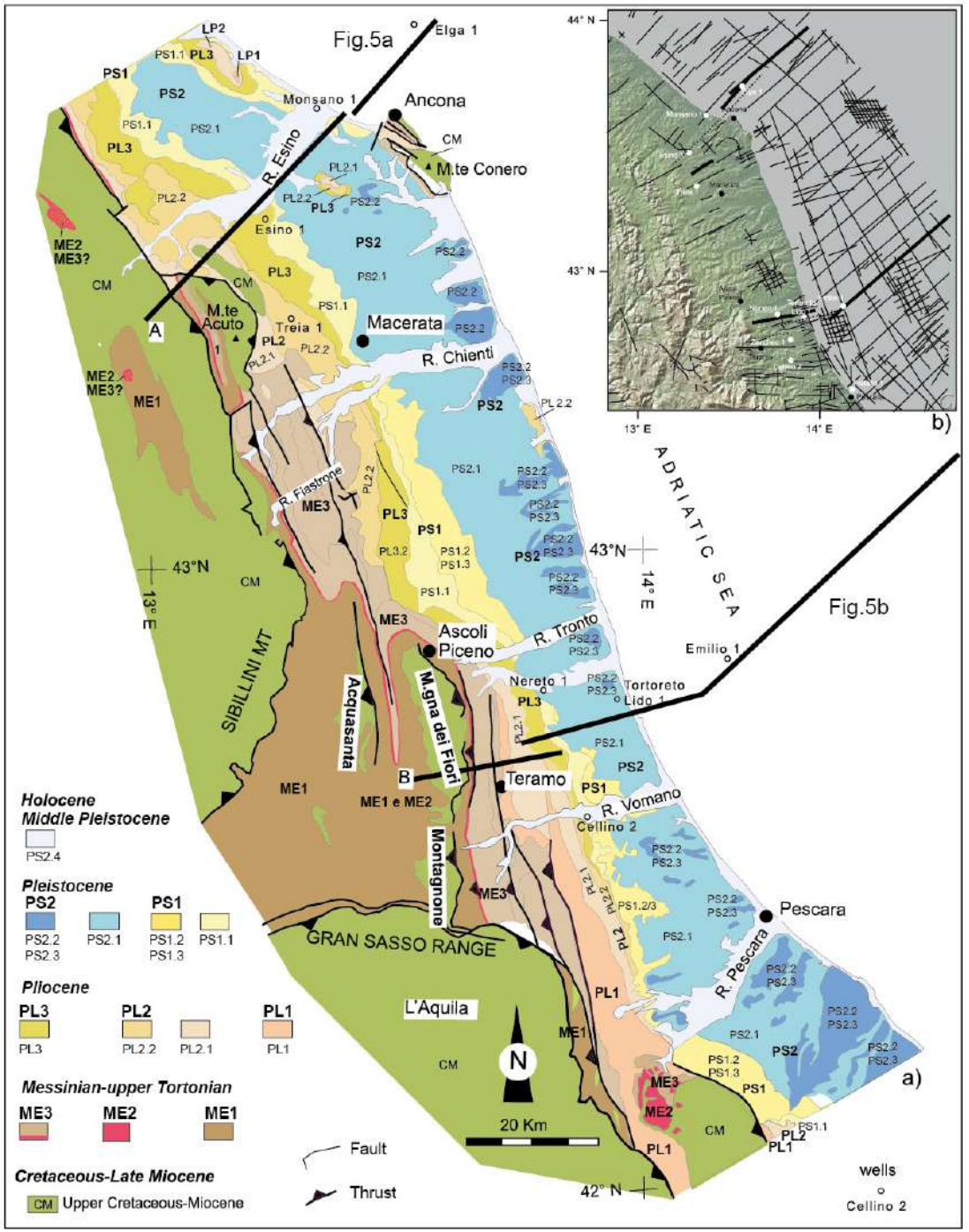

The PS1.2 subunit lower bounding surface (the u7.2 unconformity) is exposed in the vicinity of Castignano (Stops 2.1 and 2.2). In the lower part, this subunit comprises complexly alternating conglomerate, sandstone, pebbly mudstone and heterolithic packages filling a submarine canyon deeply incised in slope mudstones (Ori et al., 1991; Di Celma et al., 2012) that, in turn, are overlain by a thick succession of hemipelagic mudstones. PS1.2 also shows a lenticular shape, thinning both to the west and to the east. In the southern sector, subunit PS1.2 is the first to occur all over the area and sealing the thrust fronts (Fig. 7).

The PS1.3 subunit is bounded at the base by the u7.3 unconformity exposed at Offida (base of Unit UP in Ori et al., 1991) (Stops 2.3 and 2.4). In the lower part, this stratal unit comprises the coarse-grained fill of a slope canyon including conglomerate and sandstone packages (channel-levee complexes) alternating with pebbly mudstones (Ori et al., 1991; Di Celma, 2011), and is overlain by a thick succession of hemipelagic mudstones (Cantalamessa et al., 2009). In Figure 7, the PS1.3 is locally mapped together with the PS2.1 because of its limited lateral continuity and similarity with the coarse-grained sediment wedge (Carassai-Cossignano) at the base of the overlaying unit (see PS2.1).

Fig. 7 - Synthetic geological sketch map of Miocene to Pleistocene units of Central Periadriatic Basin in the Marche and Abruzzo regions derived from geological maps (Artoni, 1993; Artoni and Casero, 1997; Cantalamessa et al., 1986; Centamore, 1986; Servizio Geologico d'Italia, 1958, 1963a, 1963b; 1965a, 1965b, 1966, 1967, 1968, 1969a, 1969b, 1970). In the synthetic geological sketch map the locations of cross-sections of Figs. 4 and 5 are reported.

https://doi.org/10.3301/GFT.2023.03

Unit PS2 (Calabrian-Holocene)

During the early Calabrian, the decreasing or cessation of thrust activity, regional uplift, the reduction of accommodation space, and increase of sediment flux from the Apennines promoted the development of a mud-prone, margin-scale clinoforms system recording a phase of margin outbuilding and active eastward progradation (Unit 2 in Ori et al., 1986). This unit has uncompacted thicknesses ranging from 350 to 500 m (Dalla Valle et al., 2013) and it is composed of four main subunits, namely PS2.1, PS2.2, PS2.3 and PS2.4 from the oldest to the youngest, recording an overall shallowing-upward trend passing from slope, through shelf, to alluvial/fluvial settings.

In southern Marche the lower boundary of the PS2.1 subunit is placed at the base of the Carassai-Cossignano deepwater system (the u8 erosional unconformity). As well documented by seismic data (Ori et al., 1991; Dalla Valle et al., 2013), this subunit consists of a series of mud-dominated, eastward-dipping clinoforms. At outcrop, this progradation resulted into a prominent shallowing-up trend (Stop 3.1), with shelf mudstones grading upward into regressive littoral deposits (Cantalamessa and Di Celma, 2004; Ragaini et al., 2006). The top of the regressive littoral deposits is inferred to record the first phase of subaerial exposure documented in the basin-fill succession.

The PS2.2 subunit represents the slightly descending topset of the large PS2 clinoform wedge seen on seismic data. It corresponds to the shelf environment and comprises alternating shallow-marine and non-marine deposits (beachface conglomerates, shoreface sandstones, gravel-filled incised-valleys, and back-barrier lagoon mudstones). The PS2.2 subunit developed by repeated shoreline transgressions and regressions across the continental shelf, thereby hosting the shelf portion of stacked, high-frequency, unconformity-bounded depositional sequences forming the topset sequence set (Cantalamessa and Di Celma, 2004; Di Celma et al., 2016a; Pieruccini et al., 2016). During transgression, highstand, and early fall of sea level much of the sediment was stored on the shelf, whereas in off-shelf, slope settings no significant deposits were deposited beyond minor hemipelagic drapes and erosional processes were represented by rectilinear, slope-confined gullies developing thin frontal splays at the base of the slope (*Type 1* slope clinoforms of Dalla Valle et al., 2013).

On the shelf, sequence-bounding surfaces record periods of falling and low sea level stand, when great volumes of coarse-grained sediments bypass both the shelf and slope, and exhibit unambiguous evidence for subaerial exposure, such as incised fluvial valleys and/or time-equivalent, laterally extensive interfluve palaeosols (locally reworked by wave ravinement surfaces). When tracked beyond the shelf break and onto the deepwater slope, sequence boundaries are best expressed by rapidly aggrading slope foresets or basin-floor bottomsets through which river-connected slope channels were able to transfer significant amount of sediment to thick base-of-slope frontal-splay complexes (*Type 2* slope clinoforms of Dalla Valle et al., 2013). In slope conduits, in particular, sequence boundaries are widespread erosion surfaces recording intense substrate scouring by energetic, largely bypassing turbidity currents (Di Celma et al., 2010, 2013, 2014; Di Celma, 2011) during time intervals characterised by active growth of submarine fans and high aggradation and thick sediment deposition also in margin sectors away from the main turbidite conduits (Dalla Valle et al., 2013).

Sequences were deposited on the uplifting palaeo-Adriatic shelf in response to repeated high-frequency and high-amplitude eustatic changes in sea level that would promote the creation of accommodation space. By subtracting space to deposition, the contemporaneous

https://doi.org/10.3301/GFT.2023.03

regional uplift of the basin margin may be accounted for the shingled stacking pattern of subsequent sequences and their slightly descending trajectory. The lower boundary of the PS2.2 subunit (u8.2 unconformity) is a diachronous surface resulting from the downdip convergence and amalgamation of multiple erosional surfaces produced by the progressive basinward translation of succeeding sequences (Figs. 6 and 8). The PS2.3 subunit is an alluvial/fluvial sediment wedge bounded at the base by the u8.3 unconformity (Figs. 6 and 9) generated by the interplay of regional uplift and glacio-eustatic sea-level changes. This subunit is exposed on the interfluve areas (Nesci and Savelli, 2003); it is only some tens of metres thick and composed of two fining-upward cycles bracketed by prominent subaerial unconformities represented by mature red argillic palaeosols (Di Celma et al., 2015). Each cycle includes a broad, unconfined gravel-prone braidplain system abruptly overlain by floodplain fines. A detailed study of the mature red argillic palaeosols at the top of the two cycles (Di Celma et al., 2015) suggests that they were developed under humid and warm climatic conditions associated with interglacial phases, which have been tentatively attributed to MIS 11 (427 kyr) and MIS 9 (337 Kyr).

In this guide, we expand upon previous work (Ghielmi et al., 2019) by differentiating an additional PS2.4 subunit, which is bounded at the base by the composite u8.4 unconformity (Figs. 6 and 9). Onland, this subunit comprises a flight of Middle Pleistocene to Holocene alluvial terraces dominated by gravelly braided-stream alluvium, locally overlain by hydrothermal travertines and intertwining with detrital *glacis* deposits (e.g., Boni and Colacicchi, 1966; Fanucci et al., 1996; Gentili et al., 1998; Coltorti and Farabollini, 2008; Wegmann and Pazzaglia, 2009; Buccolini et al., 2010; Nesci et al., 2012; Farabollini and Scalella, 2014; Sembroni et al., 2020), which correlate offshore to coeval coastal and shelf deposits (Amorosi et al., 2016). The alluvial terraces are arranged in four different orders, commonly named T1 to T4 starting from the highest, and are characterised by a marked downstream convergence (Nesci et al., 2012 and references therein) that has been usually retained a result of the general decreasing rate of regional uplift from the chain axis towards the Adriatic. The Middle to Upper Pleistocene terraces resulted from the combination of regional uplift and climatic oscillations that forced alternating phases of fluvial aggradation and incision, whereas anthropogenic causes proved to be effective in triggering both Holocene aggradation and terrace development (e.g., Coltorti, 1997).

Tectonic-stratigraphic evolution: growth of the orogenic wedge, foreland basins system migration and mountain building

The tectono-sedimentary evolutionary stages are not affected by variations of structural styles in the two sectors of the Central Periadriatic Basin (Figs. 4 and 5); the thrust fronts propagation and migration of depocentres of the foreland basins system are similar and coeval within the entire Central Periadriatic Basin (Fig. 10). The tectonic-stratigraphic evolution provides information concerning the changes in the growth's modes of the outer orogenic wedge, associated foreland basins system and mountain building at its early stages when the outer orogenic wedge passed from submarine to subaerial condition and most of the Central Periadriatic Basin became an emerged mountain chain within the visited area (Fig. 11).

https://doi.org/10.3301/GFT.2023.03

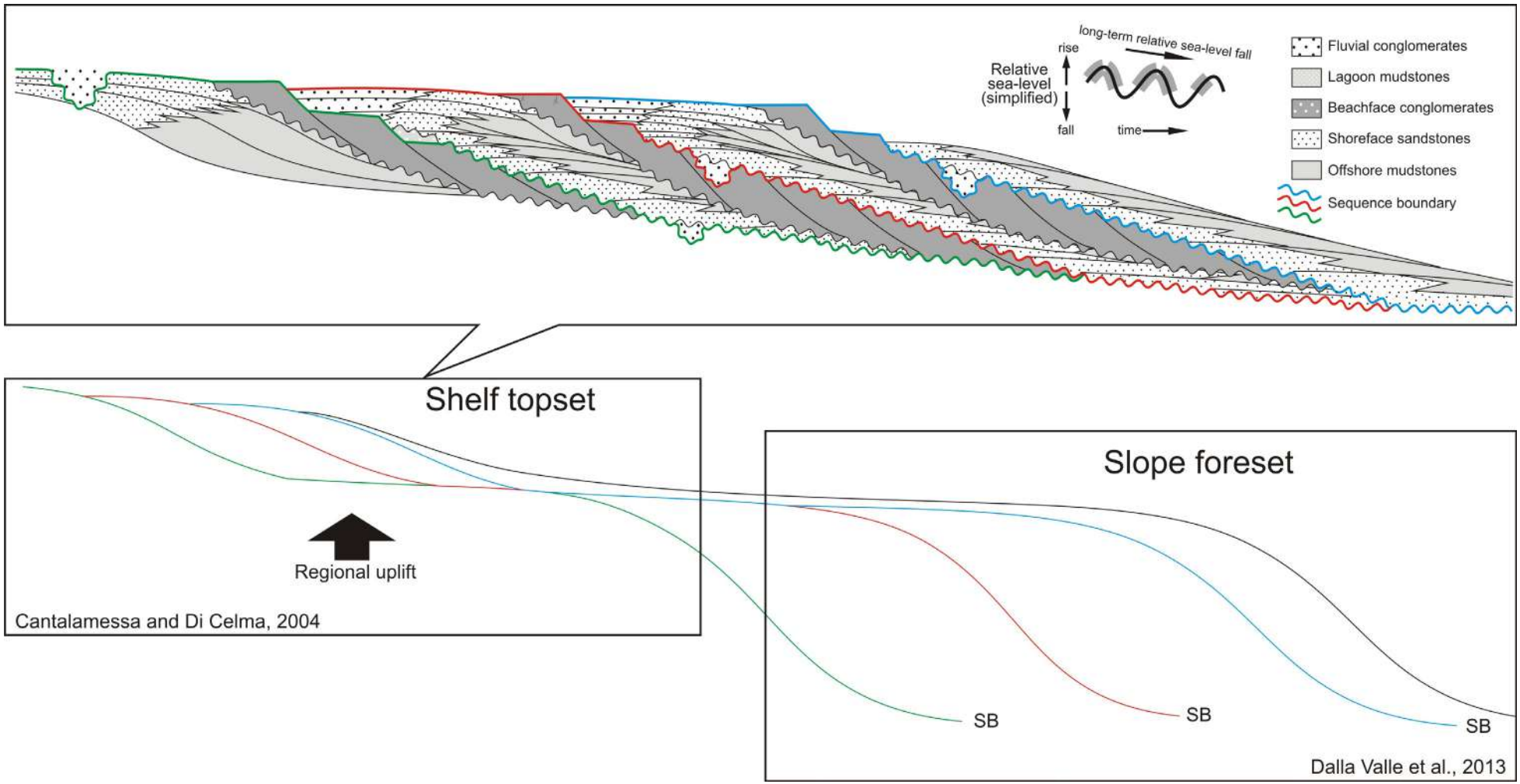

Fig. 8 - Schematic drawing of a depositional dip-oriented cross section (no scale implied) through the PS2.2 subunit within the study area showing a conceptual model for the development of the diachronous, composite sequence set boundary at the base of the topset sequence set (PS2.2 subunit). The stratigraphic architecture of the PS2.2 subunit has been established through repeated forced regressions and intervening landward shifts of shoreline controlled by glacio-eustatic sea-level changes superimposed on a long-term sea-level fall driven by contemporaneous regional uplift. Over the long-term, deposition took place in a low-accommodation setting and individual sequences were stacked with an overall downdip shingling (downstepping) configuration where each successively younger sequence occurs slightly basinward and downward of older sequences to form a tectonically enhanced, falling-stage sequence set (topset). The surface at its base is a complex erosional discontinuity that expands diachronously basinward as a result of the downdip convergence and amalgamation of successive sequence boundaries, including subaerial unconformities (interfluve palaeosols and fluvial incised valleys), regressive surfaces of marine erosion, and wave-modified subaerial unconformities. Although the above observations imply that the u8.2 composite surface is a time-transgressive erosional discontinuity and it is not a chronostratigraphically significant, effective time barrier separating older from younger strata along its full length (it is thus not a consistent unconformity), it remains a mappable surface separating shelf and slope depositional systems and in this study it is retained as a regional composite scour surface (compare Holbrook and Bhattacharya, 2012).

https://doi.org/10.3301/GFT.2023.03

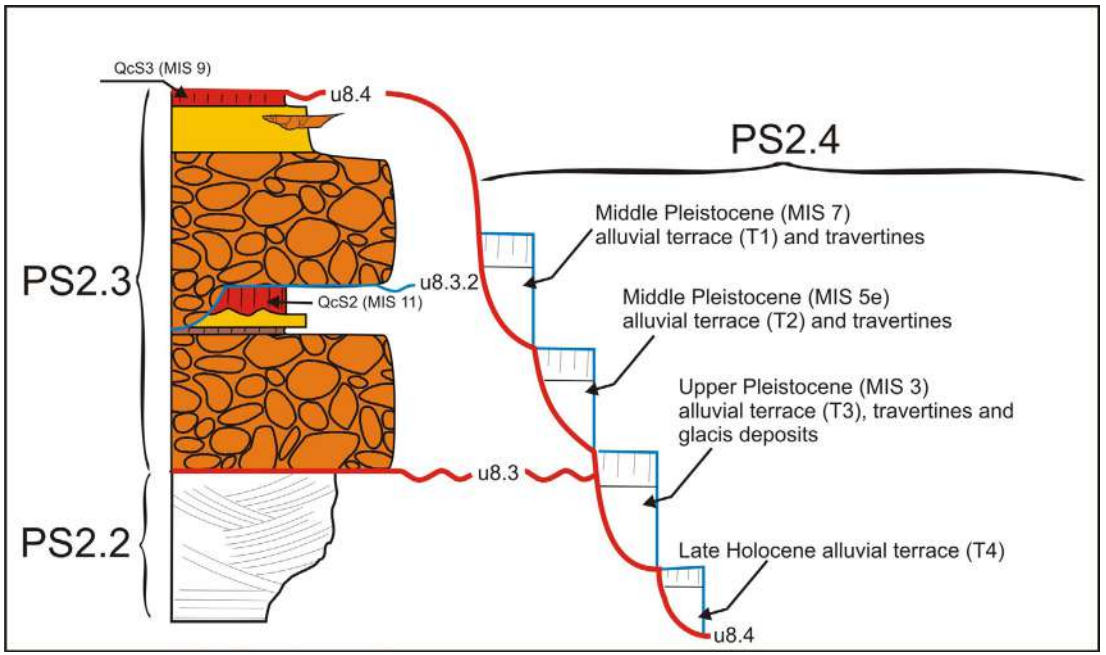

Fig. 9 - Cartoon-style summary of the stratigraphic relationships between subunits PS2.2, PS2.3, and PS2.4. QcS2 and QcS3 indicate two mature red argillic palaeosols (modified from Di Celma et al., 2015). Due to regional uplift, the initial almost-flat surface at the top of the PS2.3 subunit was gradually furrowed by river valleys where alluvial terraces started to develop extensively. Ages of the alluvial terraces are based on U-Th radiometric dating of the directly overlying travertine deposits (Janssens et al., 2020). Alluvial deposition occurred during odd-numbered MIS stages (7-5-3), while fluvial incision dominated during intervening even-numbered MIS stages (6-4-2).

Stages 1-3 reproduce a forelandward migration of foredeep depocentres associated to a piggy-back propagation of thrust fronts and large amount of shortening; at these stages deep-marine turbiditic deposits were sedimented (see Ghielmi et al., 2019) and the orogenic wedge was lengthening by eastward propagation of the outermost front (Conero-Tortoreto and Elga Adriatic fronts, respectively CT and EA in Fig. 10). During these stages 1-3 (about 2 Myr), the thrust fronts shifted in between 24 km to 40 km towards the east (average shift rates between 12 mm/yr and 20 mm/yr) with an overall shortening that varies between 11.2 km and 27.56 km (average shortening rates between 5.6 mm/yr and 13.8 mm/yr). During ***stages 4-9***, foredeep depocentres remained stationary and synchronous, breaching-back/out-of-sequence thrusting was reactivating previously formed thrust fronts producing a small amount of shortening; fluvial, coastal, shelfal to slope deposits tendentially seal the outer thrust fronts (CT, EA in Fig. 10) while internal and reactivated thrusts were tendentially eroded (MAF, SR, JNZ in Fig. 10). During these stages 4-9 (about 3.3 Myr), the forelandward shift of the thrust fronts is null and the shortening is in between 2.5 km and 4.8 km, providing an average shortening rate between 0.75 mm/yr and 1.46 mm/yr, respectively. During these later stages, the orogenic wedge is thickening with the contribution of up to 6-km-thick sedimentary succession. The balance between the tectonic thickening (uplift) and the significant sediment supply results in the first appearance of the mountain chain in this portion of the Central Periadriatic Basin (Fig. 10 – stage 8; Fig. 11d): the outer orogenic wedge passed from submarine to subaerial condition. The sedimentary sequences deposited immediately before and immediately after the emersion of the orogenic wedge are observed in this field trip. This emersion was possible also due to sediment supply which, sourced from the more internal and already emerged area, was able to fill the accommodation space made available by the interplay between eustatic sea-level changes and tectonic movements. Other orogenic wedges and associated foreland basins system present similar evolutionary trends in both structural evolution and depositional environments: the transition from deep-marine turbidites (underfilled stage, turbiditic stages, not observed during this

https://doi.org/10.3301/GFT.2023.03

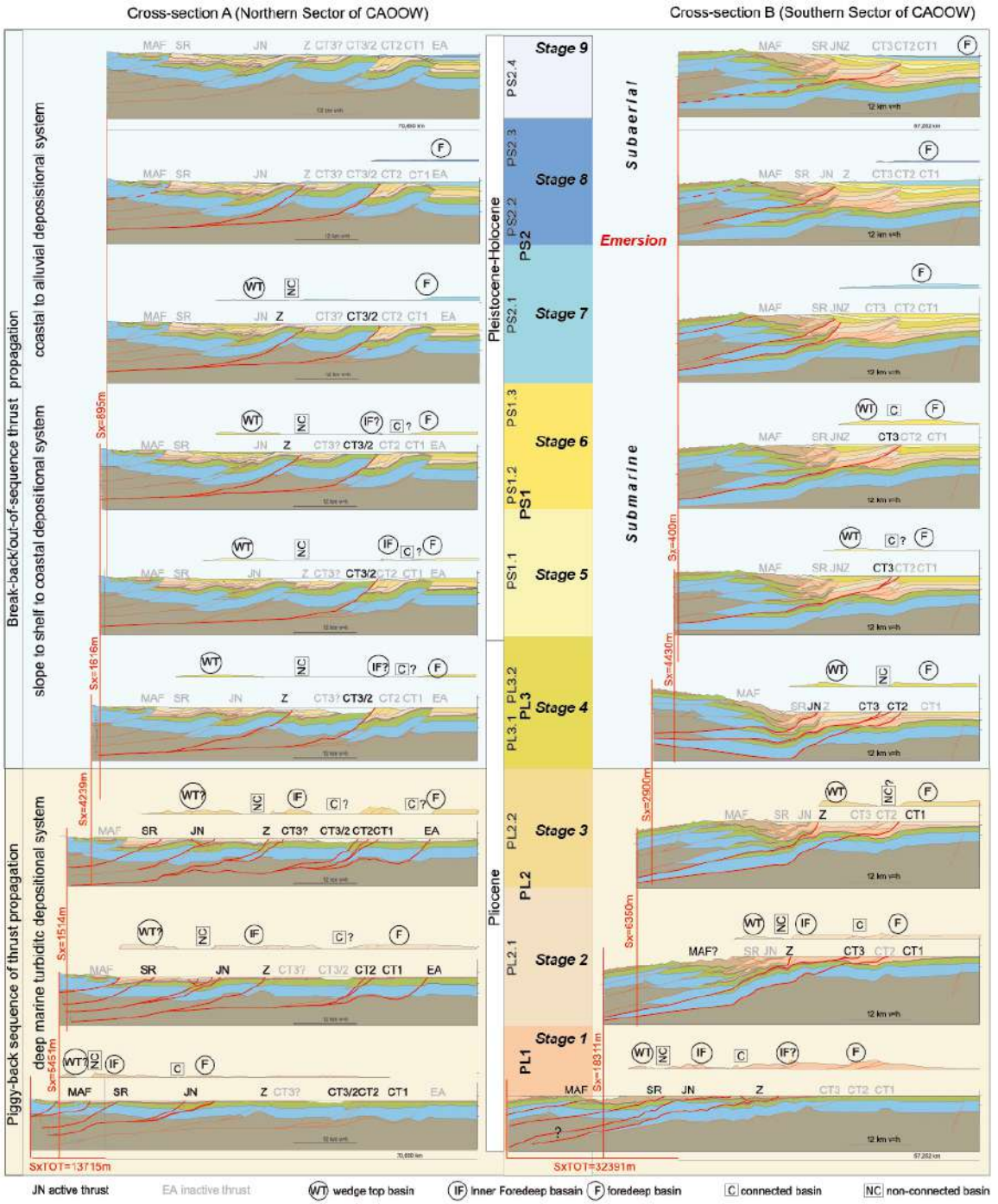

field trip) to shallow marine (overfilled stage, "molasse" stage, observed during this field trip). In the early underfilled stages, the submarine basins' depocentres shift in response to the creation of a new thrust front of the orogenic wedge inside the earlier formed foredeep basin (stages 1-3 in Figs. 10 and 11). The new thrust front creates a wedge-top basin that is progressively disconnected from the new foredeep basin ("connected" and "disconnected" sub-basins in Artoni, 2007; "open piggy-back stage" and "close piggy-back stage" of Ori et al., 1991; "fragmented foredeep" of Ghielmi et al., 2010) (Figs. 10 and 11). In the later overfilled stages, the stationary or slowly shortening-uplifting thrust fronts and the increased sediment supply enhance and allow all the thrust systems to be sealed by prograding shelfal to coastal to alluvial deposits (stages 4-9 in Figs. 10 and 11); these deposits, being strictly controlled by sea level changes, mark the emersion of the mountain chain and the coeval burial of the outermost

Fig. 10 - Sequentially restored cross-sections representative of the northern sector (cross-section A) and southern sector (cross-section B) of Central Apennine Outer Orogenic Wedge (CAOOW) (Fig. 4 for location; Fig. 5 for the cross-sections and Fig. 10 for the undeformed cross-sections). Each stage depicts the reconstructed geometry of the basin at the end of the deposition of the corresponding stratigraphic unit (see Fig. 6 for the stratigraphic scheme) and, immediately above, the restored geometry of the basin of the unit ending its deposition in the following stage (e.g. in stage 2: the geometry of PL1 at the end of its deposition is shown associated to the restored basin geometry of the following/younger PL2; the restored basin geometry of PL1 is shown below in previous stage 1). Each stage reports also the thrust faults (thicker lines) that were active during the deposition of the following/younger unit. The two cross-sections were sequentially restored with the software 2D Move (Midland Valley Exploration Ltd, 2011).

https://doi.org/10.3301/GFT.2023.03

portion of the orogenic wedge. The increased sediment supply fills the depressions at the top of the orogenic wedge so that the wedge-top and foredeep basins become hardly distinguishable.

The above dual/cyclic behaviour in the growth of the orogenic wedge responds also to lithospheric dynamics. In fact, major shifts in foredeep/wedge-top basins depocentres are clearer during the earlier evolutionary stages when few tens of kilometres wide foredeep or connected inner foredeep basins are infilled by eastward tapering out and onlapping turbiditic successions (stages 1-3 in Fig. 10). Afterward, foredeep/wedge-top basins depocentres remain at the same position till present and, at first, they are non-connected (smaller basins are formed during stages 4-6 in Fig. 10) and, finally, they are completely infilled by prograding shelfal-to-alluvial depositional systems (stages 7-9 in Fig. 10). Earlier stages 1-3 exhibit foredeep basins associated to continental lithosphere flexure in response to the load of the Apenninic orogenic wedge and likely related to eastward slab retreat of the westward subducting continental lithosphere of Adria plate (Malinverno and Ryan, 1986; Doglioni, 1991; Doglioni et al., 1999; Carminati and Doglioni, 2012). During later stages 4-9, lithospheric subduction and retreat is either halted or affected by eastward asthenosphere wedging and replacement and isostatic rebound. These later stages foresee lithospheric deformations in both subducting plate and overriding orogenic wedge. The subducting plate is still shortened by thrusting; the overriding orogenic wedge is uplifted, extended in the hinterland and shortened (out-of-sequence thrusting) toward the foreland (Doglioni, 1991; Doglioni et al., 1999; Scrocca et al., 2007; Carminati and Doglioni, 2012). The uplifting

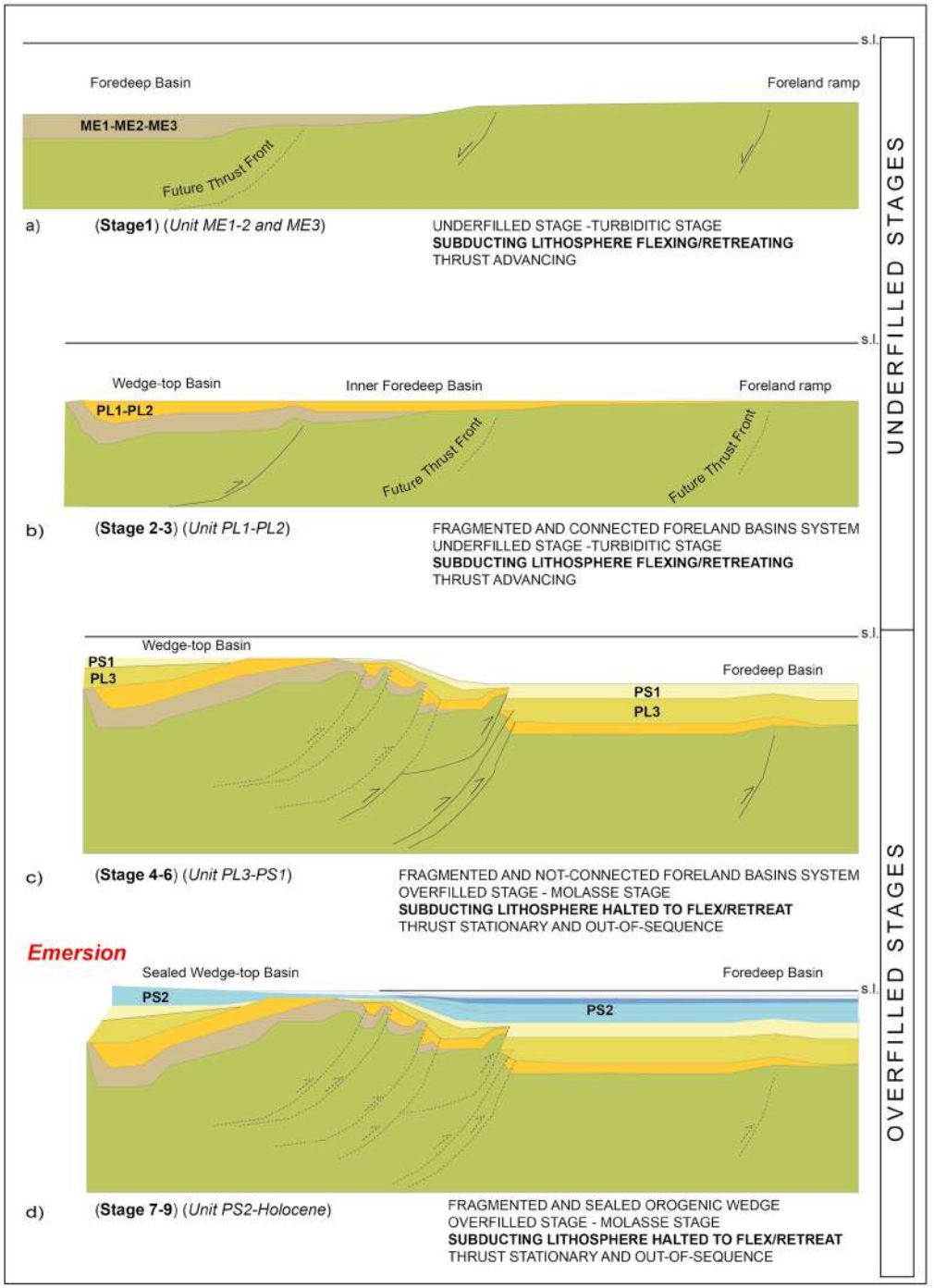

Fig. 11 - Schematic model of the foreland basins system (*sensu* DeCelles and Giles, 1996) applicable to Central Periadriatic Basin.

https://doi.org/10.3301/GFT.2023.03

and internal portion of the orogenic wedge continuously replenishes the sediments that bury the external thrust fronts closer to the foreland; these more external and buried thrust fronts contribute to rise the orogenic wedge above sea level: the subaerial mountain chain is formed.
In the reconstructed tectonic-stratigraphic evolution of the Central Apennine Outer Orogenic Wedge and Central Periadriatic Basin, it is impressive that the stage 4 (Unit PL3) marks significant tectonics and stratigraphic changes: 1) orogenic accretion mode passes from fast- to slow-accretion mode (lengthening to thickening); 2) fold-and-thrust belt structural style is dominated by thick-skinned tectonics; 3) subduction and retreat of lithosphere is either halted or affected by eastward astenospheric replacement; 4) depositional environments pass from deep marine turbidites to fluvial-coastal-shelfal-slope deposits; 5) sea-levels experience major drops related to eustatic/climatic cycles.
The effects of the advancing thrust/orogeny front and migration of foredeep/wedge-top basins that affect the stratigraphic and depositional features testifying the first appearance (emersion) of the mountain chain is investigated in this field trip; the stratigraphic and sedimentological evolution of CAOOW and associated Central Periadriatic Basin is here described since Pleistocene to Holocene.

https://doi.org/10.3301/GFT.2023.03

DAY 1

Stop PRE3-1.1 - Fosso Morignano, Rotella

Coordinates: Lat. 42°54'49"N, Long. 13°32'53"E
Topic: Structural and stratigraphic background and overview on pre-Quaternary units

The Fosso Morignano section shows four of the basin filling stratal units (Fig. 12). From base to top, these are the post-evaporitic ME3 Unit including a volcaniclastic horizon, the Pliocene hemipelagic mudstones of the PL3 Unit, the Pleistocene conglomerates of the Mt. Ascensione canyon fill (PS1.1 subunit), and the Upper Pleistocene accumulation *glacis* deposits of PS2.4. In this area, owing to the absence of PL1 and PL2 sediments, the u4 to u6 unconformities are superimposed and the contact is commonly preserved as a subtle mudstone-on-mudstone regional hiatus of approximately 2 Myr duration between the late Messinian and the early Piacenzian. Magnetostratigraphic analysis of the PL3 mudstones (Albianelli et al., 2003) indicates that the Fosso Morignano section starts with three short intervals, each 30–40 m in thickness, showing a R-N-R polarity succession followed by a relatively long (165 m) interval characterised by normal polarity. Based on the occurrence near the base of the lowermost reversed interval of *Globorotalia bononiensis* (FCO 3.31 Ma) and *Globorotalia crassaformis* (FO 3.6 Ma) and the presence in the uppermost portion of the long normal polarity interval of the calcareous nannofossil *Discoaster asymmetricus* (Lori, 2005), which according to Rio et al. (1990) is distributed up to about the *Discoaster tamalis–Discoaster pentaradiatus* zone boundary (2.82 Ma), it is possible to ascribe this interval to the planktonic foraminifera MPl4c-MPl5a zones (3.31-2.41 Ma) and the nannofossil CNPL4 Zone (3.82-2.76 Ma) of Lirer et al. (2019) and Backman et al. (2012), respectively. These biostratigraphic constraints allow a straightforward correlation of the sequence of normal and reversed polarities recorded at Fosso Morignano to the geomagnetic polarity time scale, with the short R–N–R intervals correlating with the C2An.2r (3.330-3.207 Ma), C2An.2n (3.207-3.116 Ma), and C2An.1r (3.116-3.032 Ma) subchrones, respectively, whereas the overlying long normal-polarity interval correlates with the C2An.1n subchron (3.032-2.581 Ma). By using the cyclostratigraphic distribution of its continuous magnetic signal, Albianelli et al. (2003) calculated that at Fosso Morignano the C2An.1n Chron lasts until 2.63 Ma, with the C2An.1n/C2r.2r (Gauss/Matuyama) reversal boundary (2.581 Ma), which postdates the Gelasian base (2.588 Ma), missing due to a hiatus (u7) at the base of the Mt. Ascensione conglomerates.

Bulk samples collected from the canyon fill yield poor microfossil assemblages characterised by the co-occurrence of the age-diagnostic calcareous nannofossil *Discoaster brouweri* and benthic foraminifera *Bulimina marginata* throughout the entire stratigraphic interval. According to these biostratigraphic data, the canyon fill can be assigned to the nannoplankton CNPL6 Zone (2.39-1.93 Ma) and the planktonic foraminifera MPl5b Zone (2.45-2.09 Ma), indicating an Early Pleistocene (Gelasian) age.

Directly overlying the Mt. Ascensione canyon fill, is a thick fine-grained succession composed of very thin-bedded mudstones with medium- to very fine-grained sandstone intercalations resulting from hemipelagic deposition and the periodic influx of dilute, sluggish turbidity

https://doi.org/10.3301/GFT.2023.03

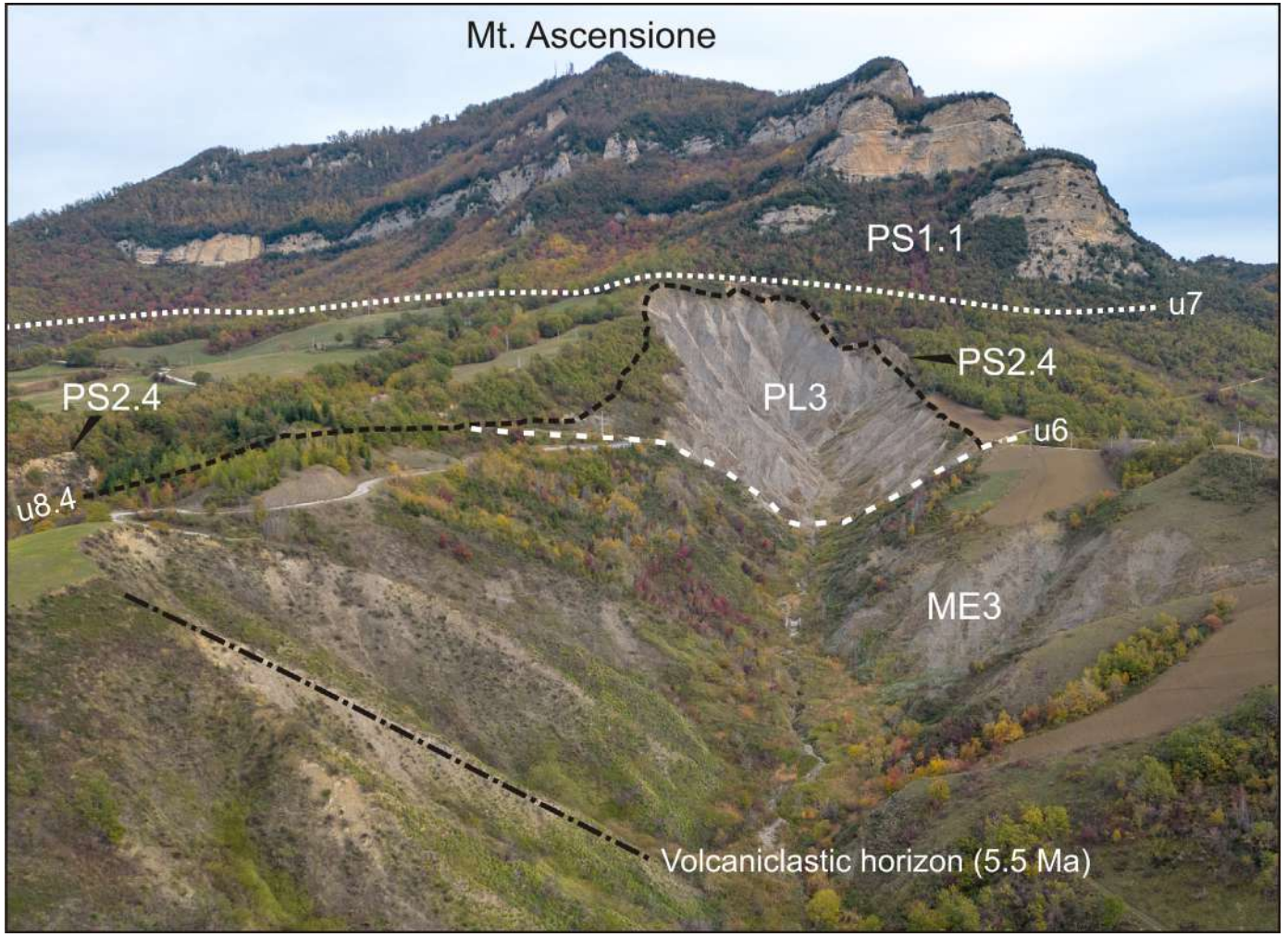

Fig. 12 - Annotated UAV-based photograph of Fosso Morignano. Three unconformities (labelled u6, u7, u8.4) divide up the stratigraphy into four sediment packages, namely ME3, PL3, PS1.1, and PS2.4.

currents, respectively. These sediments record background deposition over large tracts of the slope and are indicative of the deactivation and abandonment of the slope canyon as a conduit for the transfer of coarse-grained sediments to the deeper parts of the basin.

Several samples were collected from this portion of the sedimentary succession for micropalaeontological and magnetostratigraphic analyses (Albianelli et al., 2003; Lori, 2005). *Discoaster brouweri* and *Discoaster triradiatus* are common to abundant in the calcareous nannoplankton, while *Discoaster pentaradiatus* and *Disocoaster surculus* are totally missing, indicating deposition in the CNPL6 biozone (2.39-1.93 Ma). The foraminiferal assemblages are characterised by the occurrence of *Globorotalia crassaformis*, the absence of foraminiferal marker species *Globorotalia bononiensis* and *Globorotalia inflata*, and by abundant individuals of the transitional form between the foraminifera species *G. puncticulata* and *G. inflata*. This metres-thick interval, reported by Cantalamessa et al. (2002), is located between the appearance of *Bulimina marginata* and the FO of *G. inflata*, within the *Discoaster triradiatus* abundance acme, indicating deposition in the terminal part of the planktonic foraminifera MPl5b Zone (2.45-2.09 Ma). As such, the reversed magnetic record is correlated to the early Matuyama C2r.2r subchron (2.581–2.148 Ma).

https://doi.org/10.3301/GFT.2023.03

Stop PRE3-1.2 (optional) – Polesio, Ascoli Piceno

Coordinates: Lat. 42°54'33"N, Long. 13°33'52"E
Topic: Upper Pleistocene accumulation *glacis* deposits

At Mt. Ascensione, accumulation *glacis* represent remnants of gently sloping areas located at the foot slope of the Gelasian conglomerates (Fig. 13). According to Gentili et al. (1998) these *glacis* deposits (PS2.4 subunit) are composed of uncemented and only moderately indurated gravel and sand packages that were probably deposited on a piedmont slope under periglacial climatic conditions. Chronological constraints for this sediment wedge are provided by carbon-14 dating of charcoal fragments collected near its base (>51000 yr BP and 41640 ± 1260

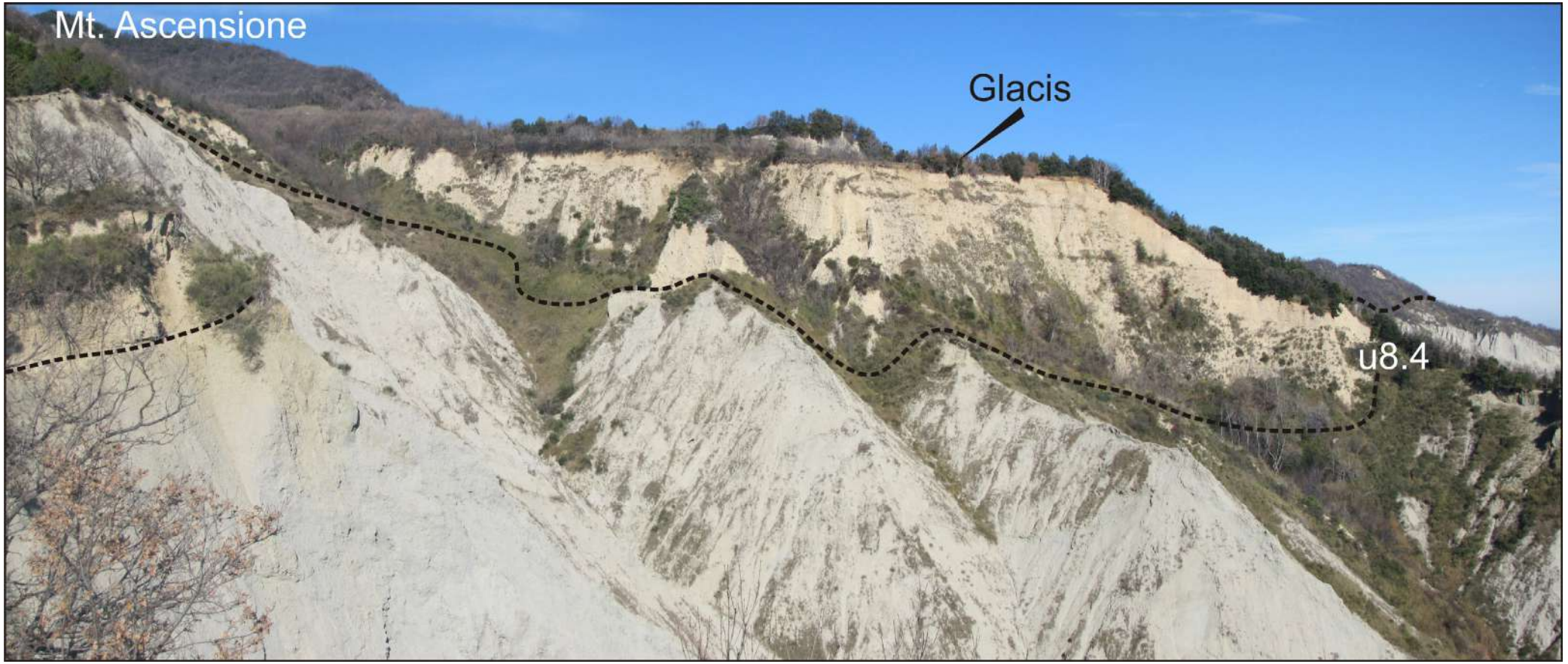

Fig. 13 – Annotated panoramic view of the coarse-grained, periglacial *glacis* deposits underlain by Pliocene hemipelagic mudstones.

https://doi.org/10.3301/GFT.2023.03

yr BP) and its top (23230 ± 170 yr BP and 22680 ± 170 yr BP) (see Gentili et al., 1998; Buccolini et al., 2010). As such, sediments of this accumulation *glacis* are coeval with those of the third-order alluvial terraces found inside the main fluvial valleys.
The base of the *glacis* deposits is a highly irregular erosion surface (u8.4) variably incised into the underlying Plio-Pleistocene mudstones, whereas the upper surface corresponds to a dissected palaeosurface (*glacis*) showing an overall concave-upward longitudinal profile sloping away from the base of the Mt. Ascensione escarpment. *Glacis* deposits were laid down by debris-flow and runoff processes and form wedge-shaped sediment bodies up to several tens of metres in thickness; they are poorly cemented and comprise large blocks of conglomerates and sandy and gravelly layers in a sandy matrix passing both upwards and distally into massive, yellowish silty sands. One or more brown palaeosols are located at different heights with respect to the basal surface. The accumulation *glacis* has been abandoned and dissected at the beginning of the Holocene following a period of climatic amelioration and drainage incision (Buccolini et al., 2010).
In a sandy layer of the *glacis* deposits exposed at Polesio, close to the dated palaeosols, a rich oligotypical assemblage of land snails was documented by D'Amico and Esu (2011). It is dominated by taxa of steppe environment, represented by *Pupilla triplicata*, *Truncatellina callicratis*, *Jaminia (J.) quadridens* and *Jaminia (J.) malatestae*, associated with minor amounts of open land species, such as *Papilla muscorum* and *Vallonia pulchella*. *C. spadae*, fairly abundant, prefers open woodland, but locally can live in semi-open to open habitats. The ecological framework of the molluscan assemblage led the authors to infer open palaeoenvironment and cold climatic conditions.

Stop PRE3-1.3 – Castel di Croce, Rotella

Coordinates: Lat. 42°55'51"N, Long. 13°31'32"E
***Topic*: Stratigraphic architecture of the proximal portion of the Mt. Ascensione canyon fill**

This vantage point provides an excellent view towards the most proximal portion of the Mt. Ascensione canyon emphasising its distinct cyclic packaging. The Mt. Ascensione canyon is one of many Gelasian sediment fairways that served as major submarine routes for the delivery of coarse-grained turbidites into the deepest reaches of the Central Periadriatic Basin and its fill consists of a south to north elongated sedimentary body that is about 2.5–3 km wide and up to 450 m in thickness.
The infill of the three exhumed submarine canyons visited during this field trip, namely Ascensione, Castignano, and Offida canyons, can be described in terms of five major lithofacies. The descriptive lithofacies scheme, considering their principal sedimentological features, is summarised in Table 1. An additional lithofacies, composed of massive mudstone, forms the canyon-confining succession.
The main purpose of this lookout is to introduce the participants to the stratigraphic evolution and architecture of mixed coarse- and fine-grained lithofacies successions in deepwater slope canyons. The canyon filling sedimentary succession displays a marked cyclic character with component lithofacies succeeding one another to form erosionally-based fining-upward cycles (labelled MA-IV with a subscript indicating the cycle from the oldest to the youngest) corresponding to individual phases of activity in the canyon. Variability in the vertical repetition of

https://doi.org/10.3301/GFT.2023.03

Table 1 - Sedimentologic attributes of canyon-filling lithofacies.

Lithofacies Code	Lithology	Description	Depositional element
LF-A	**Clast-supported conglomerates**	Poorly sorted, clast-supported, granule- to cobble-size, medium- to thick-bedded conglomerates in a coarse sandy matrix variably interbedded with a significantly minor proportion of thin lenticular sandstone beds and pebbly mudstones. Clasts are well-rounded and extrabasinal. Internally, beds are mostly massive or with subordinate inverse grading. Bed boundaries are not always obvious due to the high degree of amalgamation, however the prevalent bedding is tabular, lenticular or, to a lesser extent, cross-stratified. Extensive channelling and scouring have produced complex cross-cutting relationships. The palaeocurrent data indicate a broad dispersion about the mean direction at individual localities.	Conglomerate-dominated channel-complex: The poorly sorted but clast-supported texture of the conglomerates, their high degree of channeling, the multiple truncation surfaces, the variability and noticeable dispersion in the prevailing palaeocurrent directions, all point to suggest that this lithofacies relates to a very active, deep-marine braid plain system characterized by a dense network of shifting, multiple-thread, relatively short-lived channels within a submarine channel belt.
LF-B	**Medium- to thick-bedded amalgamated sandstones**	This lithofacies consists of medium- to coarse-grained sandstones, and subsidiary pebbly sandstones, mudstone-clast breccia, and lenses of pebble and cobble conglomerate. Sandstone beds are medium- to thick-bedded and display abundant basal scours and amalgamation surfaces. Mudstone drapes between sandstone beds are rare to absent. Internally, sandstone sedimentation units are typically ungraded or crudely normally graded and structureless, preserving only dewatering structures. Some beds show faint to well-developed parallel lamination near the top. Lateral continuity of beds is highly variable and controlled by the presence of erosional cuts. The bedding architecture between succeeding erosional surfaces displays an overall thinning-upward trend.	Sandstone-dominated channel complex: Based on the complex internal organization, each of these sandstone bodies consists of the remnants of a series of erosive-based, laterally stacked turbidite channel fills (i.e., they are sand-prone channel complexes). This type of sedimentary architecture records multiple episodes of channel incision, bypass, and filling that, in turn, can be interpreted as the product of repeated cycles of increasing than decreasing flow energy.
LF-C	**Medium- to thick-bedded sandstones**	Medium- to thick-bedded, fine- to very fine-grained, massive to subtly graded sandstones. Some thicker beds are accompanied by plane-parallel laminations in the uppermost parts. Individual sandstone beds are tabular and separated by thin packages of very thin-bedded siltstone and mudstone.	Frontal splay: The apparent absence of channelization, the overall tabular nature of the sandstone beds, characterized by absence of intense scouring at the base and preservation of intervening mudstone intervals, and some evidence for flow collapse and mass-dumping of the high-density loads of the flows, suggests that this lithofacies may have been deposited by rapidly expanding flows in a relatively unconfined setting, such as downstream of the mouth of a leveed channel as part of a frontal splay.

https://doi.org/10.3301/GFT.2023.03

Lithofacies Code	Lithology	Description	Depositional element
LF-D	**Medium- to very thin-bedded sandstones and mudstones**	This lithofacies is made up of fining- and thinning-upward packages. At the base, these packages may comprise tabular, medium-bedded, normally graded sandstone beds showing a structureless division at base and planar-parallel lamination on top intercalated with packets of thinly interbedded ripple-laminated sandstones and massive mudstones. In the upper part, the fining- and thinning-upward packages include thin- to very thin-bedded, ripple laminated, fine-grained sandstones alternating with structureless mudstone layers.	(Internal) Levee-overbank: This lithofacies is interpreted to represent levee-overbank deposits that were emplaced by decelerating, moderate- to low-concentration turbidity flows that spilled out of nearby channels. The channel levee interpretation is consistent with sedimentary processes dominated by traction, the occurrence of laterally adjacent channel fills, and the well-defined fining- and thinning-upward character of these sediments. Within levee-overbank settings, the finely-laminated sandstones and siltstones are interpreted to have been created by pulses in the thickness and grain size composition of the overspilling flows that, in turn, may have been generated by the presence of internal waves within the turbidity currents transiting the channels.
LF-E	**Pebbly mudstones and chaotic beds**	Folded and distorted thin-bedded mudstones variably interbedded with a poorly sorted mixture of pebble- to cobble-size exstrabasinal clasts floating in a muddy matrix. Typically the folds are tight to isoclinal and may have upright axial planes.	Mass-transport deposit: Similar chaotic packages are commonly referred to as mass-transport deposits or mass-transport complexes. Based on the abundance of well-rounded extrabasinal clasts, these sediments are interpreted as resulting mostly from mass wasting of the shelf-edge staging area and downslope transport, with minor contribution from local failure of steep canyon walls.
LF-F	**Massive mudstones**	Pale blue-gray, massive or faintly bedded mudstones punctuated by rare intercalations of thin, very fine-grained sandstone beds and rich in benthic and planktonic microfauna (foraminifera and nannofossils).	Slope background hemipelagic deposition

https://doi.org/10.3301/GFT.2023.03

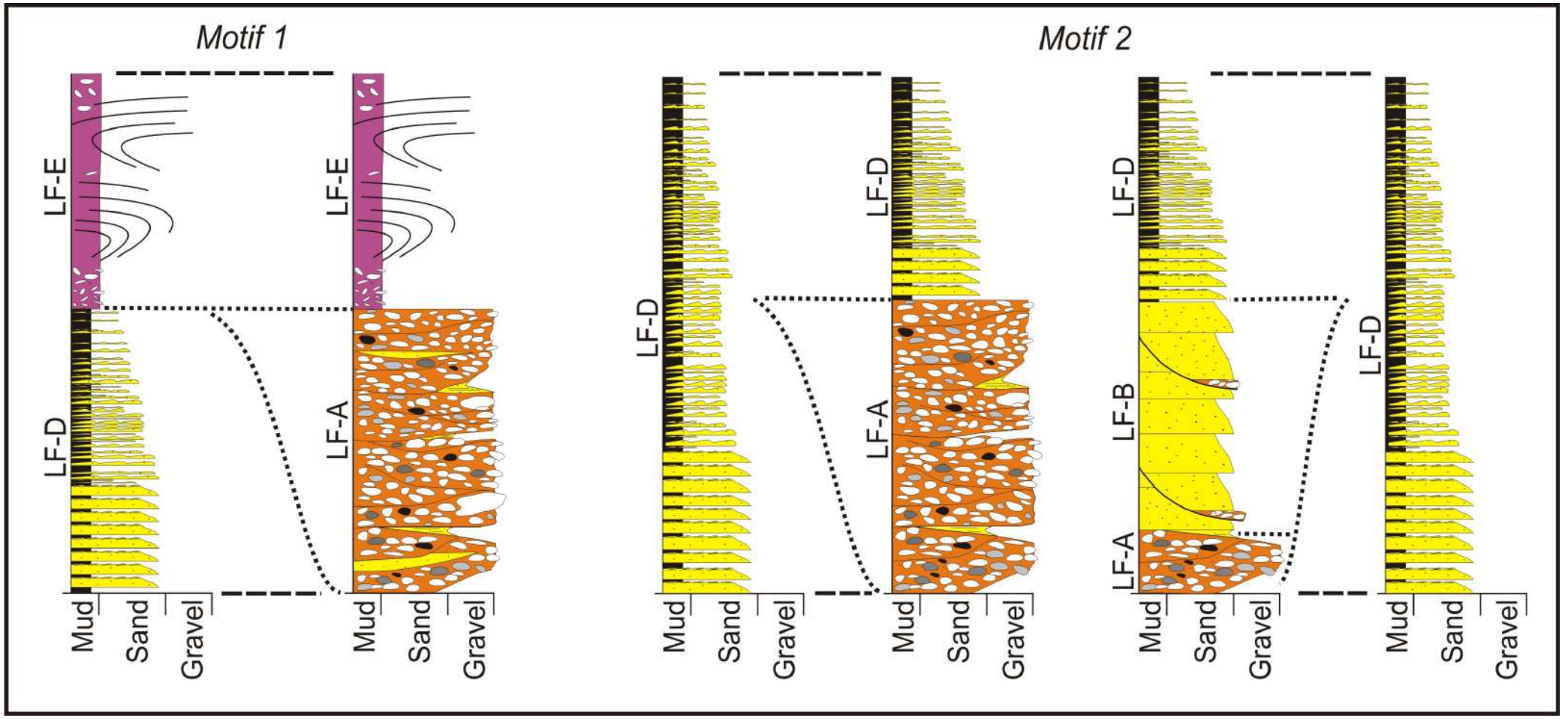

Fig. 14 - Idealised lithologic logs contrasting the main features of *Motif-1* and *Motif-2* cycles (modified after Di Celma et al., 2014). Dashed and dotted lines represent cycle- and lithofacies-bounding surfaces, respectively.

constituent lithofacies allows the identification of two basic styles of cycle architecture (Fig. 14), which can be interpreted in terms of repeated cycles of increasing then decreasing flow energy and differing positions along a conceptual down-canyon depositional profile (Fig. 15).

The *Motif-1* architecture, well represented in the most proximal reaches of the exhumed canyon fill (Fig. 16A), is a twofold-lithosome succession comprising a basal, cliff-forming channel-levee complex, including conglomerate-dominated channel complexes (Fig. 16A) and laterally adjacent levee-overbank heterolithics (Fig. 16D), which is typically overlain by recessive, mud-prone mass-transport deposits (Fig. 16B) characterised by the presence of abundant intra and extraformational clasts and disrupted slump-fold features (Fig. 16C). Generally, mass-

https://doi.org/10.3301/GFT.2023.03

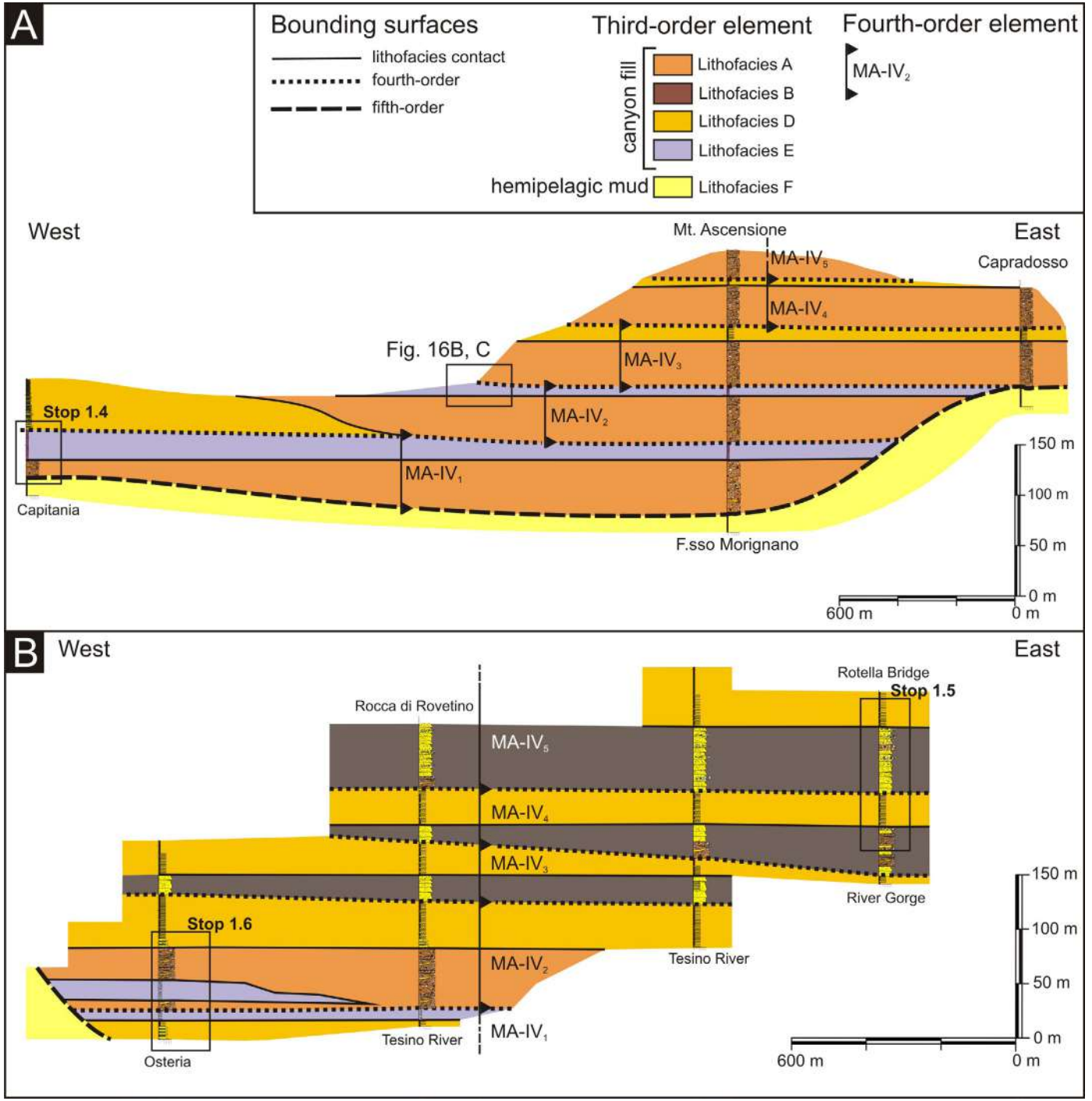

transports deposits are relatively thicker in the proximal part of the system and thin to disappear in a downslope direction. An ideal *Motif-2* cycle includes a conglomerate- or sandstone-dominated channel complex at the base that maybe flanked on either side and is overlain by thinly bedded heterolithic deposits.

Fig. 15 - Simplified, depositional-strike-oriented correlation panels of the Mt. Ascensione succession constructed with summary lithologic logs (modified after Di Celma et al., 2014). The two panels are in successive down depositional dip positions with (A) showing the proximal portion at Mt. Ascensione and (B) the middle portion along the northern side of the Tesino River, about 4.5 km farther down-depositional dip.

https://doi.org/10.3301/GFT.2023.03

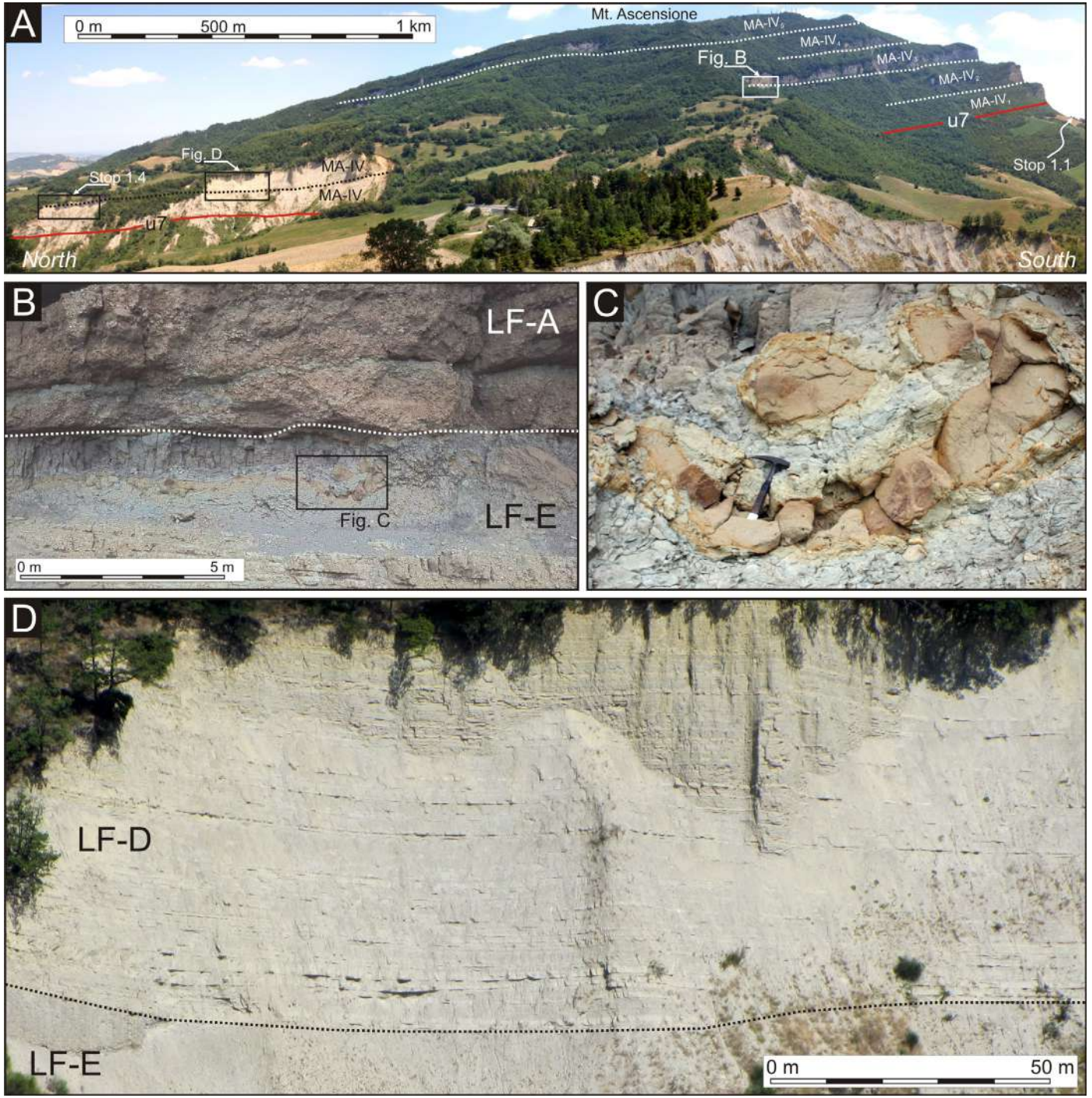

Fig. 16 - Compilation of field photographs showing the main features observed in this stop (modified after Di Celma et al., 2014). (A) Eastward panoramic view of the most proximal exposures of the Mt. Ascensione canyon fill showing the resistant, cliff-forming conglomerate units alternating with recessive-weathering, mud-prone mass-transport deposits. At this proximal site the architecture of the canyon fill can be resolved into five cycles reflecting the intermittent supply of sediment from a significant siliciclastic source. Most of the sand bypassed through this part of the canyon and accumulated farther down the system. The u7 unconformity surface represents parts of the walls and floor of the canyon and can be mapped with relative confidence only in this area, where it cuts deeply into the underlying hemipelagic mudstones. Dotted lines underscore cycle bounding surfaces; (B) Close-up illustrating the sharp contact between pebbly mudstones (LF-E) of cycle MA-IV$_2$ and the overlying channel-fill conglomerates (LF-A) of cycle MA-IV$_3$; (C) Pebbly mudstones (LF-E) are composed of well-rounded extrabasinal pebbles scattered throughout a muddy matrix and disrupted, folded and partially disaggregated sandstone beds. A 30-cm-long hammer is used for scale; (D) Photo showing the sharp contact between pebbly mudstones (LF-E) of cycle MA-IV$_1$ and the overlying thin-bedded turbidite sandstone and mudstone (LF-D) of cycle MA-IV$_2$ and the fining-and thinning-upward character of the LF-D package as a whole.

https://doi.org/10.3301/GFT.2023.03

Stop PRE3-1.4 – Bivio Capitania, Rotella

Coordinates: Lat. 42°56'13"N, Long. 13°32'19"E
Topic: pebbly mudstones

We leave the cars at an old house on the left side of a junction (Bivio Capitania) along the road between Castel di Croce and Rotella and from there we walk to the outcrop. This stop (Fig. 17A) provides a representative exposure of the mass-transport deposits (LF-E) of sequence MA-IV$_1$ and the sharp contact between them and the overlying thin-bedded turbidite sandstone and mudstone (LF-D) of sequence MA-IV$_2$(Fig. 17B). The mass-transport deposits comprise a poorly sorted mixture of extraformational limestone and chert pebbles and intraformational mud clasts in varying quantities, sizes and shapes dispersed in a matrix made of light grey, silty mudstone (pebbly mudstones) and distorted and overturned mudstone layers (Fig. 17C).
These beds are interpreted to have been deposited by cohesive sediment gravity flows within which matrix strength was the dominant sediment supporting mechanism. The disorganised and chaotic arrangement resulted from complex sliding and/or slumping processes that did not lead to complete disaggregation of material during transport. The pebbly mudstones are directly overlain by thin-bedded turbidite sandstones and mudstones intercalated in the lowermost portion by layers of conglomerates and pebbly mudstones. The heterolithic strata are interpreted to record overbank deposits laid down by dilute turbidity currents overspilling onto the levee (more details at Stop 1.6), whilst the intercalated conglomerates and pebbly mudstones were probably deposited by anomalously large flows that were able to transport gravel from a poorly confined adjacent channel onto a proximal overbank setting (compare McArthur et al., 2020).

https://doi.org/10.3301/GFT.2023.03

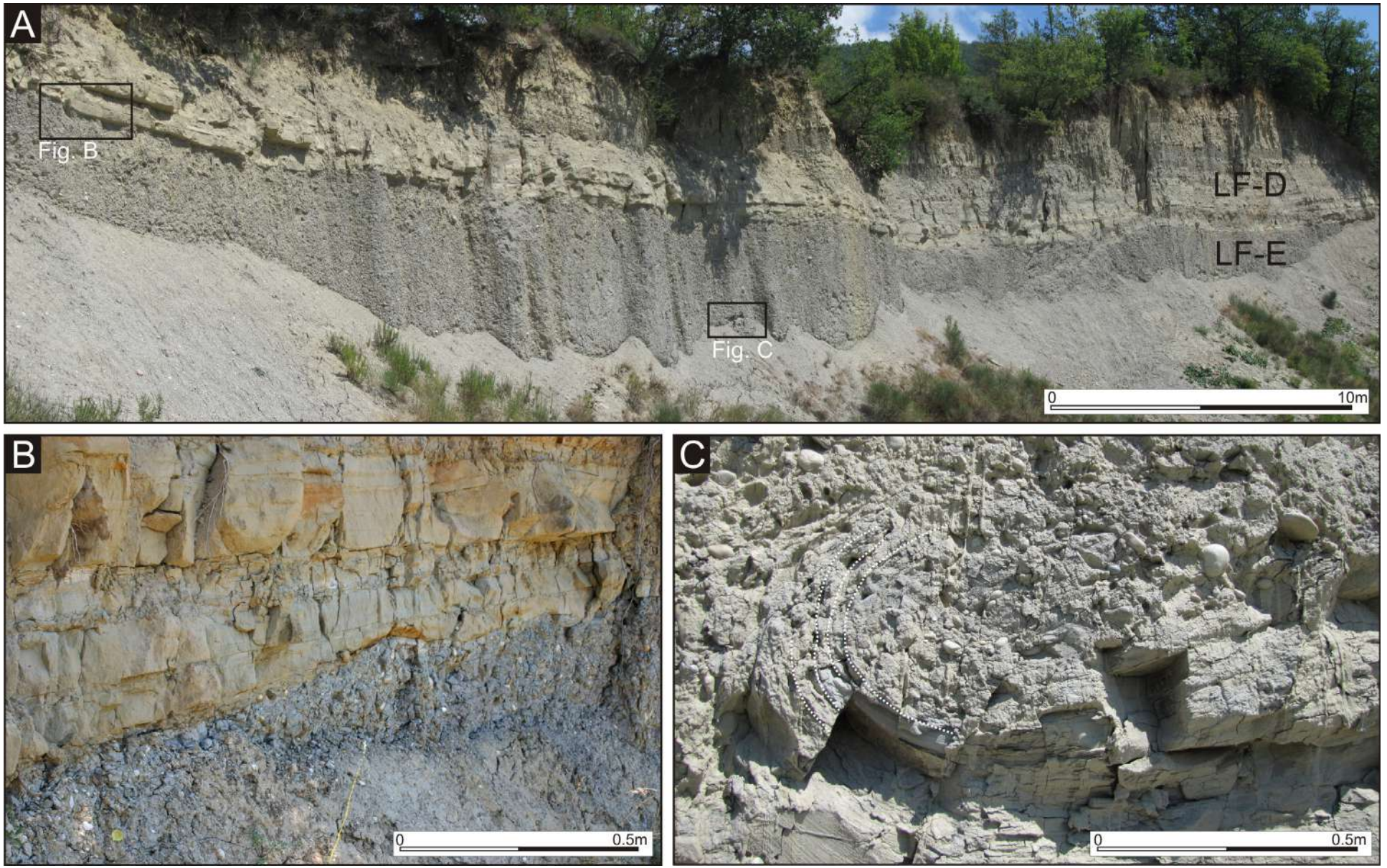

Fig. 17 - (A) The mass-transport deposits (LF-E) are composed of a mixture of mud, mudstone clasts of variable size, extrabasinal pebbles, and contorted turbidite beds. Their disorganised character is suggestive of deposition from a relatively mobile flow recording transitional stages from submarine slumps to cohesive debris flows generated by the failure of the canyon head and/or sidewalls. Boxes show areas in parts (B) and (C); (B) Detail of the contact between lithofacies LF-E and LF-D. Note the lateral change in thickness of the basal sandstone bed that compensate for the uneven top of the underlying mass-transport deposits; (C) Close-up of a recumbent fold in the LF-E lithofacies.

https://doi.org/10.3301/GFT.2023.03

Stop PRE3-1.5 – Rotella

Coordinates: Lat. 42°57'16"N, Long. 13°33'23"E
***Topic*: sedimentary facies and architecture of deepwater channel complexes**

This stop provides a rare opportunity for a close visual inspection of sedimentary facies and internal architecture of one of the Mt. Ascensione gravel- and sand-prone channel complexes and is composed of three distinct, vertically superposed exposures (namely, Stops 1.5a, 1.5b, and 1.5c).

STOP PRE3-1.5A - Access to this outcrop is only possible on foot from the gentle trail immediately adjacent to the Rotella cemetery, which means that visitors leave the vehicle in the cemetery parking area and scramble down to the outcrop from there. The outcrop is a vertical wall located at the end of the trail, on the right-hand side. It forms the lowermost portion of the Rotella section and consists mostly of extensively scoured and amalgamated pebbly sandstones, mud-clast breccias and, to a lesser degree, thin mudstone drapes (Fig. 18A). Sandstone beds range from medium-grained to pebbly; internally they are typically massive or slightly graded with dispersed mudstone-flake clasts, but in places show faint to well-developed parallel lamination. Lateral continuity of sandstone beds is highly variable and controlled by the presence of numerous scours that are typically associated with lenses of poorly sorted gravel lags and mud-clast breccias, which consist of subangular mud rip-up clasts of variable size surrounded by a coarse- to very coarse-grained sandstone matrix with scattered granules and pebbles (Fig. 18B, C). Rip up mud clasts and extraformational clasts typically of granule- to small pebble-grade are common components of these beds. Most mudstone clasts are oriented randomly in general, but upcurrent-dipping long axis imbrication may be observed locally (Fig. 18D). The occurrence of organised clast fabric may be a result of active clast interactions or pervasive shear straining of the debris flow materials, which can align or imbricate the constituent clasts. The mud clasts can be seen to have been derived from laterally discontinuous, laminated mudstone drapes and entrained through basal plucking by powerful sand-bearing turbulent flows. Armoured mud balls are also present; they were most likely formed by erosion of rip-up mud clasts and subsequent rolling over sand and pebble pavement along the sub-marine channel floor. Internal scour features suggest rapid suspension deposition by sandy high-density turbidity currents in a channel-axis setting. *Ophiomorpha* burrows and other trace fossils are common (Fig. 18E).
Sand-rich flows are interpreted to have deposited sandstone beds in these channel fills. Scour by some of these sediment gravity flows, however, was more extensive and incorporated many silty clasts into the flow during the early erosional stage. These clasts were probably transported in the lower, high-density part of the flows, and were deposited soon thereafter, forming the observed breccia layers.

https://doi.org/10.3301/GFT.2023.03

STOP PRE3-1.5B(optional) - This river-cut outcrop section is about 50 m away from Stop 1.5a and it is accessible through a very short trail in the trees. It can be visited only during the driest months of the year, when water level is considerably reduced; however, independently on water level, rubber or water-proof trekking boots are always necessary. The walls of the gorge are nearly vertical and rise for about 25 m above the Tesino River. Most of the strata exposed along the walls dip shallowly to the northeast. The gorge sidewalls provide near continuous exposures of clast-supported conglomerates that are interbedded with subordinate sandstones (Fig. 19A).

The conglomerate packages consist primarily of medium- to thick bedded conglomerates composed of well-rounded, granule- to cobble-grade clasts. Clast composition reflects a heterogeneous mixture of rock types derived from unroofing of the adjacent Apennines, including Mesozoic

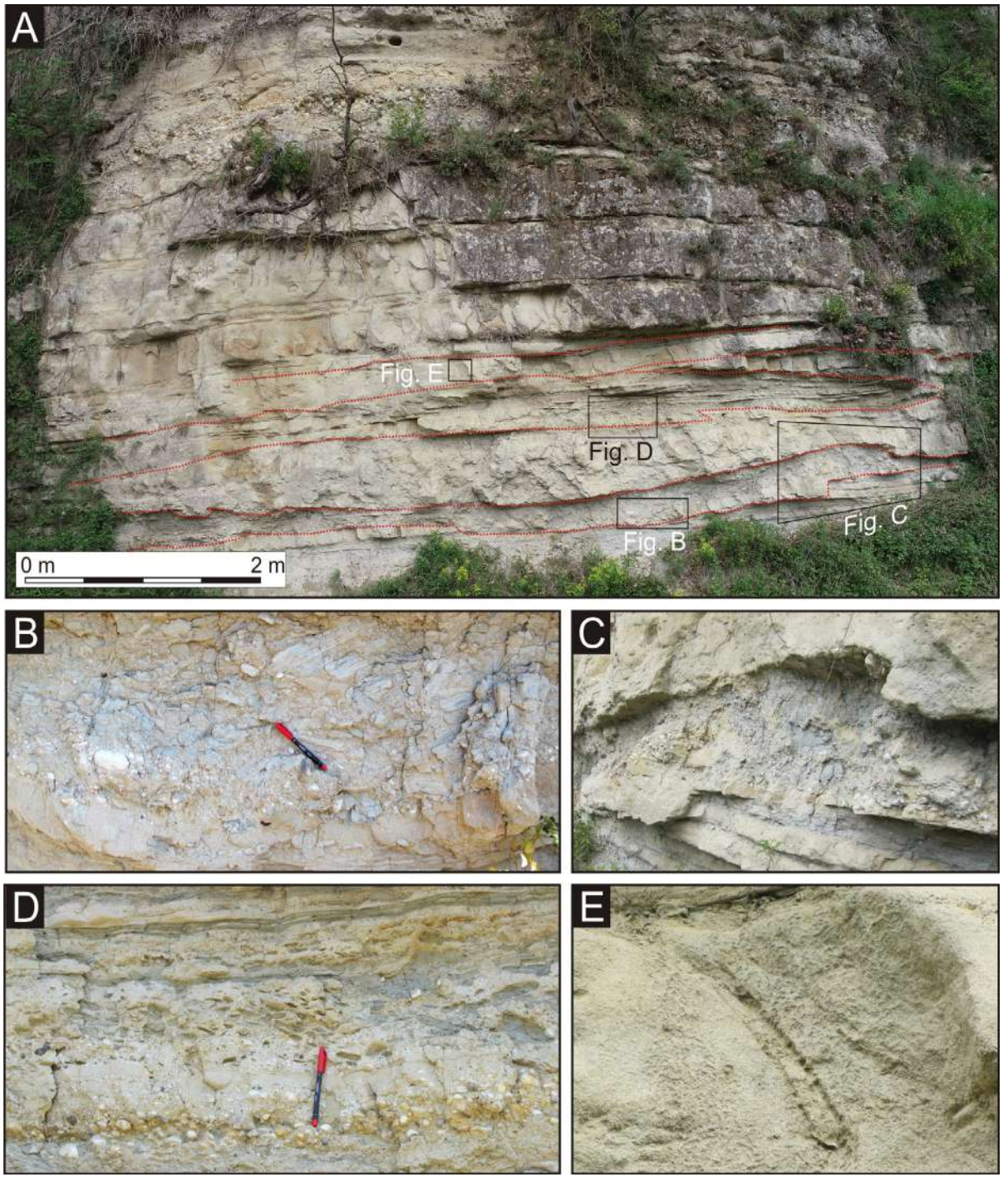

Fig. 18 - (A) Oblique UAV-based photograph of extensively scoured and amalgamated pebbly sandstone beds. Cut-and-fill erosive features (red dotted lines) are frequent at the base of sandstone beds but with erosional relief not exceeding a few tens of centimetres; (B) Mudstone-clast-rich breccia, showing the angular and disorganised gravel-size mudstone clasts jumbled in a matrix of very coarse sandstone. These sediments, which are found in irregular scoured depressions, have been derived from a former mudstone drape that has been broken and disrupted and can be interpreted as having been formed by bedload deposition from bypassing, high-concentration flows; (C) Detail of a scour surface infilled by a lenticular mud-clast conglomerate lag; (D) Mudstone-clast-rich sandstone with imbricated mud-clasts displaying a common dip towards the south (right of the photograph) consistent with emplacement by a flow travelling towards the north and suggesting that mud-clasts were fully entrained into a relatively dilute fluid–sand mix; (E) Detail showing an *Ophiomorpha* burrow with typical ornamented lining.

https://doi.org/10.3301/GFT.2023.03

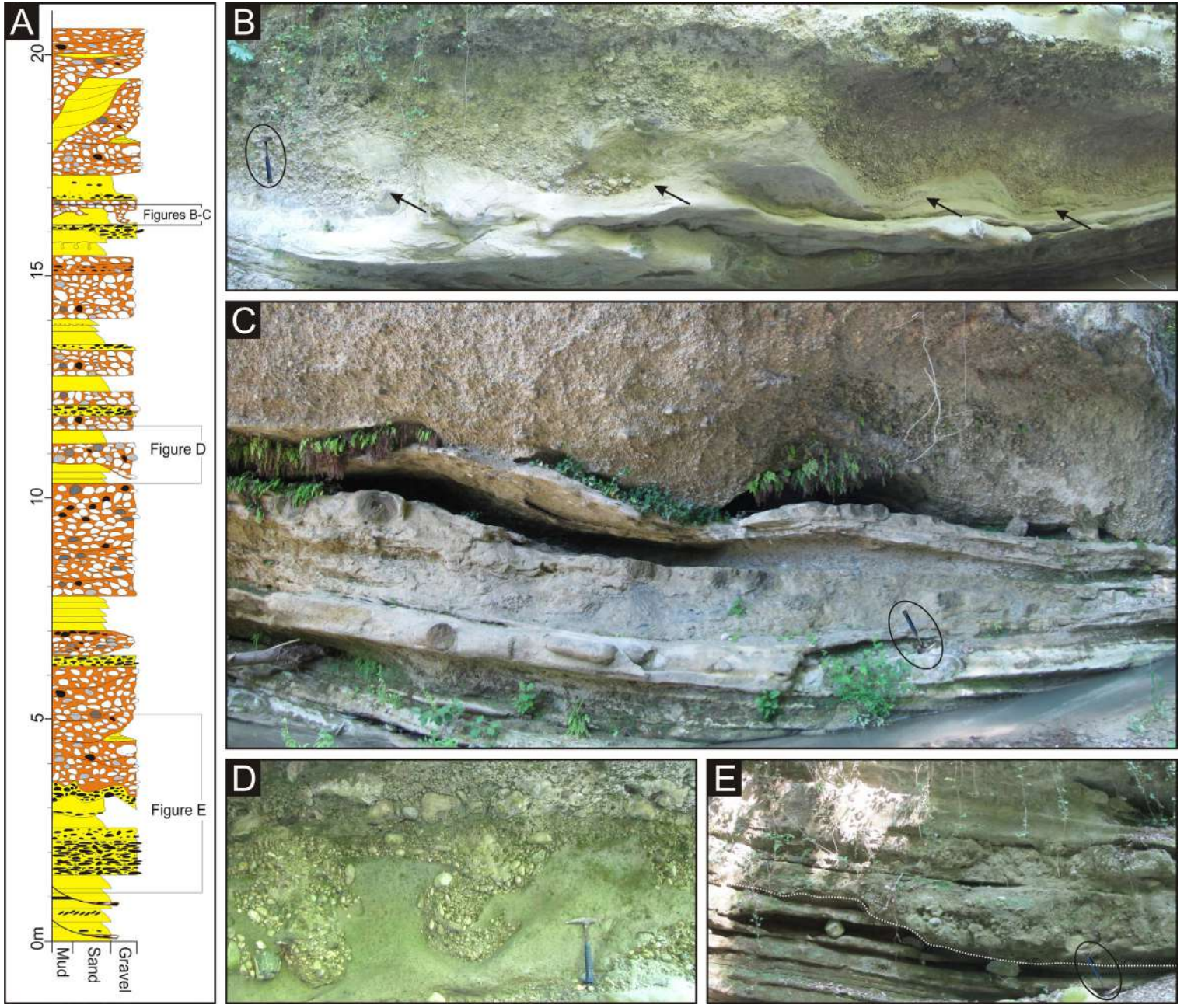

Fig. 19 - (A) Generalised stratigraphic section measured along the vertical walls of the Rotella gorge. Characteristic lithologies of the section include amalgamated, clast-supported conglomerates and thin- to thick-bedded sandstones, with sand-matrix mud-clast conglomerates representing a minor component; (B) Downwardly-directed, flame-like structures (pointed out by arrows) that are developed by overlying conglomerates injected into underlying sandstones. These interfacial markings show a curved hook-like tip, are spaced out at fairly regular intervals, and consistently verge towards the south (i.e., opposite to the general direction of flow). We suggest the sandstone that conglomerate was deposited onto was in an unconsolidated, water-saturated state, prone to deformation during loading; (C) Panoramic view of the wavy underside of a conglomerate bed characterised by the occurrence of elongated load structures. Wavy folding in the immediately underlying sandy matrix mud-clast breccia and sandstone layers fades towards below, pointing to a penecontemporaneous loading and foundering of gravels into the underlying substrate; (D) Close-up view of unusually large load structures occurring directly beneath the conglomerate at this section, consisting of coarse conglomerate material forming hook-like cusps intruding the underlying massive sandstones; (E) Detail of a small conglomerate-filled channel. The dotted white line highlights the concave-up erosional surface cutting into the underlying sandstone beds. Hammer for scale.

https://doi.org/10.3301/GFT.2023.03

and Cenozoic limestones and Messinian sandstones. The high degree of rounding of these resistant clasts implies a complex history of earlier transport. Basal contacts of conglomerate beds are typically sharp and planar but loaded basal contacts may also occur (Fig. 19B, C, D). In most of the cases conglomerate beds display little internal organisation. Pebbly mudstone intervals, usually up to 1 m thick and a few ten metres in lateral extent, occur sporadically as discontinuous lenses and, overall, are a relatively minor component of these deposits. Stratification displays a complex architecture with abundant erosional features ranging from simple shallow scours to more complex and laterally cross-cutting surfaces that define concave-upward channel-forms accounting for much of the lenticularity of individual conglomerate and sandstone layers (Fig. 19E).
Intervening sandstone bodies consist almost entirely of medium- to coarse-grained sandstones and pebbly sandstones with subsidiary discontinuous mudstone-clast breccias in coarse-grained sand matrix, lenses of pebbles and centimetre-scale mudstone layers. Internally, sandstone beds are typically ungraded or crudely normally graded and structureless. The lateral continuity of individual sandstone beds is highly variable because of erosion.
Based on the complex internal organisation, the conglomerate and sandstone packages exposed along the walls of the gorge are interpreted to represent the erosional remnants of a series of cross-cutting, vertically and laterally juxtaposed sand- and gravel-prone channel fills (channel complex) deposited by high- and low-concentration turbidity currents. In this context, the gravel lags and the mud-clast breccias that line erosional surfaces at the base of channel fills are interpreted to record material left behind in the deepest parts of channels by transiting flows in the early stages of channel development and are suggestive of flow bypass and/or erosion.

STOP PRE3-1.5C - This is a road-cut located a short walk (130 m) from the parking area, just after crossing the bridge to the north of the municipal cemetery (be careful crossing the road to examine the road cut because visibility is restricted on this corner). The sedimentary rocks exposed at this road cut form the upper portion of the Rotella section and comprise two superimposed sandstone- and conglomerate-filled turbidite channels separated by a prominent erosion surface (Fig. 20A). The sediment fill of the lower channel includes a thin pebbly mudstone layer draping the basal surface overlain by non-amalgamated to amalgamated, medium- to thick-bedded, fine- to coarse-grained sandstones commonly separated by thin mudstone partings.
The sandstone beds exhibit minor erosion at their base (Fig. 20B). Internally, sandstone beds are typically ungraded and structureless, with faint to well-developed planar laminations near the tops of same beds. The thick sandstone beds are interpreted as the result of rapid suspension deposition by collapsing, high-concentration turbidity currents and some of them preserve soft-sediment deformation structures, such as large injection structures involving upward movement of sediment. (Fig. 20C). The upper channel is bounded at the base by a steep channel-form erosional surface (Fig. 20D) and comprises lenses of pebble to cobble conglomerates, mudstone-clast breccias, pebbly sandstones, and medium- to thick-bedded sandstones (Fig. 20E). The lenticular and pebble to cobble conglomerates are bypass lags built out of clasts left behind by through-going, largely bypassing high density turbidity currents that transported sand-sized sediment farther downslope. The overlaying thick-bedded sandstones were deposited during the backfill of the channel.

https://doi.org/10.3301/GFT.2023.03

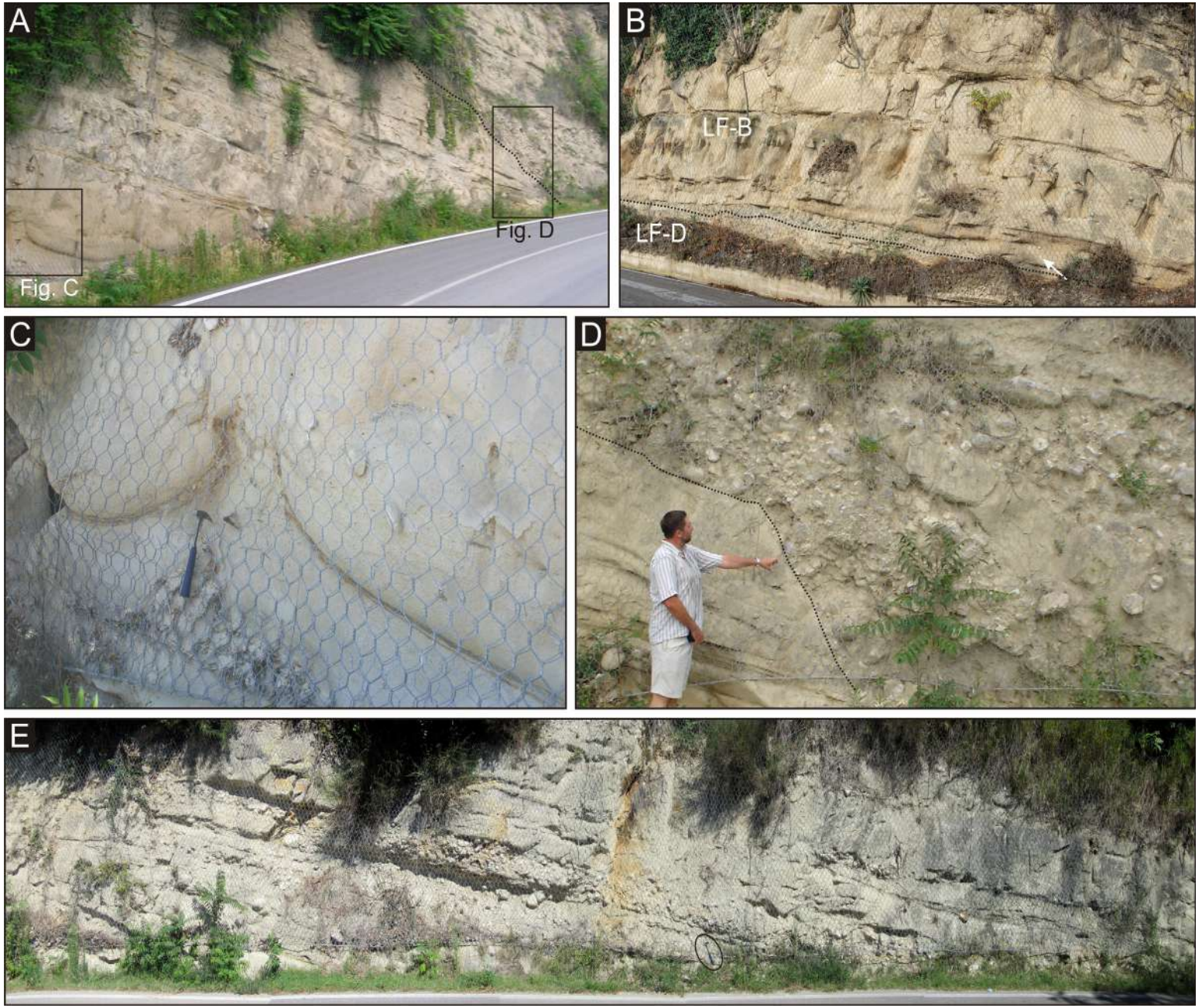

Fig. 20 - Compilation of field photographs showing the main features observed in this stop (modified after Di Celma et al., 2014). (A) Oblique view of the main outcrop showing the sedimentary fill of the two turbidite channels separated by the channel-form erosional surface; (B) Detail of the channel-form surface, demarcated by a dotted line, separating the sand-prone infill of the lower turbidite channel (LF-B) from the underlying heterolithics (LF-D). The lowest sandstone bed in LF-B (arrowed) clearly tapers and pinches out to the left in less than 3 m; (C) Close-up showing a large vertical conduit of liquified sands recording rapid loading during early burial by the overlying sandy turbidites and the upward escape of water-saturated sand with high-pore water pressure. The injection structure shows an internal homogenised texture and its top is not well defined, ending indistinctly in another sand-rich bed. Note as the sand protrusion sharply pierces through a thin mud parting, possibly acting as a permeability barrier, which has been broken, curved back, and overturned. Hammer for scale. See A for location; (D) Close-up showing the concave-upward erosional surface (dotted line) at the base of the upper channel that truncates into older sandstone beds and is directly overlain by a conglomerate lag. See (A) for location; (E) Detail of the lower portion of a channel fill comprised of a mud-clast breccia at the base and an overlying clast-supported conglomerate lag. Hammer (encircled) for scale.

https://doi.org/10.3301/GFT.2023.03

Stop PRE3-1.6 (optional) – Osteria, Rotella

Coordinates: Lat. 42°57'24"N, Long. 13°32'08"E

***Topic*: levee-overbank deposits**

Outcrops at Osteria (Fig. 21A) expose more than 20 m of interbedded mudstone and sandstone layers (LF-D) that exhibit an overall upward-thinning and -fining trend. The lower part consists mostly of laterally persistent, medium- to thick-bedded, medium- to fine-grained lower-division (T_{ab}) turbidites intercalated with thin, fine-grained, upper-division (T_{cde}) turbidites (Fig. 21B-C). Locally, large amounts of land-

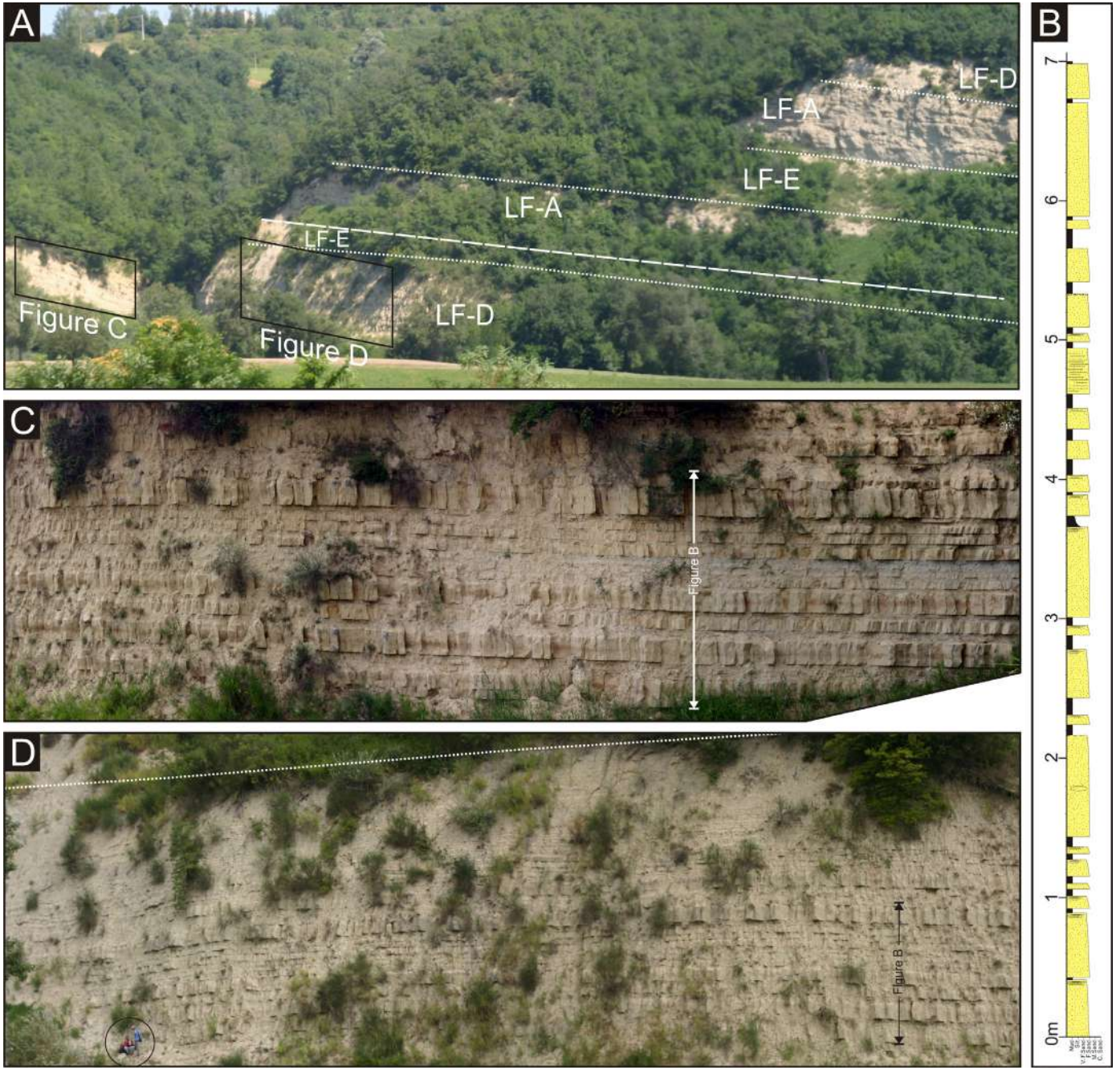

Fig. 21 - (A) Panoramic view of the sedimentary succession exposed at this stop. Dashed and dotted lines represent cycle- and lithofacies-bounding surfaces, respectively; (B) Stratigraphic section measured along the lower portion of the LF-D lithofacies. Position indicated by the vertical line in (C); (C) Outcrop photograph of the basal sandstone-rich portion of the LF-D lithofacies. See (A) for location. Centimetre- to decimetre-thick recessive packages are thin siltstone and mudstone partings; (D) Large exposure showing the overall thinning and fining-upwards trend of medium- to very thin-bedded sandstones and mudstones. See (A) for location. Sandstone beds are generally tabular and may be traced along the entire length of the exposure without appreciable irregularities or change in thickness (the vertical line indicates the position of the 7-m-long measured section in (B). Geologists (encircled) for scale.

https://doi.org/10.3301/GFT.2023.03

derived plant debris as well as coal fragments are preserved in thinly laminated divisions. Sandstone beds decrease progressively in both abundance and thickness upward, grading into an upper portion characterised by thinly interbedded, fine-grained, upper-division turbidites (T_{cde}) intercalated with uncommon medium-bedded, medium-grained, lower-division (T_{ab}) turbidites (Fig. 21D).

The section records deposition from low-density currents transporting predominantly fine-grained sediment. Based on the overall thinning- and fining-upward character of this heterolithic succession and lateral continuity of component beds, it is likely that it represents levee deposits laid down adjacent to a genetically related conglomerate-filled channel (LF-A) like that represented by the coarse-grained, sandy conglomerate exposed at Rotella (Stop 1.5). In this frame, it is suggested that the sandier lowermost portion of LF-D records deposition at a time when little relief existed between the levee crest and the base of the channel, enabling the lower, more concentrated parts of throughgoing channel flows to overspill. By contrast, the upper portion is interpreted to have been deposited as levee relief increased and only the upper, mud-rich, dilute part of the flows moving within the channels overspilled, while the coarse-grained, denser lower part remained largely confined to the channel.

https://doi.org/10.3301/GFT.2023.03

DAY 2 (MORNING)

The Castignano canyon, a generalised cross-section of which is shown in Figure 22, consists of a south to north elongated sedimentary body that is about 2–3 km wide and has a maximum total thickness of 270 m (Di Celma et al., 2013). The overall stratigraphy of this canyon fill comprises a heterogeneous succession of conglomerates, sandstones, thinly bedded sandstone and mudstone, and pebbly mudstones, which are organised into a composite upward fining trend recording at least three main episodes of incision and backfill (indicated as CST-V in Fig. 22). Palaeoflow indicators from this system all record a dominant sediment transport towards the north, roughly similar to that recorded in the Mt. Ascensione canyon. Only the most southerly exposures do not follow this trend and are instead dominated by northeasterly directed palaeoflows.

The rich foraminiferal assemblages from the thick mudstone succession underlying the turbiditic system (PS1.1) contain *Bulimina basispinosa* and *Globorotalia crassaformis* in the lower portion and the benthic foraminifer *Bulimina marginata* (FO 2.63 Ma) in the stratigraphically highest part. These sediments pre-date the canyon system, which is cut into them, and can be assigned to the planktonic foraminifera MPl5b Zone. The benthic foraminiferal fauna indicates an epibathyal (400 to 500 m palaeodepth) marine environment. Likewise, specimens of *B. basispinosa* and *B. marginata* co-occur in the low-diversity foraminiferal assemblages characteristic of the lowermost samples recovered in the turbidite system from levee and mass-transport deposits of CST-IV$_1$ and CST-IV$_2$ (PS1.2). The age diagnostic foraminifera *Globorotalia inflata* (FO 2.09 Ma) were not found in any of these samples, so these assemblages can be ascribed to the planktonic foraminifera MPl5b Zone. Samples collected from the pebbly mudstones at the top of CST-IV$_3$ yielded an abundant foraminiferal assemblage characterised by the occurrence of *B. marginata* and *Globorotalia inflata* and the absence of *Globorotalia truncatulinoides* (the first appearance of which is calibrated at 2.00 Ma). These findings suggest that the section corresponds to the planktonic foraminiferal MPL6a Zone.

Stop PRE3-2.1 – Colle della Morte, Castignano

Coordinates: Lat. 42°56’08”N, Long. 13°37’32”E)
***Topic*: Western margin of the Castignano canyon and sedimentary architecture of its channelised fill.**

This stop provides an excellent overlook to see the western margin of this canyon (u7.2), which is deeply excavated into the underlying slope mudstones (Fig. 23A). At this site the u7.2 unconformity is a sharp, eastward dipping erosion surface juxtaposing the sand-prone canyon fill against background slope mudstones (Fig. 23B). The canyon fill is composed of several channel-fill sandy turbidite deposits bounded by cross-cutting erosional surfaces resulting from multiple cut-and-fill cycles (Fig. 23C, D, E). The deepest parts of individual surfaces are often characterised by lenses of clast-supported, extrabasinal conglomerates directly overlain by structureless and plane-laminated sandstones. Towards the margins of the channels, sandstone beds either thin and onlap onto the bounding surfaces or thin rapidly laterally into thin-

https://doi.org/10.3301/GFT.2023.03

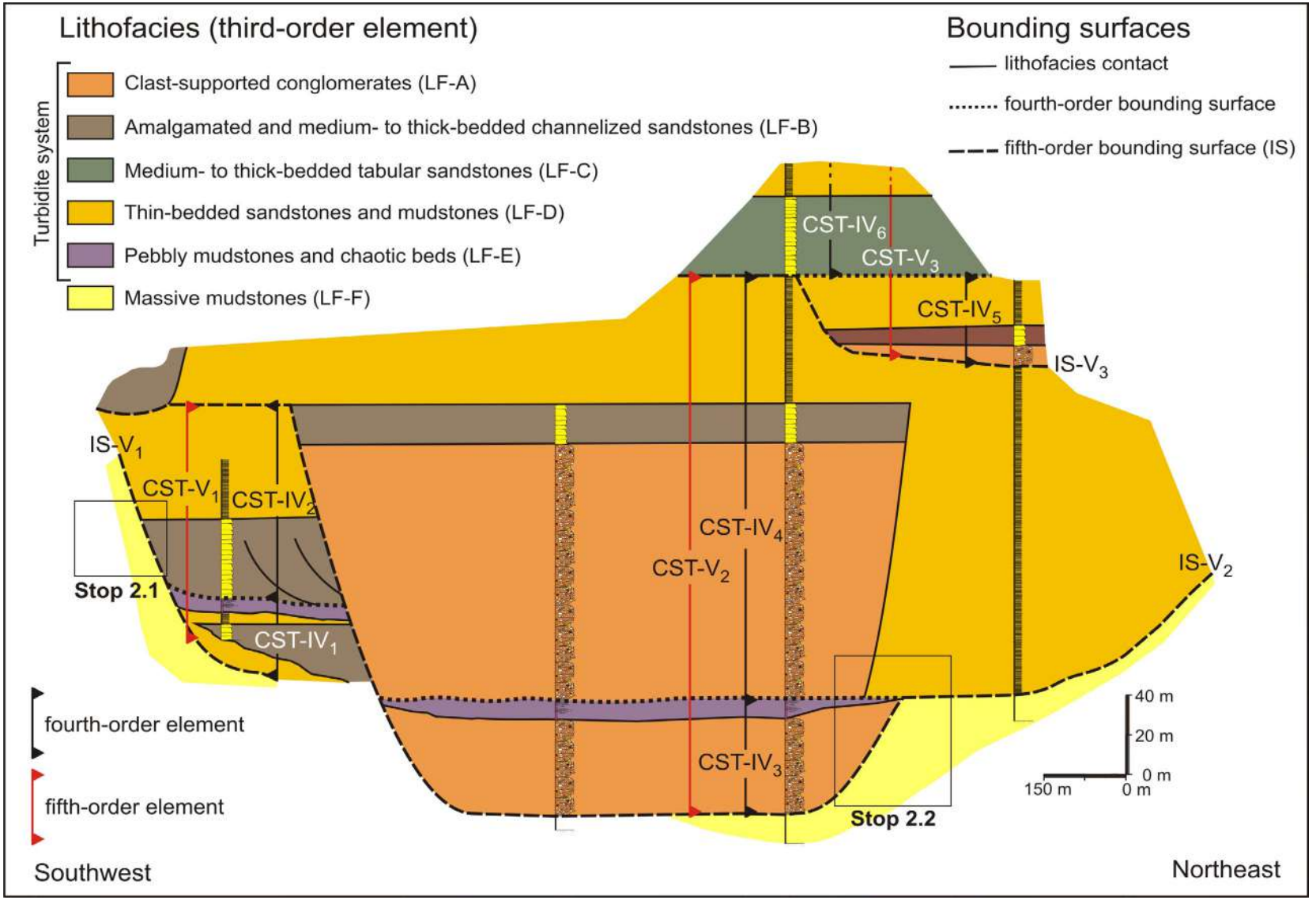

Fig. 22 - Schematic, depositional-strike-oriented correlation panel (palaeoflow is into the page) of the Castignano system illustrating the stratal hierarchy adopted to aid in organizing and classifying the observed stratigraphic architecture (modified after Di Celma et al., 2013). The turbidite deposits exposed at Castignano can be described in terms of five hierarchical levels of architectural elements. Individual lithofacies are the fundamental (third order) elements in the system. Regularly recurring groups of lithofacies represent erosionally-bounded, fining-upward fourth-order architectural elements. Fourth-order elements stack to form fifth-order elements, which lie on large-scale incisional surfaces (IS) cutting into adjacent deposits. Three stacked fifth-order elements make up the Castignano system and are designated as CST-V1 to CST-V3 in ascending stratigraphic order.

https://doi.org/10.3301/GFT.2023.03

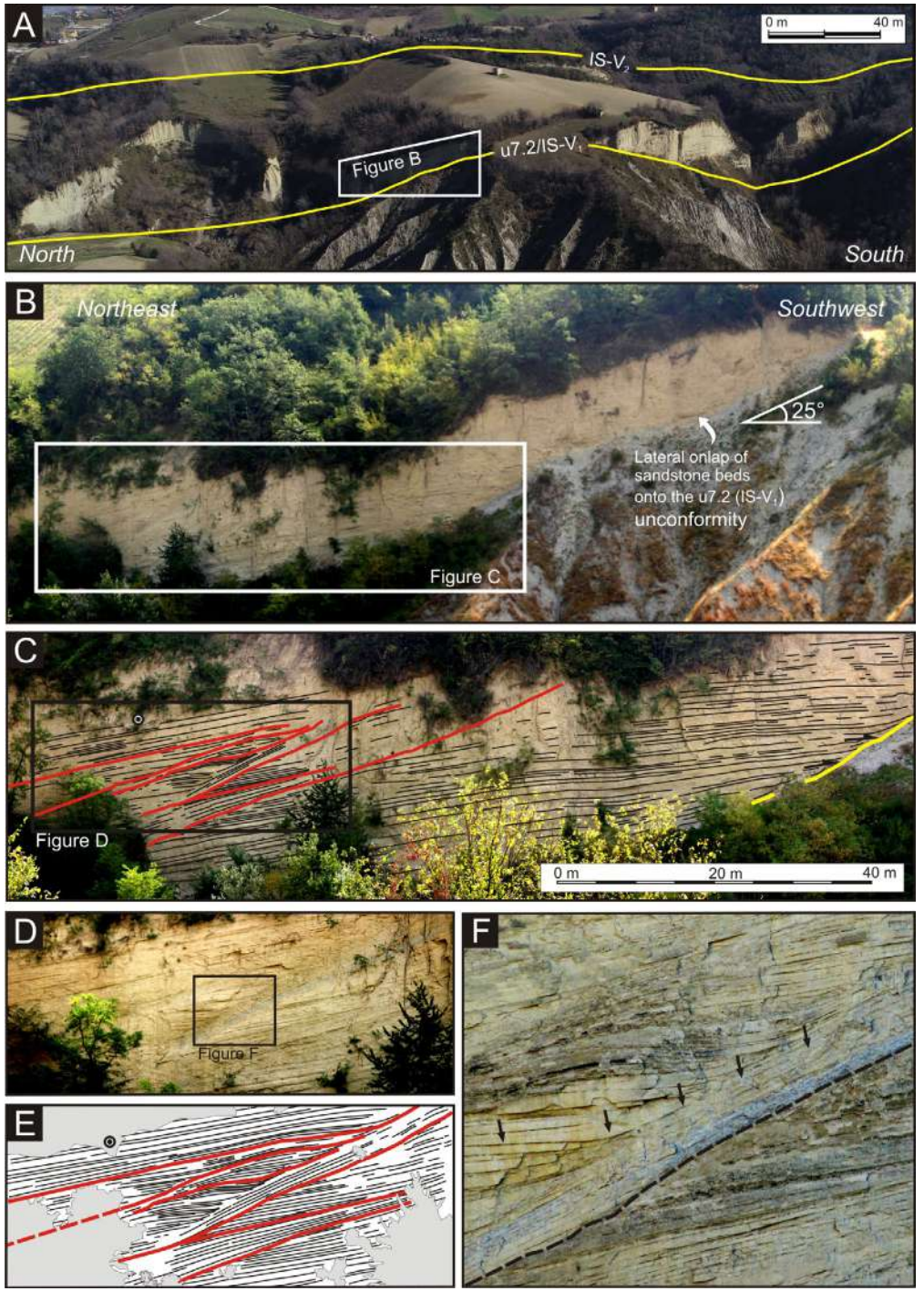

bedded sandstones and mudstones forming inclined bedsets draping the basal surface of erosion (Fig. 23F).

Stop PRE3-2.2 – San Bernardino, Castignano

Coordinates: (Lat. 42°55'15"N, Long. 13°39'04"E)

***Topic*: Eastern margin of the Castignano canyon and architecture of its fill**

We take a short walk to view the the eastern sidewall of the Castignano canyon from the south. In this locality, the canyon fill rests on an erosional surface (u7.2) deeply incised into the surrounding hemipelagic mudstones (Fig. 24A) and consists of two channel-filling conglomerate packages (LF-A) vertically separated by a mud-rich mass-transport unit (LF-E). The lowermost conglomerate channel-fill thins and lens out directly against the hemipelagic slope mudstones to the east (LF-F), whereas the upper conglomerate channel-fill (Fig. 24B) grades laterally (toward the east) into pebbly, thin- and thick-bedded sandstones (Fig. 24C) interpreted as the associated channel margin succession that, in turn, is flanked by a fine-grained, heterolithic succession interpreted as overbank (levee) deposits (LF-D).

Fig. 23 - (A) Oblique UAV-based view onto the western margin of the Castignano canyon; (B) The western margin of the turbidite system is a sharp, inclined erosion surface (u7.2/IS-V_1) juxtaposing the fill against background slope mudstones; (C) Line-drawing interpretation of the boxed area in (B), highlighting the complex cut-and-fill stratal architecture resulting from the stacking of channel-margin remnants during repeated erosion–deposition cycles (red lines indicate channel-bounding surfaces); (D) Uninterpreted, enlarged view and (E) interpretative sketch of the boxed area in panel (C); (F) Channel-filling sandstone beds (black arrows) become increasingly thin-bedded and fine-grained laterally towards the channel margin and continue some way up the channel wall as inclined, thinly bedded strata. This relation indicates that the highest energy and most competent parts of the flows were confined to the deepest parts of the active channels and that only the more dilute, higher parts of the flows lapped onto the channel margin.

https://doi.org/10.3301/GFT.2023.03

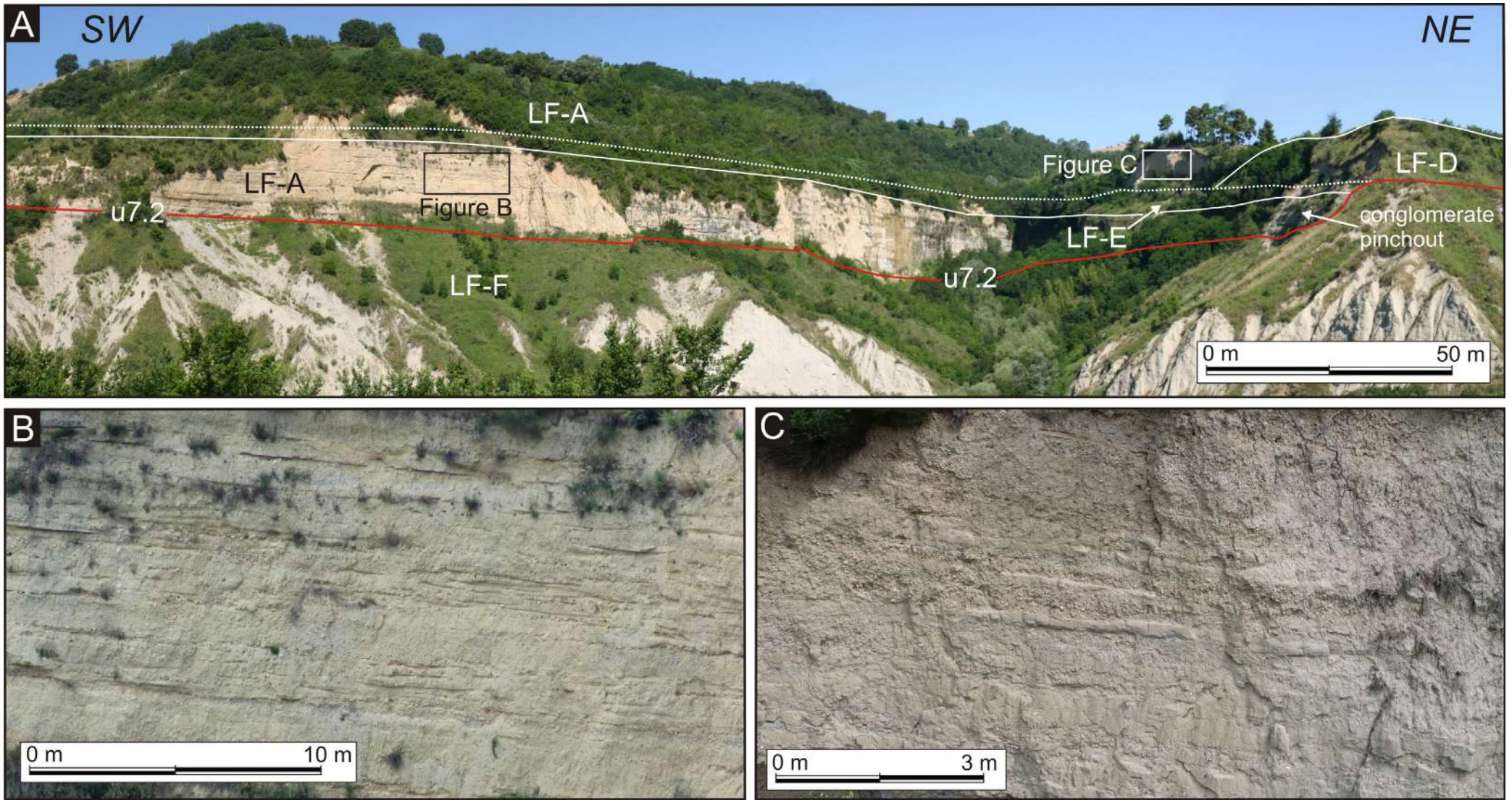

Fig. 24 - (A) South-east facing outcrop showing CST-V_2 at San Bernardino. In this area, conglomerate channel-fill strata at the base of CST-IV_3 and overlying mass-transport deposits are clearly seen to thin and lens out to the east, onlapping against the slope mudstones that mark the edge of the entrenched valley. Palaeoflow is into the hill, to the right; (B) Blow-up of the boxed area shown in (A) of the LF-A lithofacies in axial position; (C) Blow-up of the boxed area shown in (A) of the LF-A lithofacies in marginal position.

https://doi.org/10.3301/GFT.2023.03

DAY 2 (AFTERNOON)

The Offida canyon, a generalised cross-section of which is shown in Figure 25, is about 3 km wide and at least 110 m thick (Di Celma, 2011). The history of the Offida canyon comprises a major erosion event, responsible for the development of the lowermost incision surface (u7.3), followed by its sedimentary fill. A detailed facies analysis suggests that a variety of gravity-driven subaqueous flows were involved in sediment transport and deposition within the submarine canyon, including slumps, cohesive debris flows, and high- and low-density turbidity currents. Field mapping along the Offida outcrop belt reveals that the canyon fill strata display a marked cyclic character and the component lithofacies succeed one another in a well-ordered and predictable fashion to form a repetitive succession of unconformity-bounded fining-upward units (herein named O-IV$_1$ to O-IV$_5$ in ascending stratigraphic order), which range between a few and a few tens of metres in thickness. The average palaeocurrent direction from imbricate pebbles, channel-margin orientations, and current ripples is towards the northeast, approximately perpendicular to those recorded in the older Mt. Ascensione and Castignano systems.

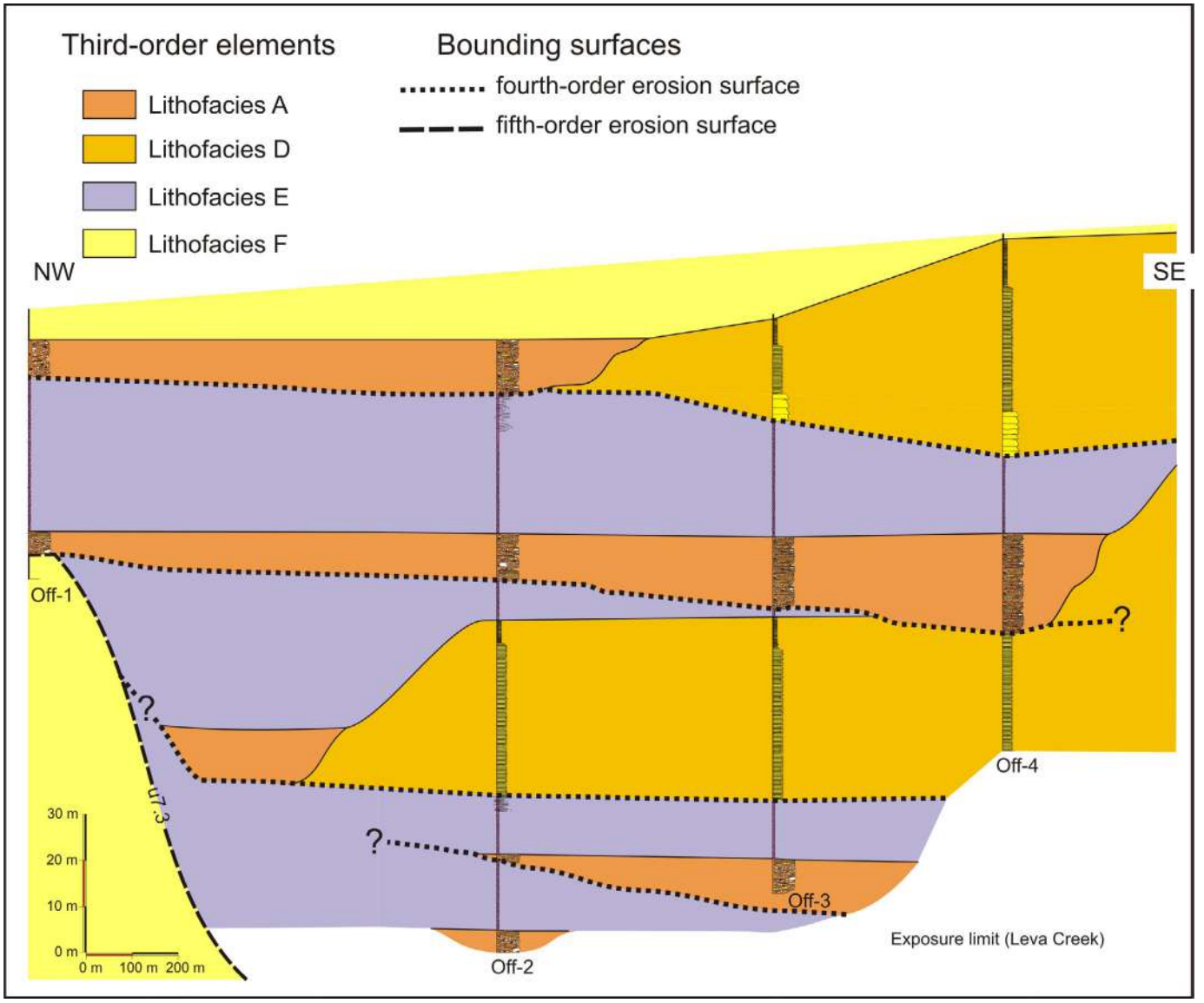

Fig. 25 - Depositional-strike correlation panel (modified from Di Celma, 2011) illustrating lithofacies distribution and stratal surfaces of the Offida Canyon between Fosso Caldarella and Fosso Borgo Cappuccini (vertical exaggeration ×10). This panel has been compiled integrating four measured sedimentary logs, field-based mapping, and photomosaic tracing.

https://doi.org/10.3301/GFT.2023.03

Biostratigraphic analyses carried out on foraminifer and calcareous nannofossil assemblages of the hemipelagic mudstones directly below and laterally adjacent to the canyon fill indicate that they are characterised by the occurrence of *Globorotalia crassaformis* and *Bulimina basispinosa* in the lower part and of *Globorotalia inflata* in the upper part (Lori, 2005), pointing to deposition during the foraminiferal MPl5b and MPl6a zones. The same section is characterised by the occurrence of *Discoaster pentaradiatus* in the lower portion and *Discoaster brouweri* and *Discoaster triradiatus* in the upper portion, pointing to deposition during the nannoplankton CNPL5 and CNPL6 zones.
Biostratigraphic analyses of samples collected in the canyon fill led to the recognition of the occurrence of *G. inflata*, *D. brouweri* and *D. triradiatus*, pointing to deposition during the lower part of the foraminiferal MPL6 and the upper part of the nannoplankton CNPL6 zones. These data allow to constrain the age of the u7.3 unconformity at the base of the canyon fill between 2.09 and 1.93 Ma. The biostratigraphic record of the normally magnetised mudstones directly overlying the canyon fill is characterised by the presence of *Globorotalia inflata*, *Calcidiscus macintyrei,* small *Gephyrocapsa* and the absence of specimens belonging to the genus *Discoaster*. This microfossil assemblage enables the identification of the foraminifera MPl6b Zone, the lower part of the nannoplankton CNPL7 Zone, and the Olduvai subchron (C2n), pointing to deposition between 1.93 Ma and 1.778 Ma.

Stop PRE3-2.4 – Ponticelli, Offida

Coordinates: Lat. 42°56’4”N, Long. 13°40’34”E
***Topic*: Strike view of the stratigraphic architecture of the Offida canyon fill**

From this vantage point one gets an excellent strike view of the Offida canyon. The canyon fill has a cyclical, *Motif-1*, appearance (Fig. 26A), with each cycle consisting of: i) a pronounced surface of erosion generated by efficient turbidity currents during a period of erosion and complete bypass of sediment to more basinward settings (Fig. 26B); (ii) a diverse assemblage of genetically related lithofacies including channel-complex conglomerates (FA-A) and laterally adjacent levee sandy heterolithics (FA-D) laid down by turbidity currents largely bypassing the area; and (iii) a mud-prone mass-transport deposit (FA-E) produced by instability and failure of shelf-edge staging areas and/or canyon sidewalls. Channel axis to margin facies changes between clast-supported conglomerates (Fig. 26B) and sandy conglomerates (Fig. 26C) can be observed. Laterally, channel-fill conglomerates either lie on erosional surfaces that cut into adjacent, genetically related levee sandy heterolithics (Fig. 26D) or wedge out into a thick succession of mud-prone mass-transport deposits (Fig. 26E).

https://doi.org/10.3301/GFT.2023.03

Stop PRE3-2.5 – Fosso Borgo Cappuccini, Offida

Coordinates: Lat. 42°55'49"N, Long. 13°41'23"E

***Topic*: Stratigraphic architecture of levee sediments flanking channel-fill conglomerates**

The final stop of the day provides a roughly down-depositional dip overview of the O-IV$_3$, O-IV$_4$, and O-IV$_5$ cycles (Fig. 27A, B). In their basal portion, the levee deposits of the stratigraphically higher channel-levee consist mostly of medium- to thick-bedded, partially amalgamated, sheet-like sandstones (FA-Dt) that are interpreted to represent deposition from relatively unconfined, moderate-concentration flows that formed an incipient overbank lobe (Fig. 27C). These sandstones are directly overlain by thinly interbedded, fine-grained sandstones, siltstones, and silty mudstones (FA-Dh) characterised by an overall thinning- and fining-upward trend (Fig. 27D) that may reflect a gradual decrease in the amount and size of ov

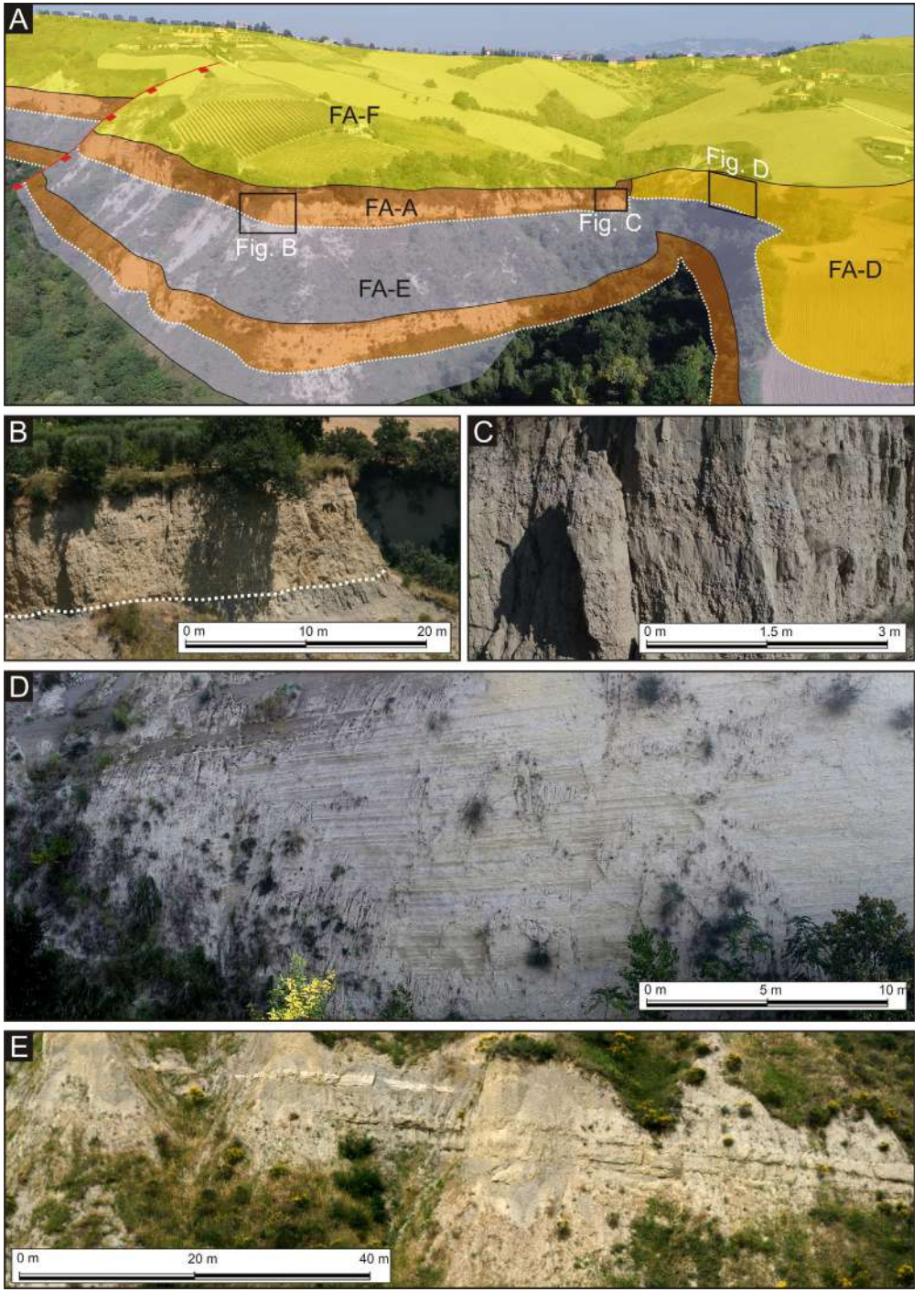

Fig. 26 - (A) UAV-based northeastward view of the stratigraphically higher (O-IV$_5$ cycle) channel-fill deposits bounded on the southern side by heterolithic levee deposits; (B) Detail showing the sedimentological characteristics of the on-axis channel conglomerates; (C) Detail of the off-axis sandy conglomerates; (D) Detail of the heterolithic levee deposits laterally adjacent to channel conglomerates; (E) Panoramic view of the progressive, lateral thinning and pinch-out of channel-fill strata (O-IV$_2$ cycle) in proximity to original northern canyon wall. In this outcrop, the lowest beds in the conglomerate unit onlap onto a basal erosional surface cut into the underlying pebbly mudstones.

https://doi.org/10.3301/GFT.2023.03

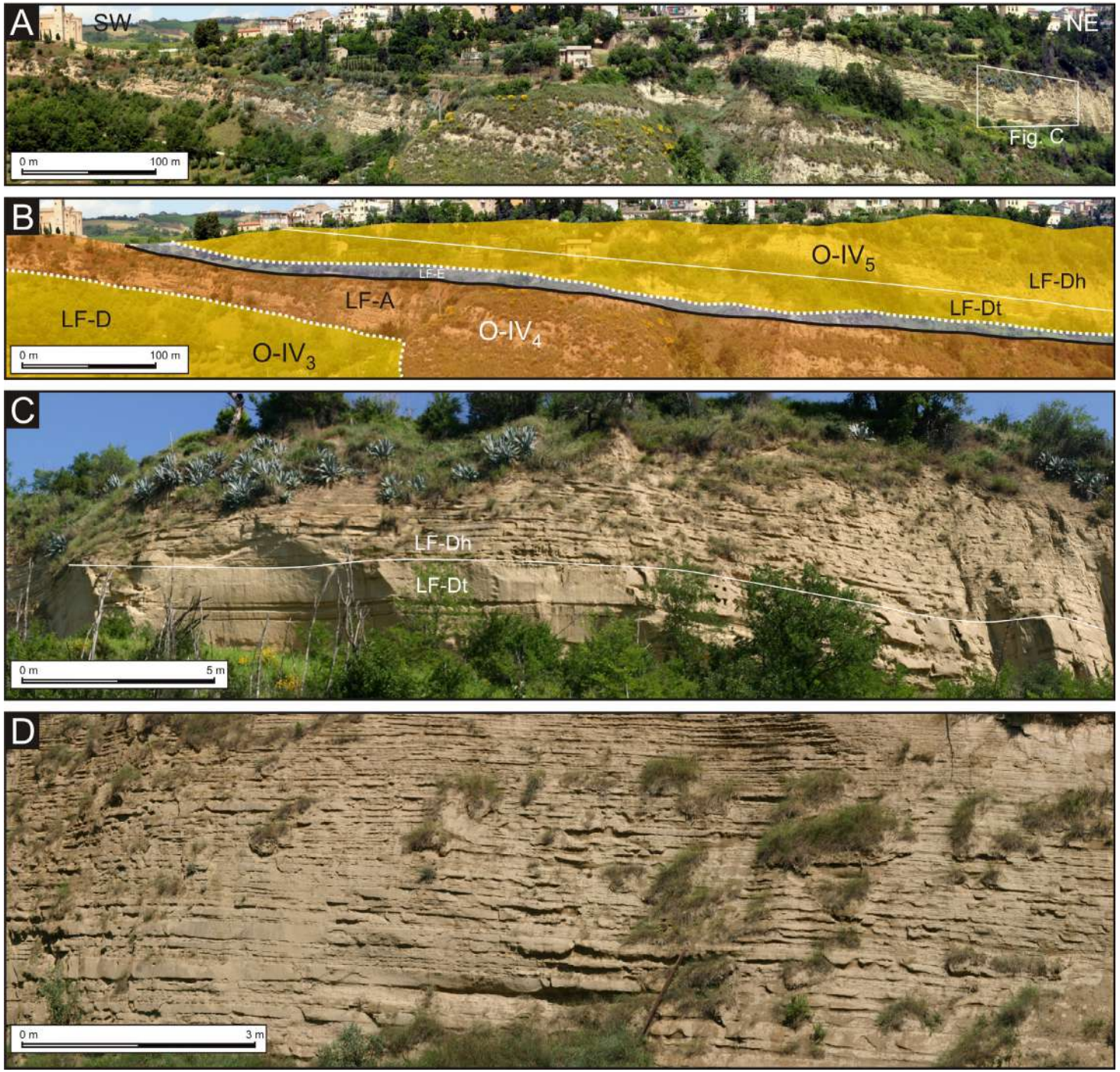

Fig. 27 - Compilation of field photographs showing the main features observed in this stop (modified from Di Celma, 2011). (A) Uninterpreted and (B) interpreted dip-oriented photomontage of the northern flank of Fosso Borgo Cappuccini showing stratigraphic relationships among the most common lithofacies within the Offida canyon fill within the upper portion of the Offida Canyon fill (O-IV_4 and O-IV_5). Note as the stratigraphy in the levee deposits is defined to include basal, sandy lobe deposits comprised of medium- to thick-bedded turbidites (LF-Dt) and overbank facies consisting primarily of packages of fining- and thinning-upward, fine-grained, thin-bedded turbidites (LF-Dh); (C) Close-up of outcrop shown in (A), illustrating thick sandstone beds interpreted as basal, sandy lobe deposits (LF-Dt); (D) Close up of thinly interbedded sandstones and mudstones exhibiting an overall thinning- and fining-upward character (LF-Dt).

https://doi.org/10.3301/GFT.2023.03

erspilling flows reaching this portion of the levee flank because of pronounced growth of the proximal levee and progressive confinement of turbidity flows to the channel.

Concluding remarks on the off-shelf sedimentary record of Unit PS1

In deepwater fold-and-thrust belts examples of slope channels and canyons being diverted by structurally related sea-floor topography are commonly found both on the modern seabed and in the subsurface, but their depositional histories have rarely been documented using examples from outcrop. The synthesis of outcrop and subsurface data sets from the Lower Pleistocene stratigraphic succession of the Periadriatic basin provides a window into the overall evolutionary pattern of large intraslope turbidite systems that, during the Gelasian, shed Apennine-derived clastic sediments into the adjacent deepwater basin. The three canyon-confined channel-levee systems visited during this field trip represent long-lived pathways for transport and deposition of coarse-grained clastics within an east-facing, fold-and-thrust belt-controlled submarine slope. A comprehensive analysis of outcrop and subsurface data (Fig. 28) enables the development of a two-phase conceptual model for evolution of the morphology of the continental slope and the downslope sediment transport as the basin progressively filled.

Phase 1: The early to middle Gelasian is characterised by deposition of the Mt. Ascensione and Castignano turbidite systems between the Mt. Acuto-M.gna dei Fiori front (MAF) to the west and the Jesi-Nereto-Zaccheo front (JNZ) to the east. Their courses and palaeocurrent directions indicate that the slope configuration had a direct impact on the sediment dispersal pattern, and suggest that although the primary source for sediment was to the west, in the uplifted Apennine orogenic belt, the sediment gravity flows were then redirected to the north (i.e. parallel to the north–south-trending strike of the east-facing slope) by the sea-floor bathymetric expression of an intraslope, thrust-related anticline (Fig. 28).

Phase 2: The late Gelasian is represented by the deposition of the Offida canyon-confined channel-levee system. Unlike the earlier depositional systems, the Offida system cuts through the hanging wall anticline above the thrust (Fig. 28), probably reflecting the filling up of the intraslope accommodation space on the western flank of the thrust-related anticline.

https://doi.org/10.3301/GFT.2023.03

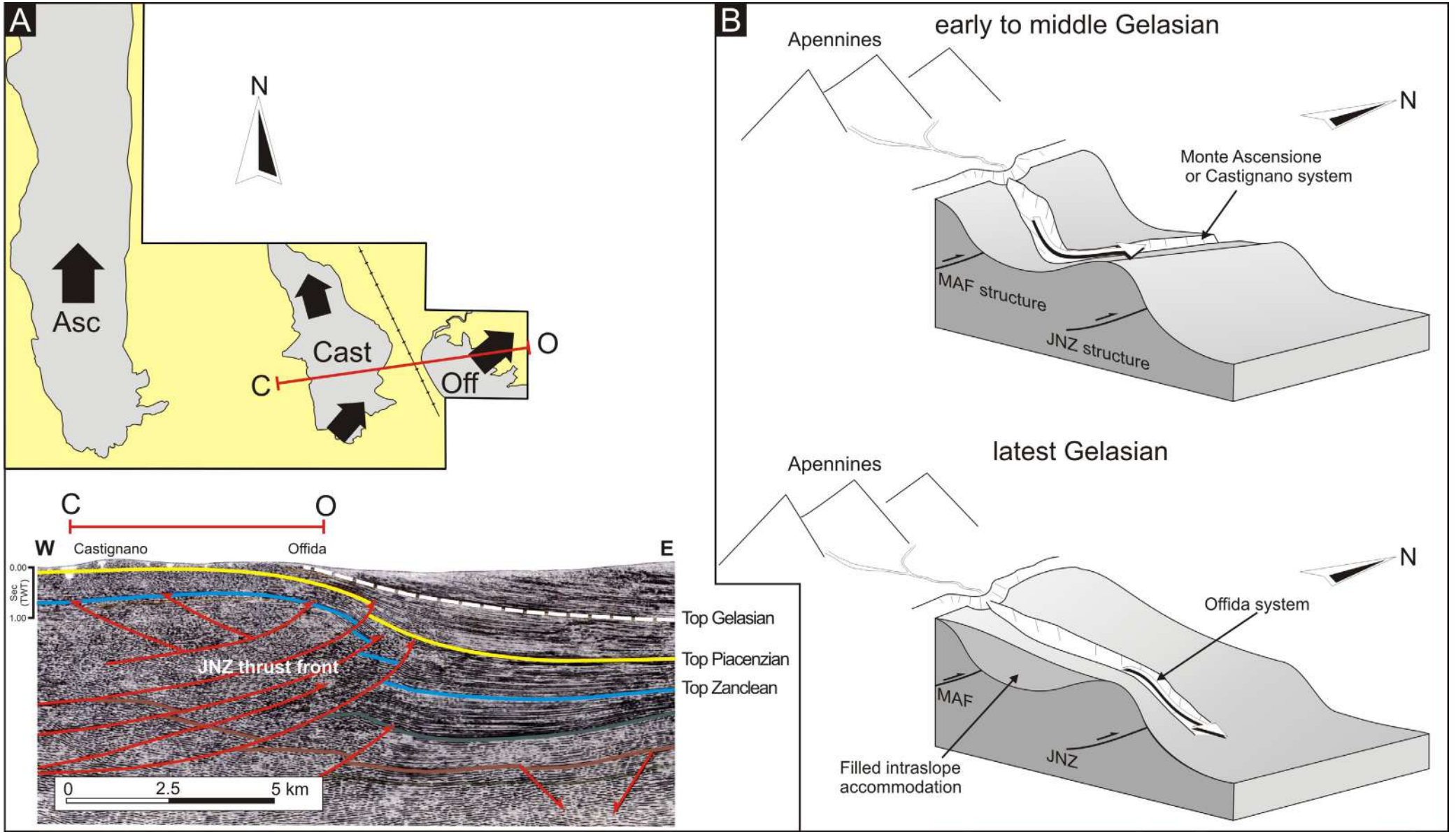

Fig. 28 - (A) Schematic geological map of the Gelasian slope turbidite systems (in grey) and enclosing hemipelagic mudstones (in yellow) exposed in the study area. Large black arrows mark the dominant palaeo-flow directions. Abbreviations: Asc, Mt. Ascensione; Cast, Castignano; Off, Offida. Interpreted seismic reflection line FTR-19-18 / APF-33-90 courtesy of UNMIG–Società Geologica Italiana–AssoMineraria. The C-O red line indicates the position of a portion of the seismic line on the geological map; (B) Depositional model for the Gelasian evolution of the visited area from an east-facing, complex submarine slope with a pronounced thrust-related step during the early to middle Gelasian to a smoother, healed sea-floor slope during the latest Gelasian (modified from Di Celma et al., 2016b).

https://doi.org/10.3301/GFT.2023.03

DAY 3

The onland exposures of the PS2 Unit (Fig. 29) represent Apennine-derived, shelf-margin scale clinoforms consisting of northeast-dipping, mud-prone foresets (continental slope) with turbidite-filled channels (PS2.1) overlain erosively by a coarse-grained topset (continental shelf) dominated by shallow-marine and non-marine sandstones and conglomerates (PS2.2).
The topset of the clinoforms is composed of offset stacked, high-frequency depositional sequences recording repeated cross- shelf shoreline transgressions and regressions (compare Steel et al., 2020). During these phases most of the coarse-grained sediments were stored in the shelf and sediment flux to deepwater settings was negligible. In contrast, the sequence bounding unconformities are marine or subaerial erosional surfaces, as well as non-depositional interfluvial exposure surfaces locally marked by palaeosols and represent periods of erosion and sediment bypass across the shelf, muddy slope accretion, and growth of contemporaneous basin floor fans. What is characteristic and particularly noteworthy in the PS2.1-PS2.2 sediment wedges is that owing to tectonically enhanced erosion during forced regressions and the ensuing transgressions, sediments of the topset-to-foreset rollover zone are not preserved in the stratigraphic record and slope deposits become truncated in updip sections. As a result, time equivalent shelf and slope segments of clinoforms are physically disconnected and coarse-grained topset deposits (PS2.2) rest erosively on foreset mudstones (PS2.1), separated by the composite, time-transgressive u8.2 stratigraphic discontinuity formed by the lateral, downdip connection of lower-rank sequence boundaries.
The benthic foraminiferal and mollusc assemblages from the mud-rich portion at the base of the exposure have been documented by Ragaini et al. (2006) and converge to indicate a neritic (infralittoral) shallow-water marine environment. Biostratigraphic investigations carried out on calcareous nannofossils and both benthic and planktonic foraminifera reveal that these deposits are characterised by the occurrence of large *Gephyrocapsa* along with *Pseudoemiliania lacunosa*, *Coccolithus pelagicus*, *Calcidiscus leptoporus*, *Gephyrocapsa oceanica* s.l., *Helicosphaera carteri*, and *Helicosphaera sellii*, which are indicative of the upper part of the CNPL8 Zone; the presence of the planktonic foraminifera *Globorotalia inflata* and *Globigerinoides tenellus* (a species characteristic of the MPle1 Zone) and of the age-diagnostic benthic foraminifer *Bulimina etnea* is in agreement with a Calabrian age.

Stop PRE3-3.1 – Ripatransone

Coordinates: Lat. 42°59’49”N, Long. 13°45’30”E
***Topic*: Stratigraphic architecture of Unit PS2**

Middle Pleistocene shoreline trends were oriented approximately northeast-to-southwest in east-central Italy. This exposure is oriented in a roughly parallel direction to the ancient shoreline and allows recognising the main stratigraphic components of the PS2 unit (Fig. 30A). In the extreme western (landward) exposures, the uppermost portion of the PS2.1 subunit (Fig. 30B) comprises an overall coarsening- and

https://doi.org/10.3301/GFT.2023.03

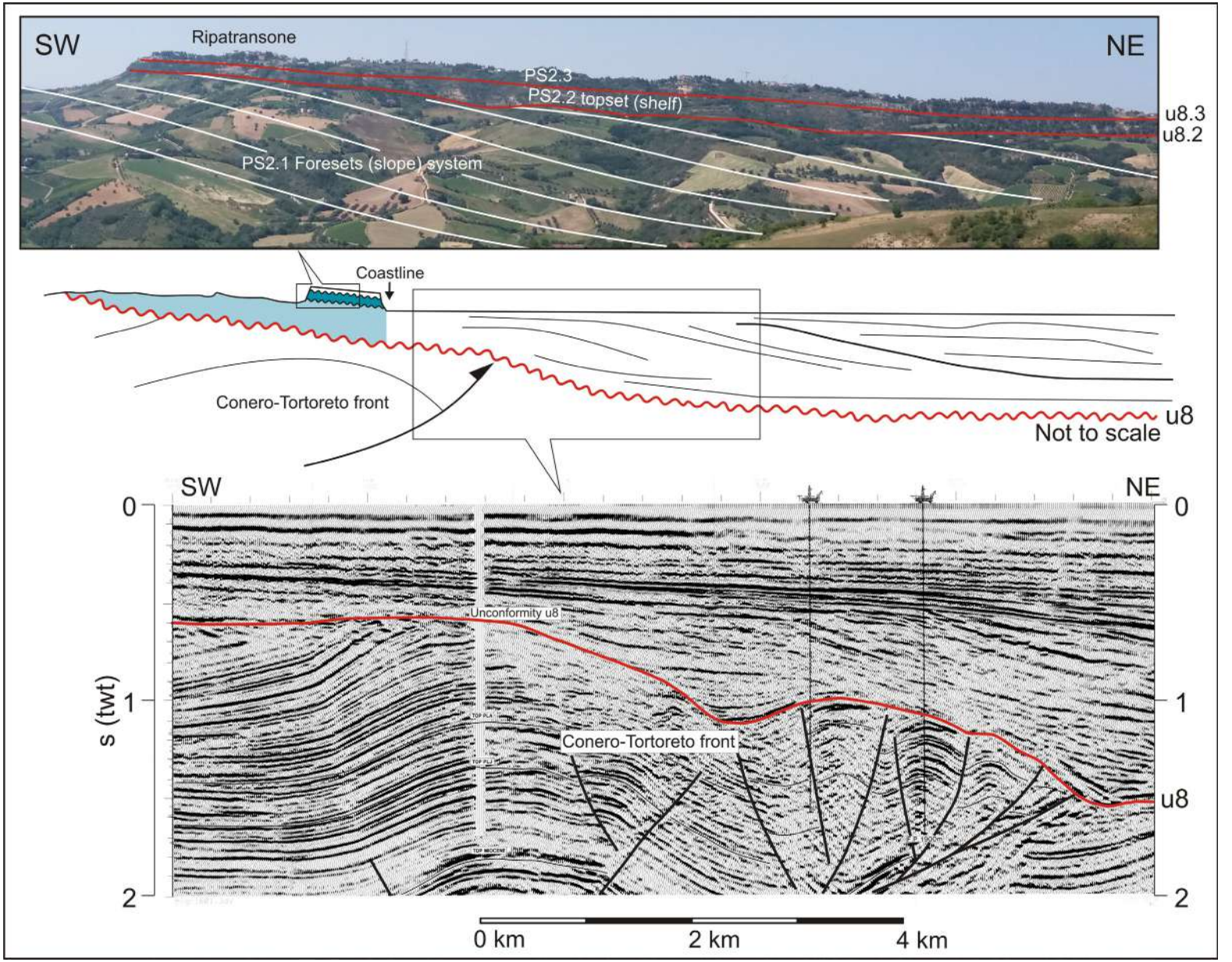

Fig. 29 - Summary diagram reconciling interpretations from onshore exposures and offshore seismic sections along the Adriatic margin (modified from Ori et al., 1991). Depositional dip-orientated seismic profile showing the internal configuration of the eastward-building PS2 Unit above unconformity u.8; shelf-slope-basin clinoforms resulting from rapid progradation can be recognised. Note the prominent erosional nature of the u.8 unconformity on top of the Conero-Tortoreto front. Seismic reflection line from: https://www.videpi.com/videpi/videpi.asp (courtesy of UNMIG–Società Geologica Italiana–AssoMineraria).

https://doi.org/10.3301/GFT.2023.03

shallowing-upward succession of facies associations indicated by Cantalamessa and Di Celma (2004) as regressive littoral deposits (hereafter referred to as RLD). Generally, the RLD is composed of a vertical succession of hemipelagic slope mudstones coarsening gradually up into thoroughly bioturbated offshore sandy mudstones with scattered mollusc shells, lower shoreface sandstones showing abundant burrowing and, through a wave-cut erosion surface, to seaward dipping gravelly beachface clinobeds. Based on the vertical succession of facies and the presence of the erosional surface separating lower shoreface sandstones below from beachface conglomerates above, these facies associations can be partitioned into the two systems tracts described below:

Highstand systems tract: The lower portion of the RLD is sandstone dominated and consists of a conformable shallowing- and coarsening-upward facies succession passing gradationally from offshore to lower shoreface facies associations reflecting normal regression under highstand conditions. This part of the stratigraphic record is thickest towards the western margin of the basin (up to about 25 m), while it is only partially preserved elsewhere beneath the overlying erosion surface.

Falling-stage systems tract: The upper portion of RLD is composed of clinostratified beachface conglomerates erosionally overlying the shoreface sandstones. In a depositional dip direction (i.e., along a profile from onshore to offshore), this conglomerate stratal unit displays a pronounced descending trajectory, suggesting that it is a product of deposition by wave- and storm-processes along a gravelly, wave-dominated strandplain during an episode of relative sea-level fall. The regressive surface of marine erosion (RSME), produced by the basinward translation of shoreface ravinement, underlies the beachface conglomerates wedge that builds seaward during forced regression. Owing to the descending trajectory of the shoreline, an increasing thickness of the underlying portion of the RLD was erosionally removed at the RSME in a seaward direction and overlain by beachface conglomerates. As a result, the thickness of the highstand offshore transition-to-lower shoreface deposits decreases northeastwards to a point where it is completely removed and seaward moving beachface conglomerates prograde directly on the underlying mudstones. The prograding conglomerate package at the top of the RLD displays a basinward (to the northeast) wedge-shape tapering geometry.

The u8.2 unconformity coincides with a poorly-defined erosional contact between the clinostratified beachface conglomerates at the top of the RLD and a massive conglomerate package that is interpreted as fluvial (Fig. 30C). This surface is interpreted as a subaerial unconformity preserved at the base of the fluvial channels and records the first evidence of subaerial exposure in the Pleistocene fill of the basin. The fluvial conglomerates represent the oldest PS2.2 sediments and are truncated by a wave ravinement surface sculpted by waves in the upper shoreface and foreshore during the ensuing shoreline transgression (Fig. 30C). An isolated channel-form oriented broadly normal to the ancient shoreline and infilled by massive conglomerates is encased in the retreating shoreface sandstones overlying the ravinement surface. It is interpreted to be a subaqueous channel cut and filled by offshore-directed hyperpycnal flows from distributary channels further updip and feeding shelf turbidite systems downdip (compare Pattison et al., 2007).

https://doi.org/10.3301/GFT.2023.03

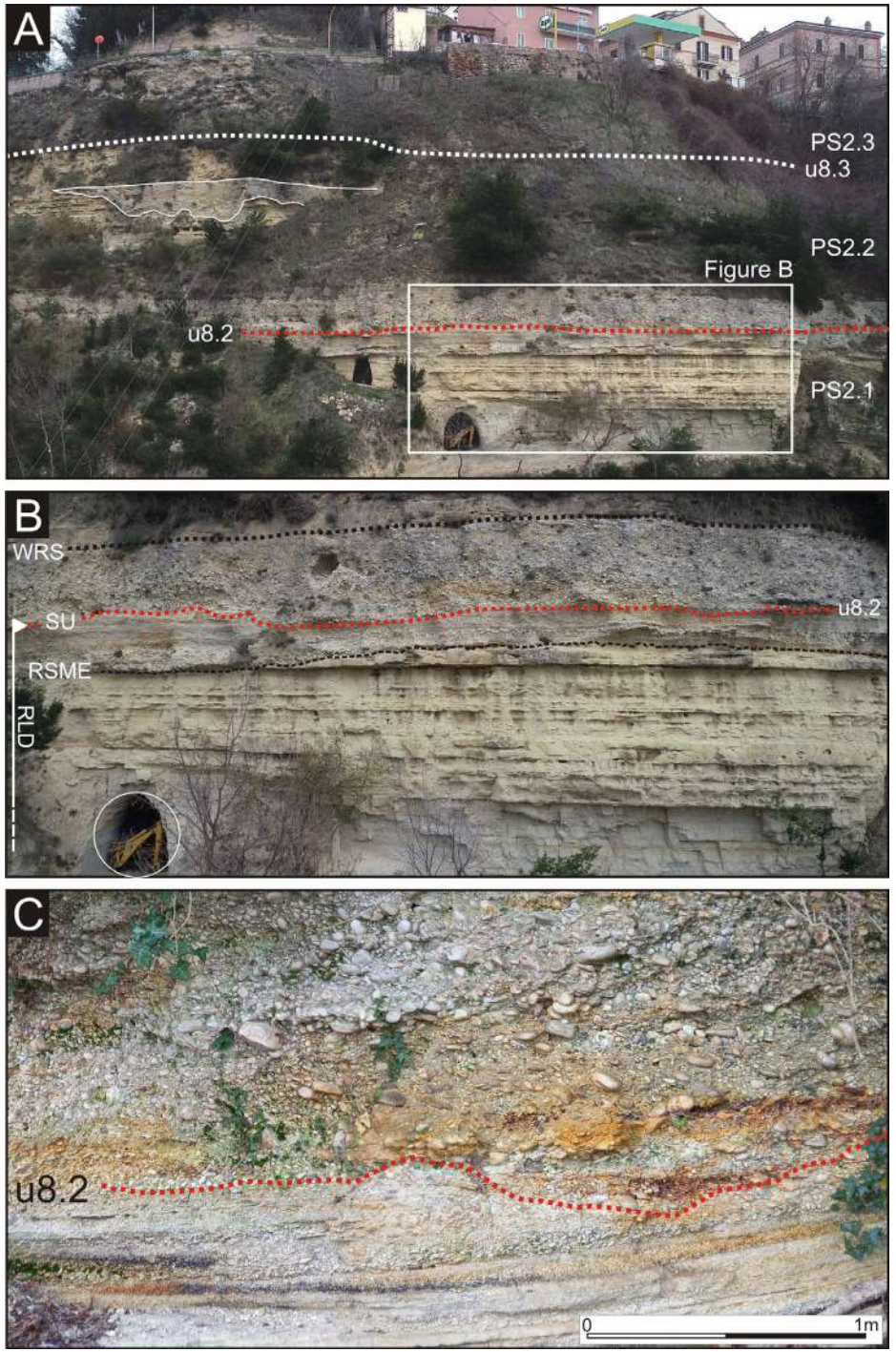

Stop PRE3-3.2 – Contrada San Salvatore, Ripatransone

Coordinates: Lat. 42°59′28″N, Long. 13°48′27″E

***Topic*: sequence architecture; clast assembling and sedimentary structures in a storm-dominated, prograding gravelly beach**

This stop provides a dip-oriented panoramic view of the PS2.2 succession exposed along the northern flank of the Tesino River showing a complete depositional sequence of the topset sequence set (Fig. 31A). The sequence comprises braided-river conglomerates and floodplain fines within the confines of an incised-valley entrenched into PS2.1 mudstones (Fig. 31B) overlain by retreating shoreface sandstones rapidly passing upward into beachface conglomerates of the falling-stage systems tract forming part of a gravelly-dominated strandplain prograding eastward into the palaeo-Adriatic Sea. At this stop the outcrop is oriented roughly normal to the palaeoshoreline and reveals a wide spectrum of beachface and shoreface deposits produced under a microtidal regime by wave- and storm-related processes (Fig. 32).

Fig. 30 - (A) UAV-based northeast-looking view of the middle Pleistocene section exposed at Ripatransone showing the three PS2 subunits and bounding surfaces (dotted lines). To the left, the 20 m wide and 4 m thick gravelly deposits encased into shoreface sandstones is outlined in white; (B) Detail documenting the gradual contact within PS2.1 between the offshore sandy mudstones and the overlying shallowing-upward succession of the regressive littoral deposits (RLD). To the left, the sharp-based seaward-dipping beachface gravelly clinobeds progressively cut into and truncate the underlying shoreface sandstones (black dashed line). A backhoe (circled) for scale. Abbreviations: SU – subaerial unconformity; WRS – wave-ravinement surface; RSME – regressive surface of marine erosion; (C) Close-up view of the u8.2 subaerial unconformity (red dotted line). It is manifested as a subtle conglomerate-on-conglomerate contact, characterised by erosional truncation below and marking a distinct basinward shift in facies association. The beachface conglomerates underlying the surface are represented by even, regularly bedded, seaward-dipping (toward the left) gravelly clinobeds. Component clasts consist of well-rounded pebbles, mainly discs and subordinate blades, displaying excellent segregation of different sizes into separate beds and well-developed seaward-dipping (toward the left) imbrication. The fluvial conglomerates directly overlying the surface are characterised by a dominance of clast-supported, poorly sorted, massive or crudely bedded clasts, which range in size from granules to small cobbles and display fair landward-dipping (toward the right) imbrication.

https://doi.org/10.3301/GFT.2023.03

Fig. 31 - (A) Annotated panoramic photograph showing the stratigraphic architecture of fluvial to shallow-marine deposits in PS2.2 recording one complete cycle of relative sea-level change. A car (circled) for scale. Abbreviations: SU – subaerial unconformity; WRS – wave-ravinement surface; (B) The conglomerates and sandstones incising at least 10 m into underlying PS2.1 mudstones are interpreted as fluvial deposits bounded by a subaerial unconformity (SU). The thin, laterally extensive conglomerate bed overlying both the incised valley fill and the PS2.1 mudstones is interpreted as a transgressive lag mantling a WRS that reworks part of the subaerial unconformity and the fluvial deposits and is overlain by retreating shoreface sandstones.

https://doi.org/10.3301/GFT.2023.03

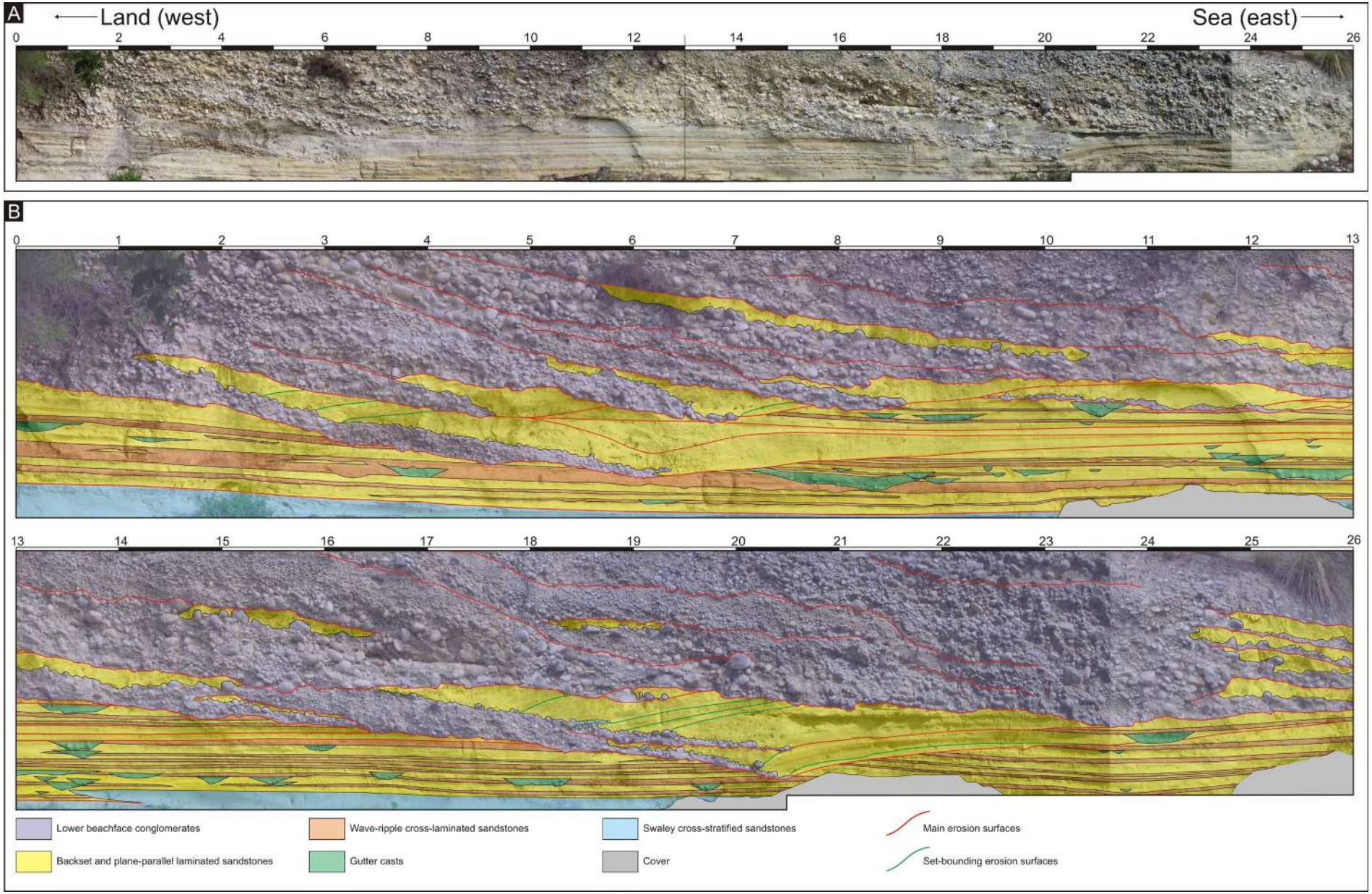

Fig. 32 - (A) Uninterpreted photomosaic of the studied cliff face oriented normal to palaeo-shoreline (land to photo left). The section preserves a progradational sediment wedge built out from the west and reflects shoaling from lower shoreface sandstones, into upper shoreface sandstones, and finally up (and laterally) into beachface conglomerates; (B) Line drawing documenting details of the facies architecture and depositional geometry of the palaeoenvironments. Red and green lines indicate main bounding surfaces and internal truncation surfaces, respectively. All the bar scales are in metres. Modified after Di Celma et al. (2020).

https://doi.org/10.3301/GFT.2023.03

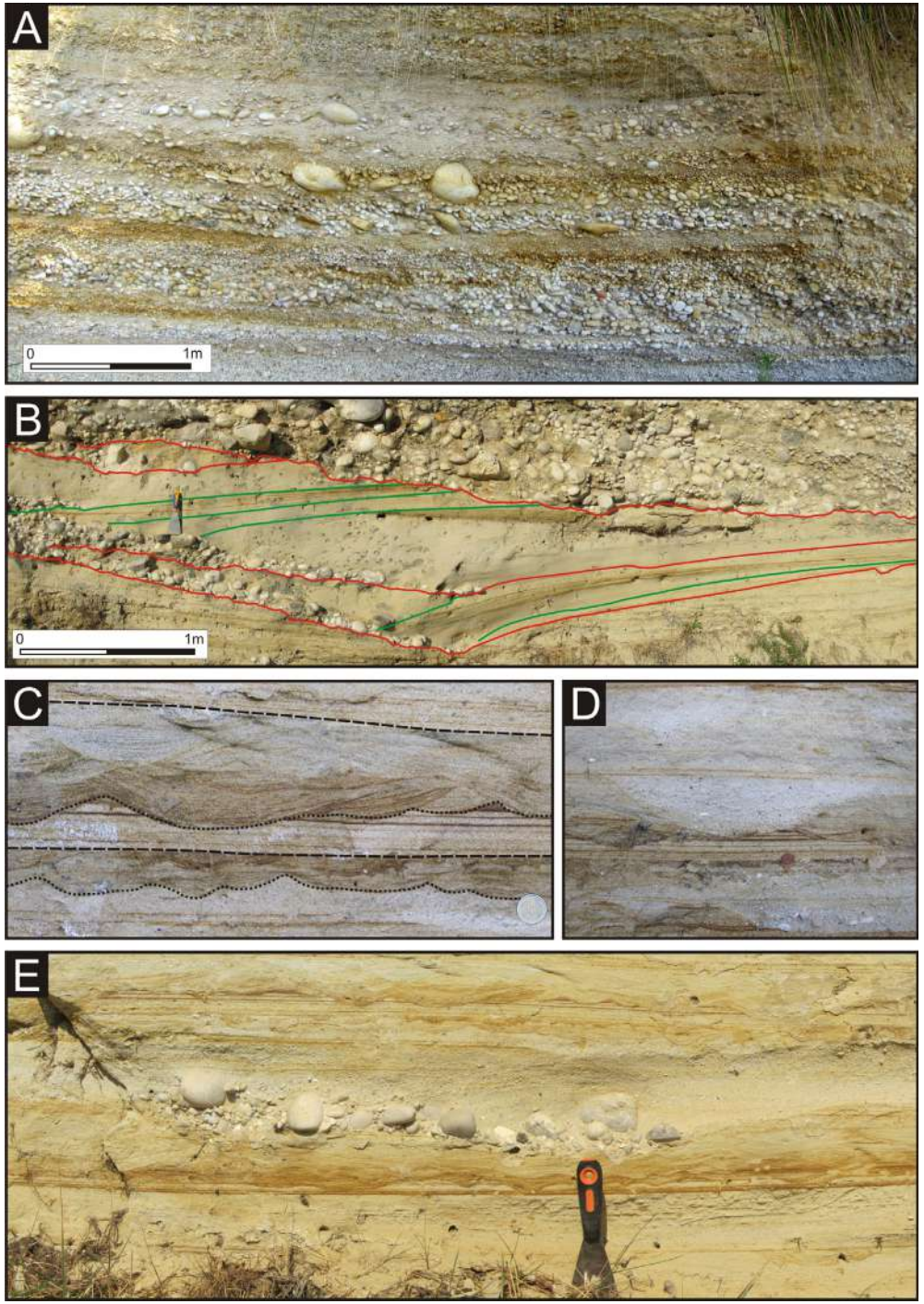

The gravelly beachface deposits show considerable variations in textural and bedding characteristics in down dip direction (Massari and Parea, 1988; Di Celma et al., 2020; Massari, 2021). In the upper beachface (Fig. 33A), conglomerates display distinct segregation of clasts of different sizes into discrete beds and occur as laterally continuous, well-developed and packed beds consisting of both openwork and clast-supported framework infilled with a fine- to coarse-grained sandy matrix. Clasts are subrounded to rounded, moderately spherical to highly disk-shaped and show clear seaward-dipping imbrication. The

Fig. 33 - Representative photographs of sedimentary structures within the gravelly beachface to sandy upper shoreface sediments exposed at this stop (modified after Di Celma et al., 2020); (A) Well-stratified, moderately- to well-sorted granule to pebble conglomerate of the upper portion of the beachface. In general, component clasts display well-developed seaward-dipping imbrication and are well-rounded and organised in a tight clast-supported texture with the interstices between clasts filled with a sandy matrix. Less frequently, these conglomerates display a matrix-free open framework or a matrix-supported texture with a matrix of sand; (B) Close-up showing the zone of lateral interfingering between seaward and landward tapering conglomerate and sandstone wedges. These sediments are filling asymmetrical concave-upward erosional surfaces (troughs) with landward margins steeper than their seaward counterpart. The seaward-dipping erosion surfaces (red lines) are sharply truncating underlying sediments and are directly overlain by a pebble lag that, in turn, is downlapped by low-angle sandy backset (upstream-dipping) laminae. Flow is to the right. The infill of individual troughs is comprised of upstream migrating backset laminae separated by set-bounding truncation surfaces (green lines); (C) In the distal upper shoreface facies association the rhythmic depositional theme was formed through multiple storm and fair-weather events. The plane-parallel laminated sandstones, which indicate upper-stage bed conditions, represent the distal expression of the storm-related bedforms described in the proximal upper shoreface and exhibit abundant evidence of high-energy conditions, including scour fillings and absence of bioturbation. The overlying ripples, displaying traces of bioturbation, indicate a return to lower flow regime conditions and are interpreted to represent temporary reworking by waves during the waning cycles of storms. Note the scooping and undulatory lower boundary of the wave ripple sets (dotted lines) marking the contact with the underlying plane parallel-laminated sandstones and the sharp, roughly horizontal erosional contacts (dashed lines) with the overlying plane parallel-laminated sandstones. Coin 2.2 cm in diameter; (D-E) Cross sections of some sand- to pebble-filled gutter casts displaying margins that widen upward and fade into the plane-parallel laminated sandstone beds. Scraper for scale.

https://doi.org/10.3301/GFT.2023.03

upper beachface deposits grade seaward into progressively thicker-bedded, coarser-grained lower beachface conglomerates displaying a comparatively lower degree of clast size and shape segregation. Clasts are dominantly spherical and rod-shaped, ranging in size from pebbles to small boulders. These sediments have yielded an elephantid tooth attributed to the southern mammoth *Mammuthus meridionalis* (Ferretti et al., 2003).

At the toe of the beachface, conglomerates interfinger with a sand-prone facies association dominated by trough-filling, landward-dipping (backset) laminae flattening and converging seaward into thinner and finer grained plane-parallel laminae (Fig. 33B). These sediments are interpreted to have been deposited in the proximal upper shoreface by strong, storm-generated, offshore-directed flows (undertow and/or backwash flows) during the transition in flow regime from supercritical to subcritical. The transition from the proximal to the distal upper-shoreface sediments records a significant increase of preserved wave ripples and burrowed intervals, in concert with a progressive decrease in thickness of individual sets of plane-parallel laminae and increase of gravel-filled gutter casts (Fig. 33C, D, E). Distal upper shoreface sediments overlie and laterally interfinger with swaley-cross stratified lower shoreface sandstones.

Stop PRE3-3.3 – Pedaso

Coordinates: Lat. 43°05'46"N, Long. 13°50'24"E

***Topic*: Shoreline trajectories and along-strike variability of the u8.2 unconformity (wave ravinement surface superimposed on subaerial unconformity)**

The 2-dimesional depositional dip view of the nearshore sediments exposed at Pedaso is sufficiently extensive to show the path of the shoreline as it migrates (Fig. 34A, B) across the u8.2 unconformity. Combining the vertical and horizontal components of migration directions, the offlapping clinobeds that make up the gravelly beachface facies association occurring in the lower portion of the outcrop define a descending, regressive shoreline trajectory, which is symptomatic of falling relative sea-level conditions. The overlying shoreface sandstones onlap onto the underlying conglomerates and illustrate an ascending transgressive shoreline trajectory, which is suggestive of transgression.

At a regional scale the u8.2 unconformity, records evidence of fluvial incision, laterally equivalent conditions of subaerial exposure and, in places, successive ravinement processes. The well-exposed transition between the PS2.2 and the PS2.3 subunits in stops 3.3, 3.4, and 3.5 offers an excellent opportunity to pinpoint the u8.2 unconformity, as well as to closely examine its sedimentary character and lateral variability along depositional strike. At this site, shoreface erosion during sea-level rise and landward translation of the shoreline removed all deposits associated with former shorelines and stripped off all the evidence of subaerial exposure, resulting in the superposition of a wave ravinement surface upon a previous surface of subaerial exposure (Fig. 34B).

https://doi.org/10.3301/GFT.2023.03

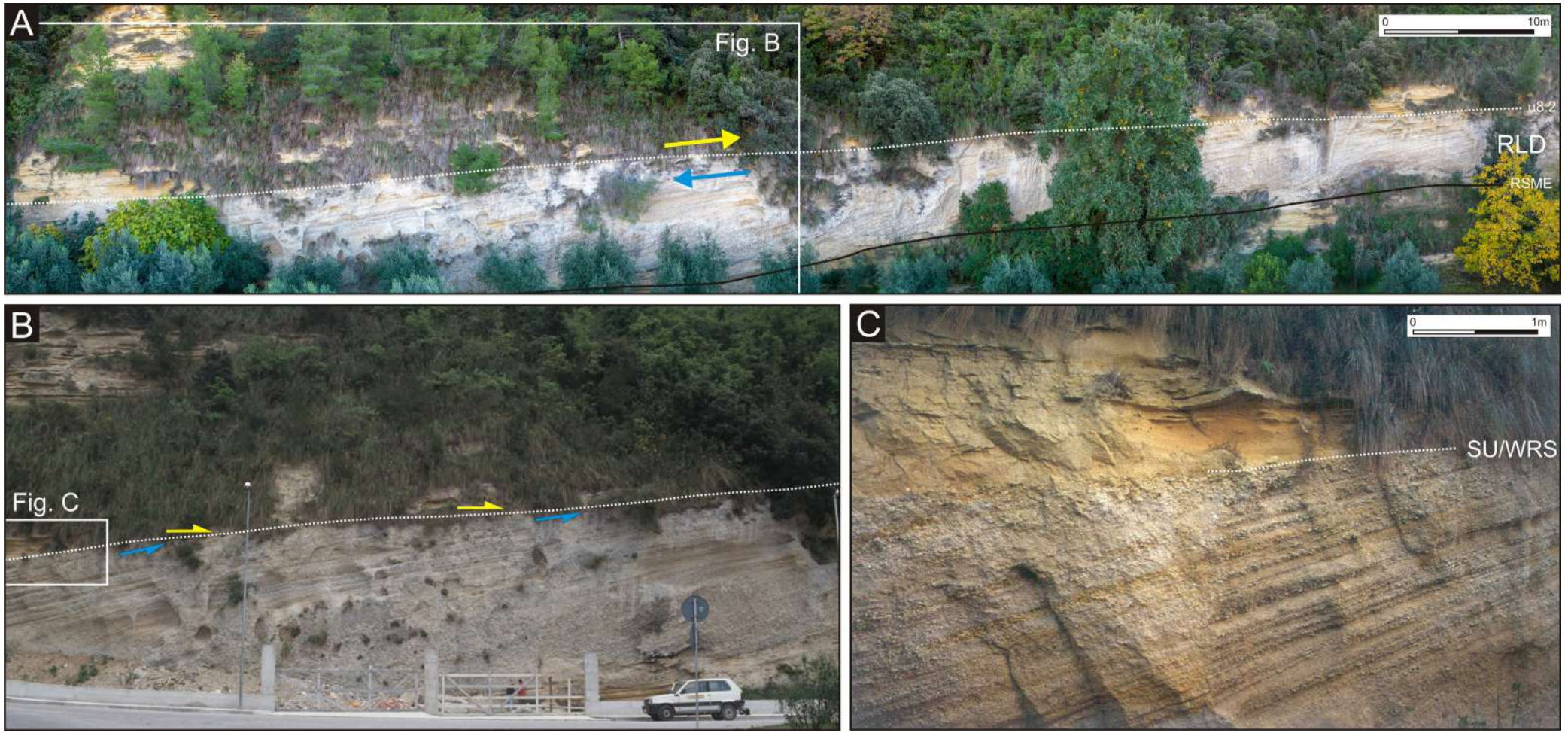

Fig. 34 - Outcrop views of the nearshore sediments exposed at Pedaso. Note that pictures in B and C were taken in the late 1990's. (A-B) Beachface conglomerates of the RLD display a descending regressive shoreline trajectory associated with offlap (blue arrows) followed by a transgressive shoreline trajectory associated with onlap (yellow arrows), which are consistent with an overall forestepping-backstepping of depositional environments due to a relative fall and successive rise of sea level, respectively. The two stratal units are separated by a prominent erosional surface (white dotted line) that climbs stratigraphically in a landward (toward the right) direction; (C) Enlargement of outcrop shown at the left-hand side of (B). The prominent erosional surface separating underlying beachface conglomerates from overlying shoreface sandstones (u8.2) is interpreted as a wave ravinement surface (WRS) produced by the landward translation of shoreface ravinement superimposed onto an older surface of subaerial exposure (SU).

https://doi.org/10.3301/GFT.2023.03

Stop PRE3-3.4 (optional) – Contrada Madonna di Manù

Coordinates: Lat. 43°07'22"N, Long. 13°48'45"E

***Topic*: along-strike variability of the u8.2 unconformity (interfluve sequence boundary)**

This stop is located about 3 km along strike of Stop 3.3. At this site the clinostratified beach conglomerates at the top of the RLD end with a 30-cm-thick, weathered reddish-brown palaeosol developed at the expense of previously accumulated deposits (Fig. 35A, B). Its composition

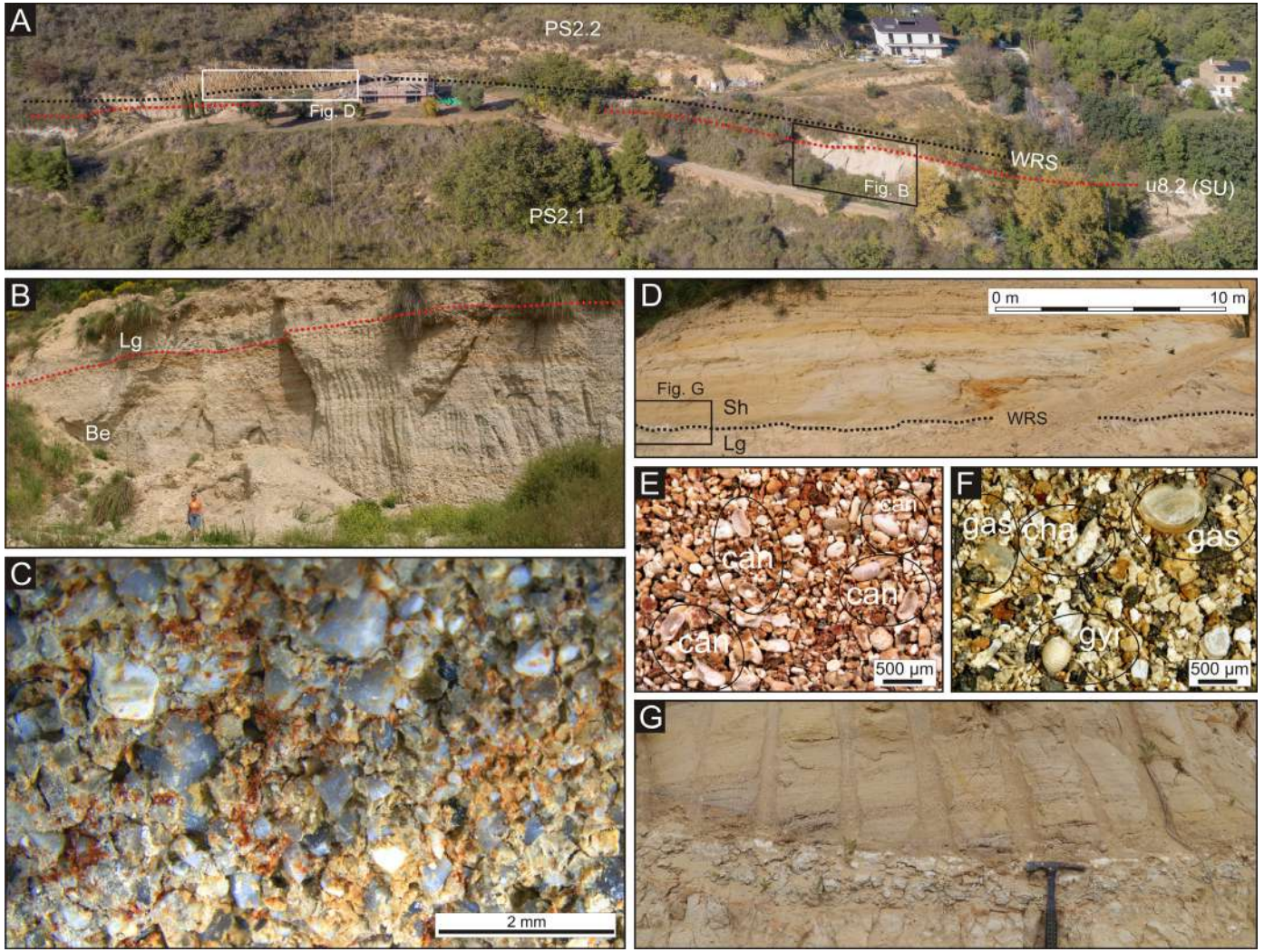

Fig. 35 - (A) Oblique UAV-based photograph looking northwards showing position of the main outcrops discussed in this stop. (B) Seaward-dipping (toward the right) beachface conglomerates (Be) capped by a reddish-brown palaeosol (red dotted line) succeeded by green-grey back-barrier lagoon mudstones (Lg). Person for scale; (C) Optical microscope image of the palaeosol sediments overwhelmingly composed of residual, sand-sized quartz grains; (D) Panoramic view showing the precursor transgressive back-barrier lagoon mudstones (Lg) overlain by the retreating shoreface sandstones (Sh). These two stratal units represent an initial sedimentation of a renewed sea-level rise following the previous regression and are separated by a wave ravinement surface (WRS); (E-F) Optical microscope images showing the micropalaeontological content of the transgressive back-barrier lagoon sediments interposed between the palaeosol below and the landward-rising wave ravinement surface above. Abbreviations: valves of *Candona candida* (can), remains of charophyte cortex (cha), charophyte gyrogonite (gyr, *Lamprothamnium papulosum*), gastropod opercula (gas); (G) Detail of the wave ravinement surface interposed between the lagoon mudstones and the shoreface sandstones. This surface was carved in the shoreface during shoreline transgression and truncates the top of the back-barrier lagoon mudstones. It is overlain by a laterally discontinuous pebble lag that grades upward into coarse- to medium-grained lower shoreface sandstones displaying landward dipping cross lamination (hammer for scale).

https://doi.org/10.3301/GFT.2023.03

ranges between silt to coarse-grained quartz sand containing a variable amount of clay minerals and iron oxide. As such, the palaeosol atop the falling-stage beachface conglomerates is interpreted as a surface of subaerial exposure marking nondeposition and prolonged pedogenic modification of what it can be considered the interfluve of widely spaced incised fluvial valleys.

Overlying this is a sediment package that is interpreted to reflect the landward migration during transgression of a coupled back-barrier/shoreface system. It consists of two transgressive stratal units (Fig. 35C): i) a 2-m-thick back-barrier wedge composed of green-grey mudstones laid down landwards of a retreating barrier island system; and ii) a retreating shoreface wedge composed of medium- to coarse-grained sandstones. The biogenic fraction recorded in the lagoon mudstones (Fig. 35D, E) comprises well-preserved valves of the freshwater ostracod *Candona candida*, possible calcified remains of charophyte cortex, calcified fructifications mostly consisting in charophyte gyrogonite with a typical spiral structure, and freshwater gastropod opercula pointing to deposition on the muddy bottom of a brackish lagoon. The boundary between these two stratal units is an erosional surface mantled with a laterally discontinuous, coarse-grained lag including limestone and rip-up mudstone clasts. This surface is interpreted as a wave ravinement surface carved in the upper shoreface during shoreline retreat that partially truncated the coeval transgressive lagoon deposits landwards of the shoreline. The reworked sediments were transported to the lower shoreface to be deposited.

Stop PRE3-3.5 (optional) – Fosso del Molinetto, Torre di Palme

Coordinates: Lat. 43°08'03"N, Long. 13°48'29"E
***Topic*: along-strike variability of the u8.2 unconformity (fluvial incision)**

This stop is about 1.3 km along strike of Stop 3.4. The outcrop belt provides a depositional-dip-oriented transect displaying a cross-sectional view through the RLD of PS2.1 and one of the topset sequences in PS2.2 (Fig. 36A). At the principal reference section, the u8.2 unconformity is characterised by a conglomerate-on-conglomerate contact with a gravelly-filled incised valley cutting into the underlying clinostratified beach conglomerates at the top of the RLD (Fig. 36B). The gravelly beach deposits display a pronounced descending trajectory developed during falling relative sea level and producing an oblique progradational pattern. The gravelly fill of the incised valley is nicely exposed a few tens of metres away, where a younger sediment package progressively onlaps and wedges out against a wave ravinement surface and is in turn truncated by the u8.3 unconformity (Fig. 36C).

In a down depositional dip direction, the valley incision tapers about 400 m away from this outcrop and the shoreface sandstones onlap directly onto the clinostratified beach conglomerates at the top of the RLD (Fig. 36D, E). At this site, the u8.2 unconformity is manifested as a seaward-dipping erosion surface interpreted to represent the wave ravinement surface superimposed upon, and coincident with, the antecedent subaerial unconformity and across which all traces of subaerial exposure have been removed by erosion during shoreface retreat (Fig. 36D).

https://doi.org/10.3301/GFT.2023.03

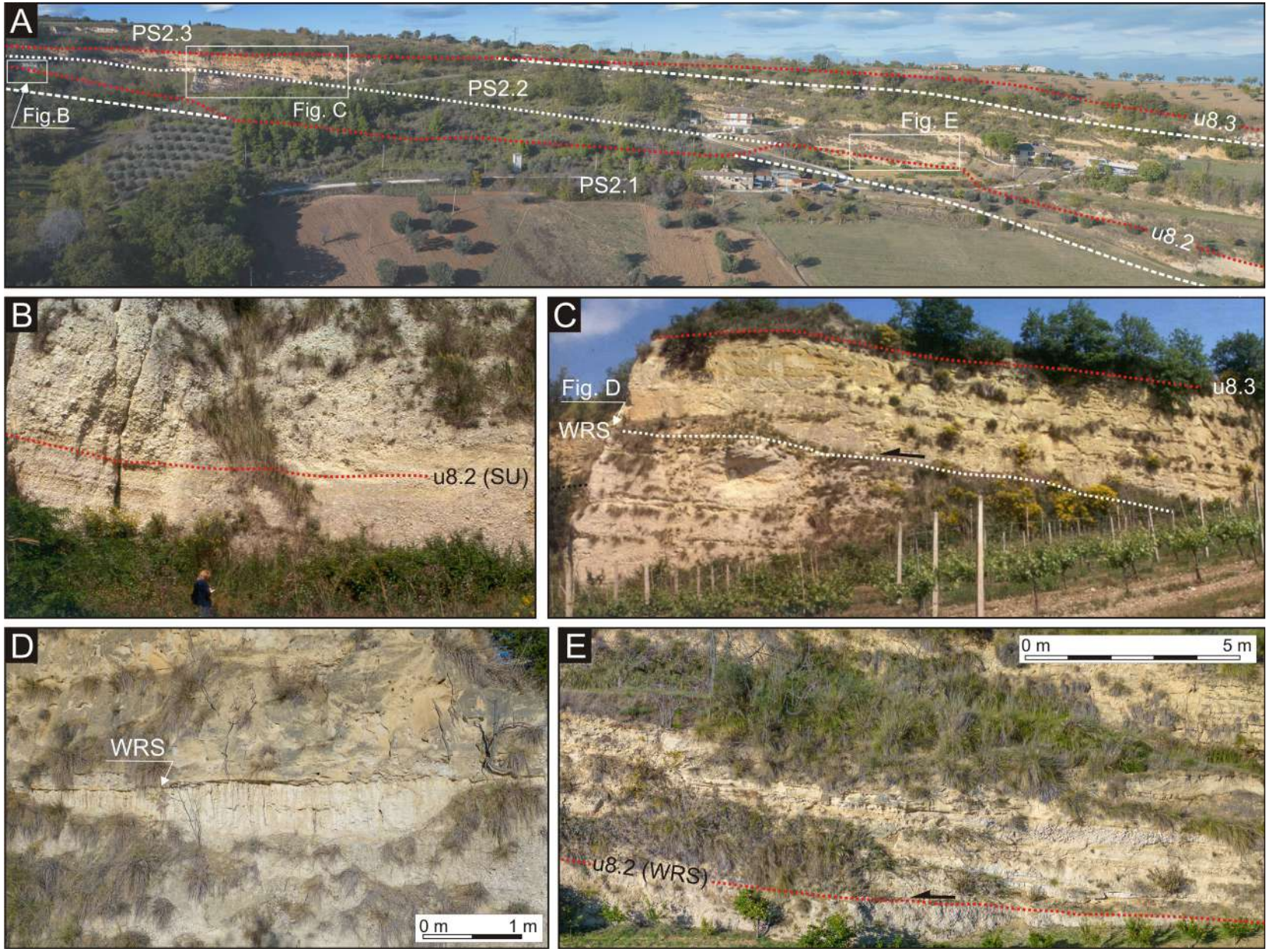

Fig. 36 - (A) Dip-oriented panoramic view of the PS2.1–PS2.2–PS2.3 succession exposed along the northern flank of the Fosso del Molinetto and its architectural interpretation. Note the gentle angular unconformity (u8.3) between the PS2.2 and PS2.3 subunits; (B) Prograding beachface conglomerates at the top of RLD overlain by an erosively based, lenticular and non-marine gravel-body, which is clearly incised into the underlying deposits. Person for scale; (C) Dip- and (D) strike-oriented views of the wave ravinement surface cut into fluvial conglomerates and siltstones and covered by sandstones of a retreating shoreface. The gravelly deposits at the base of the shoreface sandstones represent a wave winnowed transgressive lag, with coarse material being supplied to the shoreface by truncation of the underlying substrate; (E) Oblique panoramic view of the wave ravinement surface separating prograding beachface conglomerates from backstepping lower shoreface pebbly sandstones. The blue and yellow arrows indicate offlap and onlap stratal terminations, respectively.

https://doi.org/10.3301/GFT.2023.03

Stop PRE3-3.6 – Torre di Palme, Fermo

Coordinates: Lat. 43°08'31"N, Long. 13°48'43"E

***Topic*: Panoramic view of two emergent thrust-related structures of the Conero-Tortoreto thrust front**

The Conero-Tortoreto thrust front (CT) stretches along the Adriatic coastline, where it is intersected in exploration wells and imaged by seismic lines, and comprises eastward-verging, blind (nonsurfacing) thrusts and related fault-propagation folds buried under a thick succession of Pleistocene deposits. Notably exceptions are the Conero and Capodarco-Porto San Giorgio thrust folds, where these compressive structures are emerging (e.g., Cantalamessa et al., 1987; Cooper, 1988). This stop provides a northward view along the Adriatic coastline (Fig. 37). The Capodarco-Porto San Giorgio structure seems to mostly involve Pliocene units and there may be significant repetition of the Pliocene itself. The Pleistocene onlaps it and indicates little or no growth since then. The Porto San Giorgio Structure is an imbricate stack of the CAOOW. This structure preserves breaking-back thrust splays (Fig. 36): younger splay toward west – hinterlandward – cut PS1; older splays toward east – forelandward – cut PL1-3 and are sealed by PS1-2. The break-back thrust sequence can be also related to younger shallow (thick-skinned) thrust splays which interfere with older deep (thin-skinned) thrust splays as shown in regional cross-section (Fig. 5); the younger shallow thrust splay being related to thick-skinned tectonics while older deep thrust splay to thin-skinned tectonics. During the Pleistocene, the imbricate thrust splays experienced shortening rates (estimated in between 0.75 mm/yr and 1.46 mm/yr), which associated with the increased sediment supply result in the overall burial of the thrust stack.

Acknowledgments

The authors gratefully acknowledge Petros Didaskalou, who provided the micropalaeontological analysis of some of the sections, and Alan Pitts and Tiziano Volatili, who kindly provided the UAV-based photographs used in this guide. UNMIG–Società Geologica Italiana–AssoMineraria is acknowledged for providing subsurface data through the website http://unmig.sviluppoeconomico.gov.it/videpi/. Total S.A. (now TotalEnergies) and Piero Casero are greatly thanked respectively for providing additional subsurface data and discussions useful to define figures from 4 to 6. Manlio Ghielmi and Giuseppe Serafini are thanked for discussions about the stratigraphic scheme. We thank Alessandro Amorosi and an anonymous reviewer for their very useful and constructive comments. CDC is deeply indebted to Gino Cantalamessa for introducing him to the fascinating Quaternary sediments of the Central Periadriatic Basin.

https://doi.org/10.3301/GFT.2023.03

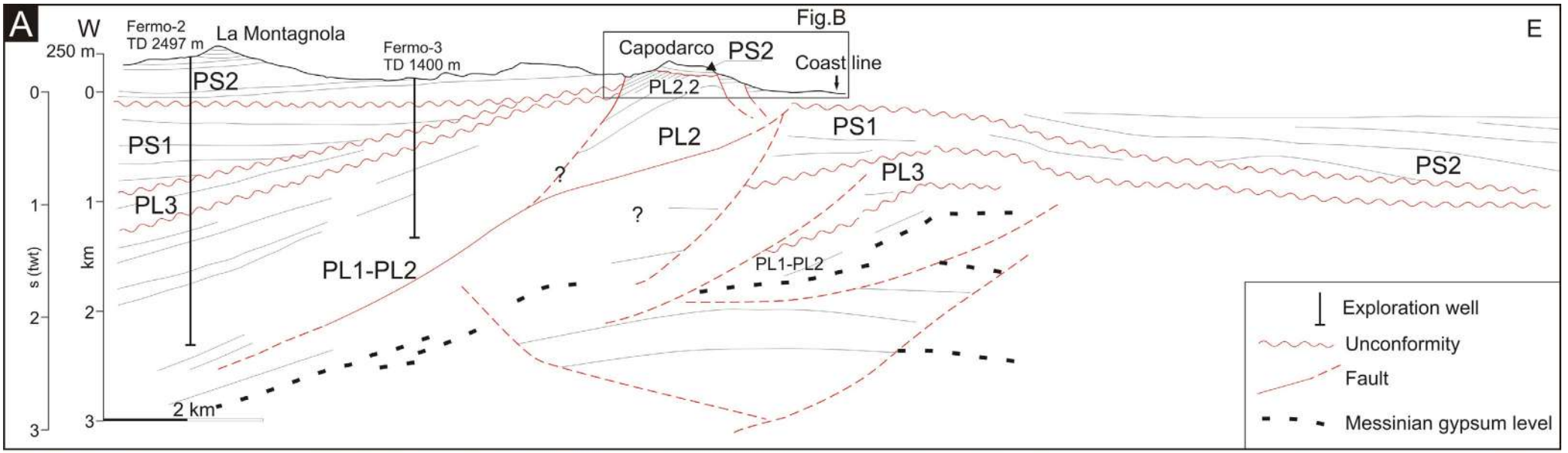

Fig. 37 - (A) Geological interpretation of the main structural elements and stratigraphy across the Fermo-Porto San Giorgio anticline obtained integrating surface data, borehole stratigraphies and interpretation of a seismic line (modified after Cantalamessa et al., 1987 and Cooper, 1988); (B) Northwards panoramic view (from Torre di Palme) along the Adriatic coastline showing position of the Capodarco-Porto San Giorgio structure in the foreground and the Conero structure in the background.

https://doi.org/10.3301/GFT.2023.03

REFERENCES

Albianelli A., Cantalamessa G., Didaskalou P., Micarelli A., Napoleone G., Potetti M. (2003) - Magnetostratigraphic dating of the middle and late Pliocene sequence in the Marchean Apennines, central Italy. Il Quaternario (Italian Journal of Quaternary Sciences), 16, 171-183.

Amorosi A., Barbieri M., Castorina F., Colalongo M.L., Pasini G., Vaiani S.C. (1998) - Sedimentology, micropalaeontology, and strontium-isotope dating of a lower-middle Pleistocene marine succession ("Argille Azzurre") in the Romagna Apennines, northern Italy. Boll. Soc. Geol. It., 117, 789-806.

Amorosi A., Maselli V., Trincardi F. (2016) - Onshore to offshore anatomy of a late Quaternary source-to-sink system (Po Plain-Adriatic Sea, Italy). Earth Sci. Rev., 153, 212-237, https://doi.org/10.1016/j.earscirev.2015.10.010.

Argnani A. (2002) - The northern Apennines and the kinematics of Africa-Europe convergence. Ital. J. Geosci. (Boll. Soc. Geol. It.), Vol. Spec. 1, 47-60.

Argnani A., Artoni A., Ori G.G., Roveri M. (1991) - L'avanfossa Centro-Adriatica: stili strutturali e sedimentazione. Studi Geol. Camerti, 1991/1, 371-381.

Argnani A. and Frugoni F. (1997) - Foreland deformation in the Central Adriatic and its bearing on the evolution of the Northern Apennines. Annali di Geofisica, XI, 771-780.

Argnani A. and Gamberi F. (1995) - Stili strutturali al fronte della catena appenninica nell'Adriatico Centro-Settentrionale. Studi Geol. Camerti, 1995/1, 19-27.

Argnani A. and Ricci Lucchi F. (2001) - Tertiary siliciclastic turbidite systems of the Northern Apennines. In: Vai G.B., Martini I.P. (Eds), Anatomy of an Orogen: the Apennines and Adjacent Mediterranean Basins, Kluwer Academic, London. pp. 327-350.

Artoni A. (1993) - Modello sedimentario e di flessurazione di un tratto del margine adriatico in un settore dell'Appennino Centrale. Ph.D. Thesis, Università di Parma.

Artoni A. (2003) - Messinian events within tectono-stratigraphic evolution of the southern Laga Basin (Central Apennines, Italy). Ital. J. Geosci. (Boll. Soc. Geol. It.), 122, 447-465.

Artoni A. (2007) - Growth rates and two-mode accretion in the outer orogenic wedge-foreland basin system of central Apennine (Italy). Ital. J. Geosci. (Boll. Soc. Geol. It.), 126, 531-556.

Artoni A. (2013) - The Pliocene-Pleistocene stratigraphic and tectonic evolution of the Central sector of the western Periadriatic Basin of Italy. Mar. Petr. Geol., 42, 82-106, https://doi.org/10.1016/j.marpetgeo.2012.10.005.

Artoni A. and Casero P. (1997) - Sequential balancing of growth structures, the late Tertiary example from the Central Apennine. Bull. Soc. Geol. Fr., 168, 35-49.

Backman J., Raffi I., Rio D., Fornaciari E., Pälike H. (2012) - Biozonation and biochronology of Miocene through Pleistocene calcareous nannofossils from low and middle latitudes. Newsl. Stratigr., 45, 221.244, https://doi.org/10.1127/0078-0421/2012/0022.

Bally A.W., Burbi L., Cooper C., Ghelardoni R. (1986) - Balanced sections and seismic reflection profiles across the central Apennines. Mem. Soc. Geol. It., 35, 257-310.

Barchi M. R., Alvarez W., Shimbukuro D.H. (2012) - The Umbria-Marche Apennines as a double orogen: Observations and hypotheses. Ital. J. Geosci. (Boll. Soc. Geol. It.), 131, 258-271, https://doi.org/10.3301/IJG.2012.17.

Barchi M., De Feyter A., Magnani M. B., Minelli G., Pialli G., Sotera B.M. (1998) - The structural style of the Umbria-Marche fold and thrust belt. Mem. Soc. Geol. It., 52, 557-578.

Barchi M. R., Minelli G., Magnani B., Mazzotti A. (2003) - Line CROP 03: Northern Apennines. In: Scrocca D., Doglioni C., Innocenti F., Manetti P., Mazzotti A., Bertelli L., Burbi L., D'Offizi S. (Eds), CROP Atlas – Seismic Reflection Profiles of the Italian Crust. Mem. Descr. Carta Geol. d'It., 52, 127-136.

Bigi S., Calamita F., Cello G., Centamore E., Deiana G., Paltrinieri W., Pierantoni P.P., Ridolfi M. (1999) - Tectonics and sedimentation within a Messinian foredeep in the Central Apennines, Italy. J. Petroleum Geol., 22, 5-18, https://doi.org/10.1111/j.1747-5457.1999.tb00456.x.

Bigi S., Milli S., Corrado S., Casero P., Aldega L., Botti F., Moscatelli M., Stanzione O., Falcini F., Marini M., Cannata, M. (2009) - Stratigraphy, structural setting and burial history of the Messinian Laga basin in the context of Apennine foreland basin system. J. Mediterran. Earth Sci., 1, 61-84, https://doi.org/10.3304/JMES.2009.006.

Boccaletti M., Calamita F., Deiana G., Gelati R., Massari F., Moratti G., Ricci Lucchi F. (1990) - Migrating foredeep-thrust belt system in the Northern Apennines and Southern Alps. Palaeogeogr. Palaeoclimatol., 77, 3-14, https://doi.org/10.1016/0031-0182(90)90095-O.

Boni C. and Colacicchi R. (1966) - I travertini della valle del Tronto: giacitura, genesi e cronologia. Mem. Soc. Geol. It., 5, 315-399.

Buccolini M., Gentili B., Materazzi M., Piacentini T. (2010) - Late Quaternary geomorphological evolution and erosion rates in the clayey peri-Adriatic belt (central Italy). Geomorphology, 116, 145–161, https://doi.org/10.1016/j.geomorph.2009.10.015.

Calamita F., Paltrinieri W., Pelorosso M., Scisciani V., Tavarnelli E. (2003) - Inherited mesozoic architecture of the Adria continental paleomargin in the Neogene central Apennines orogenic system, Italy. Ital. J. Geosci. (Boll. Soc. Geol. It.), 122, 307-318.

Cantalamessa G., Centamore E., Cristallini C., Invernizzi C., Matteucci R., Micarelli A., Piccini M., Pontoni F., Potetti M. (1987) - Nuovi dati sulla geologia dell'area di Porto San Giorgio (Ascoli Piceno, Marche). Geol. Rom., 26, 359-369.

Cantalamessa G., Centamore E., Chiocchini U., Colalongo M.L., Micarelli A., Nanni T, Pasini G., Potetti M., Ricci Lucchi F., Cristallini C., Di Lorito L. (1986) – Il Plio-Pleistocene delle Marche, In: Centamore E. and Deiana G. (Eds), La Geologia delle Marche. Studi Geol. Camerti, Num. Spec., pp. 61-81.

Cantalamessa G., Centamore E., Didaskalou P., Micarelli A., Napoleone G., Potetti M. (2002) - Elementi di correlazione nella successione marina plio-pleistocenica del bacino periadriatico marchigiano. Studi Geol. Camerti, Nuova Serie, 1, 33-49.

Cantalamessa G. and Di Celma C. (2004) - Sequence response to syndepositional regional uplift: insights from high-resolution sequence stratigraphy of late Early Pleistocene strata, Periadriatic Basin, central Italy. Sed. Geol., 164, 283-309, https://doi.org/10.1016/j.sedgeo.2003.11.003.

Cantalamessa G., Di Celma C., Potetti M., Lori P., Didaskalou P., Albianelli A., Napoleone G. (2009) - Climatic control on deposition of upper Pliocene deepwater gravity-driven strata in the Apennines foredeep (central Italy): correlations to the marine oxygen sea isotope record. In: Kneller B., Martinsen O.J., McCaffrey B. (Eds), External Controls on Deep Water Depositional Systems: Climate, Sea-level, and Sediment Flux. SEPM, Spec. Publ. 92, 247-259, https://doi.org/10.2110/sepmsp.092.247.

Carboni F., Brozzetti F., Mirabella F., Cruciani F., Porreca M., Ercoli M., Back S., Barchi M.R. (2020) - Geological and geophysical study of a thin-skinned tectonic wedge formed during an early collisional stage: the Trasimeno Tectonic Wedge (Northern Apennines, Italy). Geol. Mag., 157, 213-232, https://doi.org/10.1017/S001675681900061X.

Carminati E. and Doglioni C. (2012) - Alps vs. Apennines: The paradigm of a tectonically asymmetric Earth. Earth Sci. Rev., 112, 67–96, https://doi.org/10.1016/j.earscirev.2012.02.004.

Carruba S., Casnedi R., Perotti C.R., Tornaghi M., Bolis G. (2006) - Tectonic and sedimentary evolution of the Lower Pliocene Periadriatic foredeep in Central Italy. Int. J. Earth Sci., 95, 665-683, https://doi.org/10.1007/s00531-005-0056-4.

Casnedi, R. (1983) - Hydrocarbon-bearing submarine fan system of Cellino Formation, Central Italy. AAPG Bull., 67, 359-370, https://doi.org/10.1306/03B5AD18-16D1-11D7-8645000102C1865D.

Casnedi R., Crescenti U., D'Amato C., Mostardini F., Rossi U. (1981) - Il Plio-Pleistocene del sottosuolo molisano. Geol. Rom., 20, 1-42.

Casnedi R., Ghielmi M., Rossi M., Cazzola A.L., Serafini G. (2006) - Geometrical analysis and seismic modelling of an outer foredeep margin in the lower Messinian Laga turbidite complex (Central Apennines, Abruzzo, Italy). Ital. J. Geosci. (Boll. Soc. Geol. It.), 125, 203-220.

Castellarin A., Colacicchi R., Praturlon A. (1978) - Fasi distensive, trascorrenze e sovrascorimenti lungo la "linea Ancona-Anzio", dal Lias medio al Pliocene. Geol. Rom., 17, 161-189.

Cavazza W., Roure F.M., Spakman W., Stampfli G.M., Ziegler P.A. (Eds) (2004) - The TRANSMED atlas. The Mediterranean region from crust to mantle. Springer, Berlin Heidelberg.

Centamore E. (1986) - Carta Geologica delle Marche alla scala 1:250.000. In: Centamore E. and Deiana G. (Eds), La Geologia delle Marche. Studi Geol. Camerti, Camerino.

https://doi.org/10.3301/GFT.2023.03

Centamore E., Adamoli L., Berti D., Bigi S., Casnedi R., Cantalamessa G., Fumanti F., Morelli C., Micarelli A., Micarelli A., Ridolfi M., Salvucci R., Chiocchini M., Mancinelli A., Potetti M. (1992) - Carta geologica dei bacini della Laga e del Cellino e dei rilievi carbonatici circostanti (Marche meridionali, Lazio nordorientale, Abruzzo settentrionale). Scala 1:100.000. S.E.L.C.A., Firenze.

Centamore E., Cantalamessa G., Micarelli A., Potetti M., Berti D., Bigi S., Morelli C., Ridolfi M. (1991) - Stratigrafia ed analisi di facies dei depositi del Miocene e del Pliocene inferiore dell'avanfossa Marchigiano-Abruzzese e delle zone limitrofe. Studi Geol. Camerti, Vol. Spec. 1, 125-131.

Centamore E., Cantalamessa G., Micarelli A., Potetti M., Ridolfi M., Cristallini C., Morelli C. (1993) - Contributo alla conoscenza dei depositi terrigeni neogenici di avanfossa del teramano (Abruzzo settentrionale). Boll. Soc. Geol. It., 112, 63-81.

Centamore E. and Nisio S. (2003) - Significative events in the Periadriatic foredeeps evolution (Abruzzo – Italy). Studi Geol. Camerti, Num. Spec., 39-48.

Coltorti M. (1997) - Human impact in the Holocene fluvial and coastal evolution of the Marche region, Central Italy. Catena, 30, 311-335, https://doi.org/10.1016/S0341-8162(97)00007-6.

Coltorti M. and Farabolini P. (2008) - Late Pleistocene and Holocene fluvial–coastal evolution of an uplifting area: The Tronto River (Central Eastern Italy). Quat. Int., 189, 39-55, https://doi.org/10.1016/j.quaint.2007.09.032.

Cooper J.C. (1988) - The geology of the central Apennines and foreland basin, Italy. (Volumes I and II). Ph.D. Thesis, Rice University.

Costa M., Chicco J., Invernizzi C., Teloni S., Pierantoni P.P. (2021) - Plio–Quaternary structural evolution of the outer sector of the Marche Apennines south of the Conero Promontory, Italy. Geosciences, 11, 184, https://doi.org/10.3390/geosciences11050184.

Costa E. and Vendeville B. (2002) - Experimental insights on the geometry and kinematics of fold-and-thrust belts above weak, viscous evaporitic decollement. J. Struct. Geol, 24, 1729-1739, https://doi.org/10.1016/S0191-8141(01)00169-9.

Coward M.P., De Donatis M., Mazzoli S., Paltrinieri W., Wezel F.C. (1999) - Frontal part of the northern Apennines fold and thrust belt in the Romagna-Marche area (Italy): shallow and deep structural styles. Tectonics, 18, 559-574, https://doi.org/10.1029/1999TC900003.

Crescenti U., Milia M.L., Rusciadelli G. (2004) - Stratigraphic and tectonic evolution of the Pliocene Abruzzi basin (Central Apennines, Italy). Ital. J. Geosci. (Boll. Soc. Geol. It.), 123, 163-173.

D'Agostino N., Jackson J.A., Dramis F., Funiciello R. (2001) - Interactions between mantle upwelling, drainage evolution and active normal faulting: an example from the central Apennines (Italy). Geophys. J. Int., 147, 475-497. https://doi.org/10.1046/j.1365-246X.2001.00539.x.

D'Ambrosio A., Lipparini L., Bigi S., Cassola T., Roblet Bambridge V., Derks J.F., Trippetta F. (2021) - Structural restoration and basin modelling of the central Apennine orogen/foredeep/foreland system: New insights on the regional petroleum system. Mar. Petr. Geol., 27, 104948, https://doi.org/10.1016/j.marpetgeo.2021.104948.

D'Amico C. and Esu D. (2011) - *Jaminia (Jaminia) malatestae* Esu, 1988 (Mollusca, Gastropoda, Enidae) from the Middle and Late Pleistocene of central-southern Italy. Paleoecological implications. Il Quaternario (Italian Journal of Quaternary Sciences), 24, 67-74.

Dalla Valle G., Gamberi F., Trincardi F., Baglioni L., Errera A., Rocchini P. (2013) - Contrasting slope channel styles on a prograding mud-prone margin. Mar. Petrol. Geol., 41, 72-82, https://doi.org/10.1016/j.marpetgeo.2012.02.003.

Dattilo P., Pasi R., Bertozzi G. (1999) - Depositional and structural dynamics of the Pliocene Peri-Adriatic Foredeep, NE Italy. J. Petrol. Geol., 22, 19-36, https://doi.org/10.1111/j.1747-5457.1999.tb00457.x.

Davis D.M. and Engelder T. (1985) - The role of salt in fold-and-thrust belts. Tectonophysics, 119, 67-88, https://doi.org/10.1016/0040-1951(85)90033-2.

DeCelles P.G. and Giles K.A. (1996) - Foreland basin systems. Basin Res., 8, 105-123, https://doi.org/10.1046/j.1365-2117.1996.01491.x.

De Donatis M. and Mazzoli S. (1994) - Kinematic evolution of thrust-related structures in the Umbro-Romagnan parautochthon (Northern Apennine). Terra Nova, 6, 563-574, https://doi.org/10.1111/j.1365-3121.1994.tb00523.x.

https://doi.org/10.3301/GFT.2023.03

Dercourt J., Zonenshain L.P., Ricou L.E., Kazmin V.G., Le Pichon X., Knipper A.L., Grandjacquet C., Sbortshikov I. M., Geyssant J., Lepvrier C., Pechersky D.H., Boulin J., Sibuet J.-C., Savostin L.A., Sorokhtin O., Westphal M., Bazhenov M.L., Lauer J.P., Biju-Duval B. (1986) - Geological evolution of the Tethys belt from the Atlantic to the Pamirs since the Lias. Tectonophysics, 123, 241-315, https://doi.org/10.1016/0040-1951(86)90199-X.

Di Celma, C. (2011) - Sedimentology, architecture, and depositional evolution of a coarse-grained submarine canyon fill from the Gelasian (early Pleistocene) of the Peri-Adriatic basin, Offida, central Italy. Sed. Geol., 238, 233-253, https://doi.org/10.1016/j.sedgeo.2011.05.003.

Di Celma C. and Cantalamessa G. (2012) - Off-shelf sedimentary record of recurring global sea-level changes during the Plio-Pleistocene: evidence from the cyclic fills of exhumed slope systems in central Italy. J. Geol. Soc. London, 169, 643-646. https://doi.org/10.1144/jgs2012-041.

Di Celma C., Cantalamessa G., Didaskalou P. (2013) - Stratigraphic organization and predictability of mixed coarse- and fine-grained successions in an upper slope turbidite system of the Peri-Adriatic basin. Sedimentology, 60, 763-799, https://doi.org/10.1111/j.1365-3091.2012.01359.x.

Di Celma C., Cantalamessa, G., Didaskalou P., Lori P. (2010) - Sedimentology, architecture, and sequence stratigraphy of coarse-grained, submarine canyon fills from the Pleistocene (Gelasian-Calabrian) of the Peri-Adriatic basin, central Italy. Mar. Petrol. Geol., 27, 1340-1365, https://doi.org/10.1016/j.marpetgeo.2010.05.011.

Di Celma C., Pieruccini P., Farabollini P. (2015) - Major controls on architecture, sequence stratigraphy and paleosols of Middle Pleistocene continental sediments ("Qc Unit"), eastern central Italy. Quat. Res., 83, 565-581, https://doi.org/10.1016/j.yqres.2015.01.006.

Di Celma C., Pitts A., Jablonská D., Haynes J.T. (2020) - Backset lamination produced by supercritical backwash flows at the beachface-shoreface transition of a storm-dominated gravelly beach (middle Pleistocene, central Italy). Mar. Petrol. Geol., 112, 103987, https://doi.org/10.1016/j.marpetgeo.2019.08.015.

Di Celma C., Ragaini L., Caffau M. (2016a) - Marine and nonmarine deposition in a long-term low-accommodation setting: an example from the Middle Pleistocene Qm2 Unit, eastern Central Italy. Mar. Petrol. Geol, 72, 234-253, https://doi.org/10.1016/j.marpetgeo.2016.02.010.

Di Celma C., Teloni R., Rustichelli A. (2014) - Large-scale stratigraphic architecture and sequence analysis of an early Pleistocene submarine canyon fill, Mt. Ascensione succession (Peri-Adriatic basin, eastern central Italy). Intern. J. Earth Sci. (Geol Rundsch), 103, 843-875, https://doi.org/10.1007/s00531-013-0984-3.

Di Celma C., Teloni R., Rustichelli A. (2016b) Evolution of the Gelasian (Pleistocene) slope turbidite systems of southern Marche (Peri-Adriatic basin, central Italy). J. Maps, 12, 137-151, https://doi.org/10.1080/17445647.2014.995724.

Doglioni C. (1991) - A proposal of kinematic modelling for W-dipping subductions - Possible applications to the Tyrrhenian - Apennines system. Terra Nova, 3/4, 423-434, https://doi.org/10.1111/j.1365-3121.1991.tb00172.x.

Doglioni C., Harabaglia P., Merlini S., Mongelli F., Peccerillo A., Piromallo C. (1999) - Orogens and slabs vs. their direction of subduction. Earth Sc. Rev., 45, 1667-208, https://doi.org/10.1016/S0012-8252(98)00045-2.

Doglioni C., Mongelli F., Pialli G. (1998) - Boudinage of the alpine belt in the Apenninic back-arc. Mem. Soc. Geol. It., 52, 457-468.

Faccenna C., Piromallo C., Crespo-Blanc A., Jolivet L., Rossetti F. (2004) - Lateral slab deformation and the origin of the western Mediterranean arcs. Tectonics, 23, 1012-1033, https://doi.org/10.1029/2002TC001488.

Fantoni R. and Franciosi R. (2010) - Tectono-sedimentary setting of the Po Plain and Adriatic foreland. Rend. Fis. Acc. Lincei 21 (Suppl 1), 197-209, https://doi.org/10.1007/s12210-010-0102-4.

Fanucci F., Moretti E., Nesci O., Savelli D., Veneri F. (1996) - Tipologia dei terrazzi vallivi ed evoluzione del rilievo nel versante adriatico dell'Appennino centro-settentrionale. Il Quaternario, 9, 255-258.

Farabollini P. and Scalella G. (2014) - Itinerari geoturistici nel comprensorio del Monte dell'Ascensione e dei calanchi. Mem. Descr. Carta Geol. d'It., 102, 57-72.

Fellin M.G., San Jose M., Faccenna C., Willett S.D., Cosentino D., Lanari R., Gourbet L., Maden, C. (2022) - Transition from slab roll-back to slab break-off in the central Apennines, Italy: Constraints from the stratigraphic and thermochronologic record. Geol. Soc. Am. Bull., 134, 1916–1930, https://doi.org/10.1130/B36123.1.

https://doi.org/10.3301/GFT.2023.03

Ferretti M., Di Celma C., Lori P., (2003) - Occurrence of *Mammuthus meridionalis* (Proboscidea, Elephantidae) in the Lower Pleistocene deposits of Ripatransone (Periadriatic Basin, Ascoli Piceno, Italy): Stratigraphic contest and biochronologic implication. Studi Geol. Camerti, Vol. I, 37-44.

Gentili B., Materazzi M., Pambianchi G., Scalella G. (1998) - I depositi di versante del Monte dell'Ascensione (Marche meridionali, Italia). Geogr. Fis. Dinam. Quat., 21, 205-214.

Ghielmi M., Minervini M., Nini C., Rogledi S., Rossi M. (2013) - Late Miocene–Middle Pleistocene sequences in the Po Plain – Northern Adriatic Sea (Italy): The stratigraphic record of modification phases affecting a complex foreland basin. Mar. Petr. Geol., 42, 50-81, https://doi.org/10.1016/j.marpetgeo.2012.11.007.

Ghielmi M., Minervini M., Nini C., Rogledi S., Rossi M., Vignolo A. (2010) - Sedimentary and tectonic evolution in the eastern Po-Plain and northern Adriatic Sea area from Messinian to Middle Pleistocene (Italy). Rend. Fis. Acc. Lincei 21 (Suppl 1), 131-166, https://doi.org/10.1007/s12210-010-0101-5.

Ghielmi M., Serafini G., Artoni A., Di Celma C., Pitts A. (2019) - From Messinian to Pleistocene: tectonic evolution and stratigraphic architecture of the Central Adriatic Foredeep (Abruzzo and Marche, Central Italy). In: Vigliotti, M., Tropeano, M., Pascucci, V., Ruberti, D., Sabato, L. (Eds.), Field Trips - GUIDE BOOK, 34th IAS Meeting of Sedimentology, Rome (Italy) September 10-13 2019, Pre-Meeting Field Trip A4, 53-91 (A4 1-38). ISBN 978-88-944576-0-5

Giacomuzzi G., De Gori P., Chiarabba C. (2022) - How mantle heterogeneities drive continental subduction and magmatism in the Apennines. Sci. Rep., 12, 13631, https://doi.org/10.1038/s41598-022-17715-w.

Holbrook J.M. and Bhattacharya J.P. (2012) - Reappraisal of the sequence boundary in time and space: Case and considerations for an SU (subaerial unconformity) that is not a sediment bypass surface, a time barrier, or an unconformity. Earth Sci. Rev., 113, 271-302, https://doi.org/10.1016/j.earscirev.2012.03.006.

Janssens N., Capezzuoli E., Claes H., Muchez P., Yu T.-L., Shen C.-C., Ellam R.M., Swennen R. (2020) - Fossil travertine system and its palaeofluid provenance, migration and evolution through time: Example from the geothermal area of Acquasanta Terme (Central Italy). Sed. Geol., 398, 105580, https://doi.org/10.1016/j.sedgeo.2019.105580.

Kruse S.E. and Royden, L.H. (1994) - Bending and unbending of an elastic lithosphere: the Cenozoic history of the Apennine and Dinaride foredeep basins. Tectonics, 13, 278-302, https://doi.org/10.1029/93TC01935.

Krzywiec P. and Vergés J. (2007) - Role of the foredeep evaporites in wedge tectonics and formation of triangle zones: Comparison of the Carpathian and Pyrenean thrust fronts. In: Lacombe O., Roure F., Lavé J., Vergés J. (Eds), Thrust Belts and Foreland Basins. Springer, Berlin, Heidelberg, https://doi.org/10.1007/978-3-540-69426-7_20.

Lavecchia G., Boncio P., Creati N. (2003) - A lithospheric-scale seismogenic thrust in Central Italy. J. Geodyn., 36, 79-94, https://doi.org/10.1016/S0264-3707(03)00040-1.

Lirer F., Foresi L.M., Iaccarino S.M., Salvatorini G., Turco E., Cosentino C., Sierro F.J., Caruso A. (2019) - Mediterranean Neogene planktonic foraminifer biozonation and biochronology. Earth Sci. Rev., 196, 102869, https://doi.org/10.1016/j.earscirev.2019.05.013.

Lori P. (2005) - Stratigrafia integrata dei sedimenti plio-pleistocenici del bacino Periadriatico marchigiano. Ph.D. Thesis, Università degli Studi di Camerino.

Malinverno A. and Ryan W.B.F. (1986) - Extension in the Tyrrhenian sea and shortening in the Apennines as result of arc migration driven by sinking of the lithosphere. Tectonics, 5, 227-245, https://doi.org/10.1029/TC005i002p00227.

Mancinelli P., Pauselli C., Minelli G., Barchi M.R., Simpson G. (2018) - Potential evidence for slab detachment from the flexural backstripping of a foredeep: Insight on the evolution of the Pescara basin (Italy). Terra Nova, 30, 222-232, https://doi.org/10.1111/ter.12329.

Mantovani E., Babbucci D., Tamburelli C., Viti M. (2009) - A review on the driving mechanism of the Tyrrhenian-Apennines system: Implications for the present seismotectonic setting in the Central-Northern Apennines. Tectonophysics, 476, 22-40, https://doi.org/10.1016/j.tecto.2008.10.032.

Marroni M., Meneghini F., Pandolfi L. (2017) - A revised subduction inception model to explain the Late Cretaceous, double-vergent orogen in the precollisional western Tethys: Evidence from the Northern Apennines. Tectonics, 36, 2227-2249, https://doi.org/10.1002/2017TC004627.

Mascle A., Puigdefàbregas C., Luterbacher H.P., Fernàndez M. (1998) - Cenozoic Foreland Basins of Western Europe. Geol. Soc. Spec. Publ., 134, London, pp. 427

https://doi.org/10.3301/GFT.2023.03

Massari F. (2021) - Storm signature in the Messinian and Pleistocene record of drift-and swash-aligned Mediterranean gravel beaches. Role of precession-driven intensification of the Mediterranean cyclogenesis. Journal of Mediterranean Earth Sciences, 13, 31-76, https://doi.org/10.13133/2280-6148/17480.

Massari F. and Parea G.C. (1988) - Progradational gravel beach sequences in a moderate- to high-energy, microtidal marine environment. Sedimentology, 35, 881-913, https://doi.org/10.1111/j.1365-3091.1988.tb01737.x.

Mazzoli S., Pierantoni P.P., Borraccini F., Paltrinieri W., Deiana G. (2005) - Geometry, segmentation pattern and displacement variations along a major Apennine thrust zone, central Italy. J. Struct. Geol., 27, 1940-1953, https://doi.org/10.1016/j.jsg.2005.06.002.

McArthur A., Kane I., Bozetti G., Hansen L., Kneller B.C. (2020) - Supercritical flows overspilling from bypass- dominated submarine channels and the development of overbank bedforms. Depos. Rec., 6, 21-40, https://doi.org/10.1002/dep2.78.

Midland Valley Exploration Ltd (2011) - 2D Move ®vers. 2011.

Milli S., Moscatelli M., Stanzione O., Falcini F. (2007) - Sedimentology and physical stratigraphy of the Messinian turbidites deposits of the Laga Basin (Central Apennines, Italy). Ital. J. Geosci. (Boll. Soc. Geol. It.), 126, 37-48.

Molli G., Crispini L., Malusà M.G., Mosca P., Piana F., Federico L. (2010) - Geology of the Western Alps-Northern Apennine junction area: a regional review. In: Beltrando M., Peccerillo A., Mattei M., Conticelli S., Doglioni C. (Eds), The Geology of Italy: tectonics and life along plate margins, Journal of the Virtual Explorer, 36, 10, https://doi.org/10.3809/jvirtex.2010.00215.

Nesci O. and Savelli D. (2003) - Diverging drainage in the Marche Apennines (central Italy). Quat. Int., 101-102, 203-209, https://doi.org/10.1016/S1040-6182(02)00102-7.

Nesci O., Savelli D., Troiani F. (2012) - Types and development of stream terraces in the Marche Apennines (central Italy): a review and remarks on recent appraisals. Géomorphologie, 18, 215-238, https://doi.org/10.4000/geomorphologie.9838.

Ori G.G., Roveri M., Vannoni F. (1986) - Plio-Pleistocene sedimentation in the Apenninic-Adriatic foredeep (Central Adriatic Sea, Italy). In: Allen P.A., Homewood P. (Eds.), Foreland Basins, IAS Spec. Publ., 8, 183-198, https://doi.org/10.1002/9781444303810.ch9.

Ori G.G., Serafini G., Visentin C., Ricci Lucchi F., Casnedi R., Colalongo M.L., Mosna S. (1991) - The Pliocene-Pleistocene Adriatic Foredeep (Marche and Abruzzo, Italy): an integrated approach to surface and subsurface geology. In: Adriatic Foredeep Field Trip, 3rd EAPG Conference, Florence May 26-30, pp. 85.

Pattison S.A.J., Ainsworth R.B., Hoffman T.A. (2007) - Evidence of across-shelf transport of fine-grained sediments: Turbidite-filled shelf channels in the Campanian Aberdeen Member, Book Cliffs, Utah, USA. Sedimentology, 54, 1033-1063.

Pieruccini P., Di Celma C., Di Rita F., Magri D., Carnevale G., Farabollini P., Ragaini L., Caffau M. (2016) - Sedimentology, faunal content and pollen record of Middle Pleistocene palustrine and lagoonal sediments from the Peri-Adriatic basin, Abruzzi, eastern central Italy. Quat. Res., 86, 359-372, https://doi.org/10.1016/j.yqres.2016.08.003.

Ragaini L., Cantalamessa G., Di Celma C., Didaskalou P., Impiccini R., Lori P., Marino M., Potetti M., Ragazzini S. (2006) - First Emilian record of the boreal affinity bivalve *Portlandia impressa* Perri, 1975 from Montefiore dell'Aso (Marche, Italy). Boll. Soc. Paleontol. It., 45, 227-234.

Ricci Lucchi F. (1986) - The Oligocene to Recent foreland basins of the northern Apennines. In: Allen P.A. and Homewood P. (Eds), Foreland Basins, IAS Spec. Publ., 8, 105-140, https://doi.org/10.1002/9781444303810.ch6.

Ricci Lucchi F., Colalongo M.L., Creminini G., Gasperi G., Iaccarino S., Papani G., Raffi I., Rio D. (1982) – Evoluzione sedimentaria e paleogeografica del margine appenninico. In: Cremonini G. and Ricci Lucchi F. (Eds), Guida alla geologia del margine appenninico-padano. Guide Geologiche Regionali della Società Geologica Italiana, 17-46.

Rosenbaum G. and Lister G.S. (2004) - Formation of arcuate orogenic belts in the western Mediterranean region. In: Sussman A. and Weil A. (Eds), Orogenic Curvature, GSA Special Papers, 383, 41-56, https://doi.org/10.1130/0-8137-2383-3(2004)383[41:FOAOBI]2.0.CO;2.

Rosenbaum G., Lister G.S., Duboz C. (2002) - Reconstruction of the tectonic evolution of the western Mediterranean since the Oligocene. In: Rosenbaum G. and Lister G.S. (Eds), Reconstruction of the evolution of the Alpine-Himalayan Orogen. Journal of the Virtual Explorer, 8, 107-130, https://doi.org/10.3809/jvirtex.2002.00053.

Roveri M., Bassetti M., Ricci Lucchi F. (2001) - The Mediterranean salinity crisis: an Apennine foredeep perspective. Sed. Geol., 140, 201-214, https://doi.org/10.1016/S0037-0738(00)00183-4.

Royden L. and Karner G.D. (1984) - Flexure of the lithosphere beneath Apennine and Carpathian foredeep basins: evidence for an insufficient topographic load. AAPG Bull., 68, 704-712, https://doi.org/10.1306/AD461372-16F7-11D7-8645000102C1865D.

Rio D., Raffi I., Villa G. (1990) - Pliocene-Pleistocene calcareous nannofossil distribution patterns in the western Mediterranean. In: Kastens K.A., Mascle J. et al. (Eds), Proc. ODP, Sci. Results, 107, 513-533. College Station, TX, https://doi.org/10.2973/odp.proc.sr.107.164.1990.

Ryan W.B.F., Carbotte S.M., Coplan J., O'Hara S., Melkonian A., Arko R., Weissel R.A., Ferrini V., Goodwillie A., Nitsche F., Bonczkowski J., Zemsky R. (2009) - Global Multi-Resolution Topography (GMRT) synthesis data set. Geochem. Geophys. Geosyst., 10, Q03014, https://doi.org/10.1029/2008GC002332. Data: https://doi.org/10.1594/IEDA.100001.

Salvador A. (1994) - International stratigraphic guide. In: I.U.G.S.C. o. Stratigraphy (Eds), I.U.G.S. and Geol. Soc. Am., Trondheim. pp. 214.

San Jose M., Caves Rugenstein J.K., Cosentino C., Faccenna C., Fellin M.G., Ghinassi M., Martini I. (2020) - Stable isotope evidence for rapid uplift of the central Apennines since the late Pliocene. Earth Planet. Sci Lett., 544, 116376, https://doi.org/10.1016/j.epsl.2020.116376.

Scisciani V. and Montefalcone, R. (2005) - Evoluzione neogenico-quaternaria del fronte della catena centro-appenninica: vincoli del bilanciamento sequenziale di una sezione geologica regionale. Ital. J. Geosci. (Boll. Soc. Geol. It.), 124, 579-599.

Scisciani V. and Montefalcone R. (2006) - Coexistence of thin- and thick-skinned tectonics: An example from the Central Apennines, Italy. In: Mazzoli S. and Butler R.W.H. (Eds), Styles of Continental Contraction. GSA Special Papers, 414, 33-54, https://doi.org/10.1130/2006.2414(03).

Scisciani V., Tavarnelli E., Calamita F., Paltrinieri W. (2002) - Pre-thrusting normal faults within syn-orogenic basins of the Outer Central Apennines, Italy: implications for Apennine tectonics. Boll. Soc. Geol. It., Vol. Spec. 1, 295-304.

Scrocca D. (2006) - Thrust front segmentation induced by differential slab retreat in the Apennines (Italy). Terra Nova, 18, 154-161, https://doi.org/10.1111/j.1365-3121.2006.00675.x.

Scrocca D., Carminati E., Doglioni C., Marcantoni D. (2007) - Slab retreat and active shortening along the central northern Apennines. In: Lacombe O., Lavé J., Roure F., Vergés J. (Eds), Thrust belts and Foreland Basins: From Fold Kinematics to Hydrocarbon Systems, Springer, 471-487, https://doi.org/10.1007/978-3-540-69426-7_25.

Sembroni A., Molin P., Soligo M., Tuccimei P., Anzalone E., Billi A., Franchini S., Ranaldi M., Tarchini L. (2020) - The uplift of the Adriatic flank of the Apennines since the Middle Pleistocene: New insights from the Tronto River basin and the Acquasanta Terme Travertine (central Italy). Geomorphology, 352, 106990, https://doi.org/10.1016/j.geomorph.2019.106990.

Servizio Geologico d'Italia (1958) - Carta Geologica d'Italia alla scala 1:100.000, F. 125 Fermo.

Servizio Geologico d'Italia (1963a) - Carta Geologica d'Italia alla scala 1:100.000. F. 141 Pescara.

Servizio Geologico d'Italia (1963b) - Carta Geologica d'Italia alla scala 1:100.000, F. 140 Teramo.

Servizio Geologico d'Italia (1965a) - Carta Geologica d'Italia alla scala 1:100.000, F. 118 Ancona.

Servizio Geologico d'Italia (1965b) - Carta Geologica d'Italia alla scala 1:100.000, F. 110 Senigallia.

Servizio Geologico d'Italia (1966) - Carta Geologica d'Italia alla scala 1:100.000, F. 117 Jesi.

Servizio Geologico d'Italia (1967) - Carta Geologica d'Italia alla scala 1:100.000, F. 124 Macerata.

Servizio Geologico d'Italia (1968) - Carta Geologica d'Italia alla scala 1:100.000, F. 148 Vasto.

Servizio Geologico d'Italia (1969a) - Carta Geologica d'Italia alla scala 1:100.000. F. 133-134 Ascoli Piceno-Giulianova.

Servizio Geologico d'Italia (1969b) - Carta Geologica d'Italia alla scala 1:100.000, F. 109 Pesaro.

https://doi.org/10.3301/GFT.2023.03

Servizio Geologico d'Italia (1970) - Carta Geologica d'Italia alla scala 1:100.000, F. 147 Lanciano.

Steel R.J., Olariu C., Zhang J., Chen S. (2020) - What is the topset of a shelf-margin prism? Basin Res., 32, 263-278, https://doi.org/10.1111/bre.12394.

Tavarnelli E., Butler R.W.H., Decandia F.A., Calamita F., Grasso M., Alvarez W., Renda P. (2004) - Implications of fault reactivation and structural inheritance in the Cenozoic tectonic evolution of Italy. Boll. Soc. Geol. It., Spec. Vol. for IGC 32 Florence, 209-222.

Tozer R.S.J., Butler R.W.H., Corrado S. (2002) - Comparing thin- and thick-skinned thrust tectonic models of the Central Apennines, Italy. EGU Stephan Mueller Special Publication Series, 1, 181–194.

Van der Meulen M.J., Meulenkamp J.E., Wortel M.J.R. (1998) - Lateral shifts of Apenninic foredeep depocenters reflecting detachment of subducted lithosphere. Earth Planet. Sci Lett., 154, 203-219, https://doi.org/10.1016/S0012-821X(97)00166-0.

Wegmann K.W., Pazzaglia F.J. (2009) - Late Quaternary fluvial terraces of the Romagna and Marche Apennines, Italy: climatic, lithologic, and tectonic controls on terrace genesis in an active orogen. Quat. Sci. Rev., 28, 137-165, https://doi.org/10.1016/j.quascirev.2008.10.006.

Manuscript received 14 January 2023; accepted 03 May 2023; published online 31 May 2023;
editorial responsibility and handling by M.L. Pampaloni.

https://doi.org/10.3301/GFT.2023.03